Lep S. Lee
Gregory B. Baecher

Acoustic Data and Uncertainty in Geotechnical Site Characterization Offshore

MIT Sea Grant
College Program

Massachusetts
Institute of Technology
Cambridge
Massachusetts 02139

Report Number
MITSG 83-13
April 1983

Acoustic Data and Uncertainty in Geotechnical Site Characterization Offshore

by

Lep S. Lee
Gregory B. Baecher

Sea Grant College Program
Massachusetts Institute of Technology
Cambridge, Massachusetts 02139

Report No. MITSG 83-13

Grant No. NA81AA-D-00069
Project No. R/O-4

April 1983

Research Group

Gregory B. Baecher is Associate Professor of Civil Engineering in the MIT Department of Civil Engineering

At the time the research was in progress,

Lep S. Lee was a research assistant in the MIT Department of Civil Engineering

RELATED SEA GRANT REPORTS

Baecher, Gregory B., Mark Chan, Thomas S. Ingra Thomas Lee, Louis A. Nucci. GEOTECHNICAL RELIABILITY OF OFFSHORE GRAVITY PLATFORMS. MITSG 80-20. NTIS: PB81 224438. Cambridge: Massachusetts Institute of Technology, 1980. 271 pp. $8.00

MIT/Marine Industry Collegium. OFFSHORE GEOTECHNICAL EVALUATION: OPPORTUNITY BRIEF #27. MITSG 82-3. Cambridge: Massachusetts Institute of Technology, 1982. 16 pp. $3.50.

The Sea Grant Marine Information Center maintains an inventory of technical publications. We invite orders and inquiries to:

Sea Grant Marine Information Center
MIT Sea Grant College Program
Massachusetts Institute of Technology
Building E38-302
Cambridge, Massachusetts 02139

(617) 253-5944

ABSTRACT

The velocity parameter is an important parameter in acoustical profiling. Methods of determining this parameter are discussed. The empirical relationships between the acoustical properties of deep sea sediments and their physical properties are examined and good correlations are found to exist. The physical properties are also found to correlate well with the sediments' geotechnical elastic properties. This then gives an indirect means of correlating between the acoustical properties and the elastic properties.

Next the reliability of predicting the state of regions outside and between parallel seismic (acoustical) profile lines is examined. From these predictions, a two-color map of the region examined is drawn.

Finally, the government's role in leasing the Outer Continental Shelf lands is examined and a policy model for leasing OCS lands is discussed.

ACKNOWLEDGEMENTS

The authors wish to express appreciation to Daniele Veneziano, whose contribution to this work came at a crucial time; and also to their other colleagues at MIT for helpful criticism and suggestions.

TABLE OF CONTENTS

LIST OF FIGURES

LIST OF TABLES

1. Acoustic Profiling - Introduction

The identification of sub-bottom stratigraphy and geological structure often is necessary for the design and construction of foundations of structures on the ocean floor. Acoustical profiling technique provides a flexible, convenient means of identifying general types of ocean-bottom materials and of determining the geometry of sub-bottom layers of soil and rock prior to sampling.

Acoustic profiling is part of the general category of sub-bottom profiling methods known as seismic profiling. Acoustic profiling refers principally to seismic profiling methods using high frequency signals, and therefore having high resolution but limited penetration. Current literature uses the terms 'seismic' and 'acoustic' somewhat interchangeably when referring to offshore exploration, and here both of these terms will be used as applied to a water environment.

Two general types of acoustic profiling are available: refraction profiling and reflection profiling. Refraction profiling uses refraction at strata boundaries and horizontal travel times of seismic waves through strata to infer sub-bottom geometry. Refraction is quite common in terrestial exploration. Reflection uses reflected seismic waves and return travel times to infer sub-bottom geometry. Reflection is much more common than refraction offshore. Here, only reflection surveys are considered, although much of the present discussion could apply to refraction as well.

In acoustic (reflection) profiling, the sound source is usually towed close to the ship while the hydrophone array is towed at a distance behind. This reduces the noise level of the ship, which has frequencies in the range of signal frequencies. Figure 1.1 illustrates an arrangement for a continuous profiling system. The reflected signals are detected by the towed hydrophone array, amplified, filtered and displayed on a precision variable density recorder.

1.1 Basic Concepts

This section discusses basic concepts of reflection profiling which are referred to in later chapters. Figure 1.2 illustrates basic definitions and concepts of reflection profiling.

1.1.1 Acoustic Reflection

A propagating sound wave encountering an interface between materials of different acoustic impedance (see later in this section) has part of its energy reflected back in the direction from which it came, while some is transmitted forward. A normally reflected wave is one encountering such an interface perpendicular to the direction of travel. An obliquely reflected wave is one encountering the interface at an angle. Figure 1.2 illustrates two basic relations for analyzing wave propagation through layered media; first, the angle of incidence = angle of reflection; and second, Snell's Law. At the liquid-solid interface, the two types of refracted waves are generated

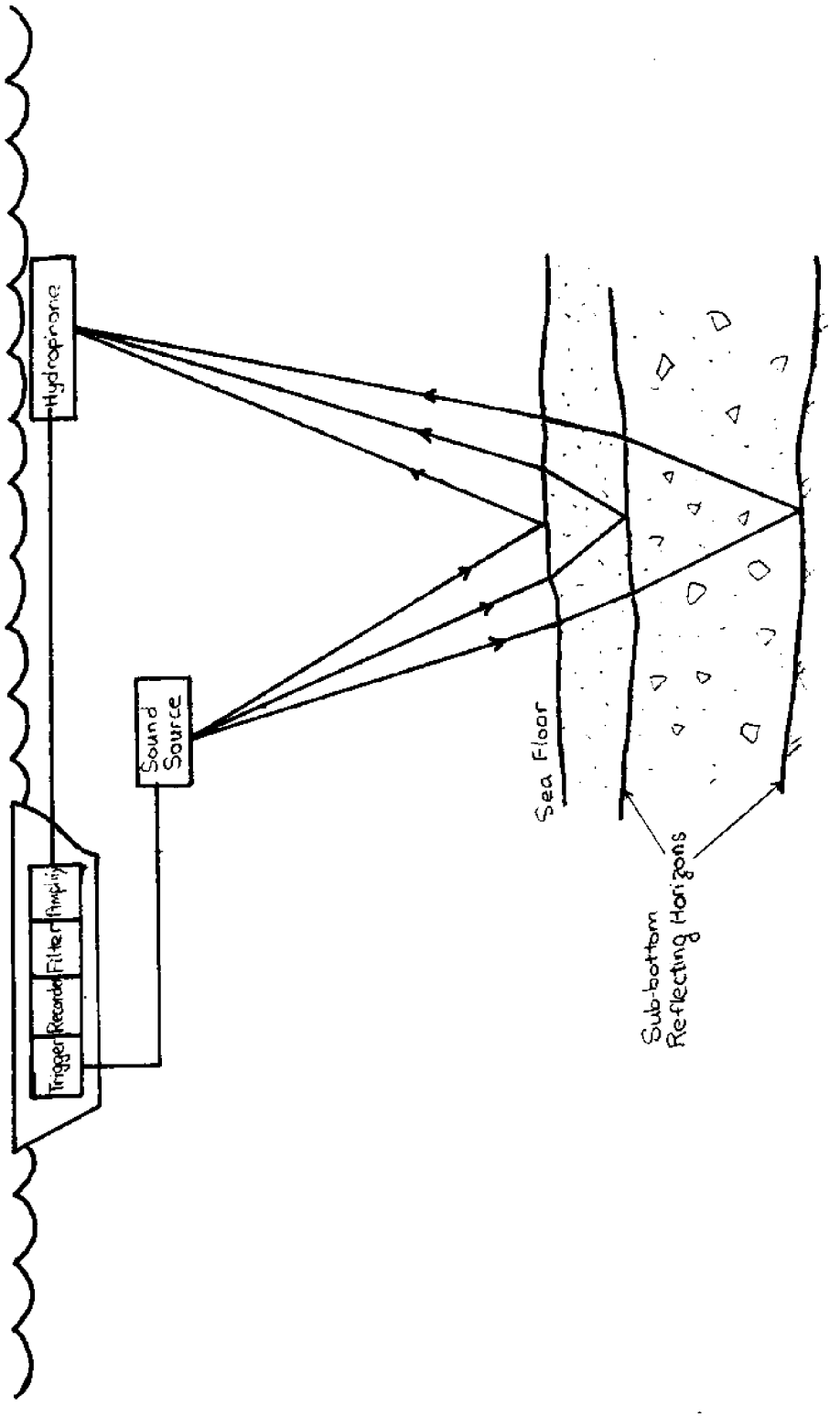

Figure 1.1 Schematic of continous profiling system.

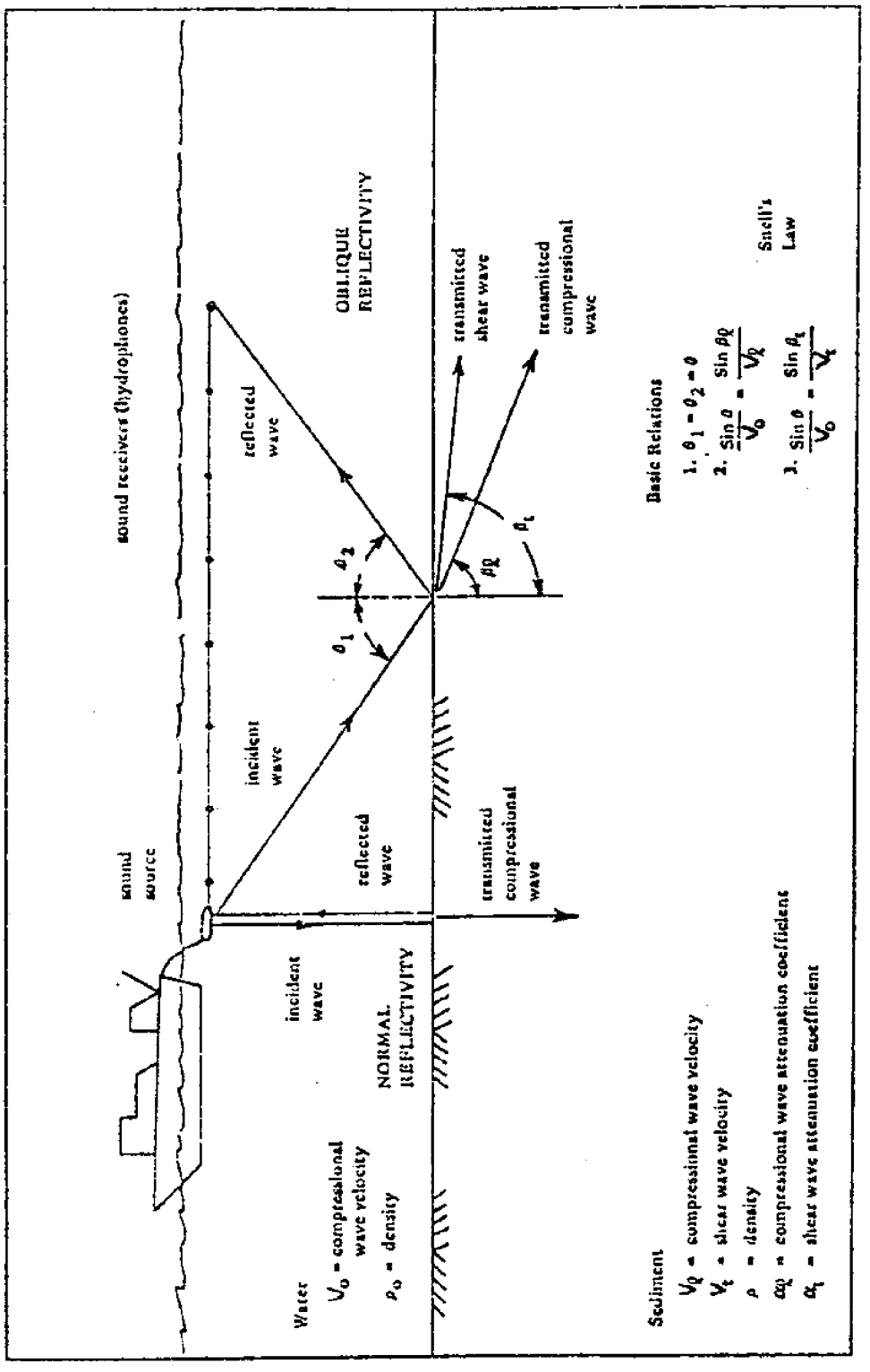

Figure 12. Diagram illustrating basic definitions and concepts. (from Lee & Mallow)

from an obliquely incident wave, a compressional wave and a shear wave. Both obey Snell's Law.

1.1.2 Reflection Coefficient

The reflection coefficient, R, for reflection at the water-sediment interface is given by Raleigh (1945) as

$$R = \frac{A_r}{A_i} = \frac{\rho_2/\rho_1 - \dfrac{\sqrt{V_1^2/V_2^2 - \sin^2\theta}}{\sqrt{1 - \sin^2\theta}}}{\rho_2/\rho_1 + \dfrac{\sqrt{V_1^2/V_2^2 - \sin^2\theta}}{\sqrt{1 - \sin^2\theta}}} \qquad (1.1)$$

where θ is the angle of incidence,

A_r and A_i are the amplitudes of the reflected and incident signals,

ρ_1 and V_1 are the density and sound velocity in water,

ρ_2 and V_2 are the density and sound velocity in the sediment.

Equation [1.1] is commonly used for adjacent sediment layers, as well. However, this application should be made only under restricted conditions of sediment layering, sound energy levels and frequency. Generally, it is valid only when a second, or other, layer in the seabottom does not reflect sound interfering with that reflected from the water-sediment interface.

For normal reflection and incidence Equation [1.1] reduces to

$$R = \frac{\rho_2 V_2 - \rho_1 V_1}{\rho_2 V_2 + \rho_1 V_1} \qquad (1.2)$$

Since most surficial sediments have about the same sonic velocity, as measured by simple oblique reflection techniques, equation [1.2] further reduces to

$$R = \frac{\rho_2 - \rho_1}{\rho_2 + \rho_1} \qquad (1.3)$$

Equation [1.3] can be used in a progressive technique, starting at the water-sediment interface where the water density is known or easily determined, and knowing the values of R for the different layers (from the acoustic record, i.e. $R = A_r/A_i$), to obtain the bulk density of progressive layers.

1.1.3 Compressional Wave and Shear Wave

The compressional wave, also known as the longitudinal or P wave, is transmitted by materials alternately compressing and expanding, and propagates at the compressional wave speed V_c, given by

$$V_c = \sqrt{\frac{K + 4G/3}{\rho}} \qquad (1.4)$$

where K is the bulk modulus

G is the shear modulus

ρ is the material density

Particle movement is along the axis of wave propagation.

The shear wave, also known as transverse or S wave, is generated by an oscillating force transversely stressing a solid. The shear wave speed V_s is given by

$$V_s = \left(\frac{G}{\rho}\right)^{1/2}$$

Particle movement is perpendicular to wave propagation direction.

1.1.4 Attenuation and Energy Loss

Both compressional and shear waves are reduced in amplitude as they propagate through a medium. Energy is lost when the sound spreads out spherically from the source, and by absorption as the wave propagates through water and sub-bottom materials.

Energy loss in the water column is of two types, spherical spreading loss, proportional to 1/L where L is the signal path length, and attenuation loss, proportional to $e^{-\alpha_w L}$ where α_w is the attenuation coefficient of sea water.

In the water-saturated sediment, energy is lost due to Rayleigh scattering, solid friction losses and viscous losses. Solid friction losses occur at the points of contact between the particles and are characterized by a linear variation of the attenuation coefficient with frequency, over a frequency range of 1 to 10^8 Hz. Viscous losses are due to interaction between solid and liquid and are characterized by an attenuation coefficient proportional to the square root of the frequency. The Rayleigh scattering losses are dependent on the fourth power of frequency. Buchan et al. (1972) related the attenuation coefficient α (for compressional waves) to frequency f as

$$\alpha = kf^n \qquad (1.5)$$

where k, n are constants.

1.1.5 Common Depth Point (CDP) Method

The CDP method is a method of acoustic profiling developed by Mayne (1956); and is considered to be among the most important recent developments in seismic profiling. Using the CDP Method, the hydrophone signal traces are recorded from shot points at different horizontal locations below the water surface. Signals reflected from the same sub-bottom point are stacked. The stacking of CDP traces improves data signals because the primary common point reflections are in phase and add constructively, whereas ambient noise and other seismic signals which are not in phase, cancel each other.

Figure 1.3 illustrates how the CDP technique is performed. An acoustic source is triggered at position 1. Part of this energy is reflected from sub-bottom bed 3 to hydrophones 4. The hydrophones and source are then removed to positions 5 and 2 respectively, and the firing repeated. The spacing of 2 from 5 is such that the energy transmitted to hydrophones 5 impinges on the sub-bottom bed (i.e., bed 3) at about the same point. The received signals from the two shots should therefore correspond. Thus when the received energy derived from the two shots is combined, the reflected energy will be reinforced, whereas random energy, being non-coincidental, will be averaged over, improving the clarity of the resulting record.

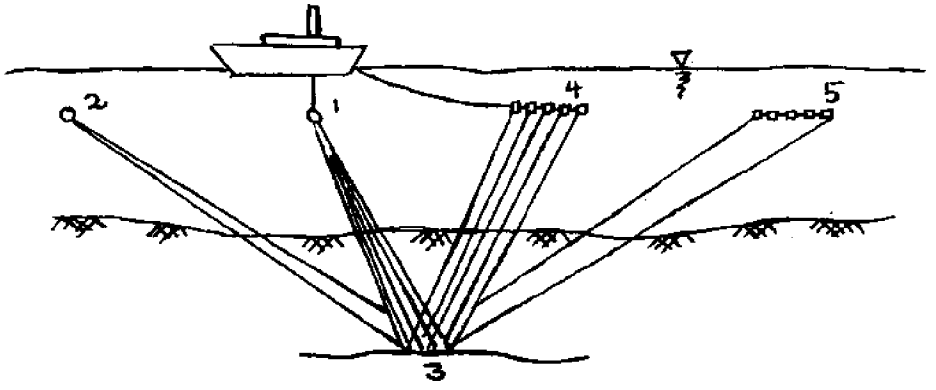

Figure 1.3 Representation of common depth point stacking technique.

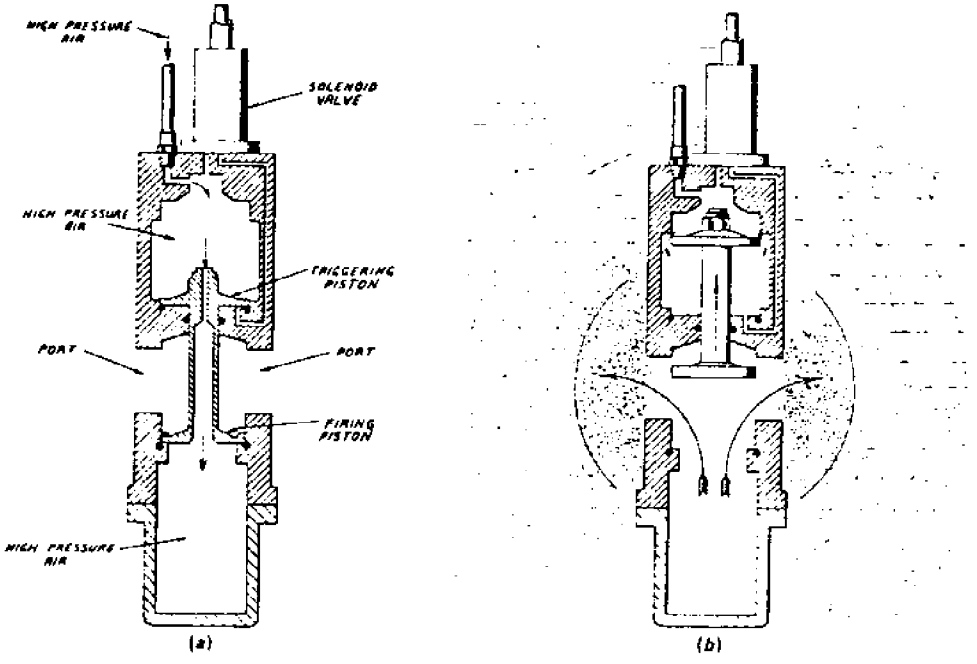

Figure 1.4 Bolt PAR air gun, showing two stages of the firing cycle: (a) armed; (b) fired. (Bolt Associates, Inc.)

1.2 Acoustic Source - The Air Gun

Acoustic profiling sources can be divided into two groups, explosive sources (e.g., dynamite) and non-explosive sources. The Flexotir and Maxipulse systems are examples of explosive sources, while the most common non-explosive sources are the sparker and air gun. The air gun system shall be discussed here.

1.2.1 The Air Gun

The air gun is the most widely used of all non-explosive sources. The Bolt Par, which is a trademark of Bolt Associates, is the most extensively used air gun and has capacities of 1 to 2000 in^3 of air, operating at pressures up to 2000 lb/in^2. Figure 1.4 shows the operation of the PAR air gun. In this system, high pressure air passes through a hose from compressor on the ship to the towed submerged unit. The force in the triggering piston forces the shuttle with the triggering piston to rest on the base of the upper chamber. A high pressure air is then injected by way of the solenoid valve to the base of the triggering piston. This upsets the equilibrium of the system, and the shuttle moves upward at a high velocity, causing high pressure air from the lower chamber to be suddenly released into the water, creating an air bubble and tailing oscillations (which creates return signals that have to be filtered).

The most effective way of reducing the effect of bubble oscillations in the field is to use an array of air guns, all

fired in synchronism. The pressure signal recorded consists of an impulse representing the sum of the initial pulses from all the guns, followed by a train of much weaker bubble pulses, spread out over a period of time and partially cancelling each other.

1.2.2 Signature and Amplitude of Linear Air Gun Arrays

An air gun array is designed with the objective of generating a short signature of high amplitude. To generate such a pulse, with respect to linear arrays of non-interacting air guns, the total available air volume has to be distributed over the individual guns in such a way that the tail of the signal is as flat as possible.

Air guns are ordered according to volume. The flat signal tail can be achieved by designing the volumes such that the difference in bubble times of two adjacent guns is proportional to their volumes to the power 2/3. The amplitude of the signal expected from a linear array of non-interacting air guns is limited by the physical length of the array. Nooteboom (1978) proposed that a good gun combination of non-interacting air guns in a linear array can be achieved by selecting the separate guns such that the difference in bubble times between adjacent guns are proportional to their bubble times squared.

1.3 Characteristics of Seismic Events

In the process of distinguishing features of events from an acoustic record, the interpreter has to perform the

following basic tasks. Initially, he has to select these events on the record which represents primary reflections. Then the arrival times for these reflections are translated into depths and dips. The reflecting horizons are then mapped. The interpreter also has to be aware of other events which may yield valuable or distracting information, such as multiple reflections and diffractions.

Recognition of acoustic events are based on five characteristics. These are coherence, amplitude standout, character, dip moveout and normal moveout. Figure 1.5 illustrates these concepts. The coherence of the event is the most important characteristic in recognizing an event. Coherent events are caused by return signals producing similar effects on each hydrophone in an array, from trace to trace. The amplitude standout relates to an increase in energy of the return signals due to reflection from an interface of two media with different acoustic impedances. Amplitude standouts are associated with coherent events. The character of the event refers to the distinctive appearance of the waveform which identifies a particular event. The distinction involves primarily the shape of the envelope, the number of cycles showing amplitude standout and irregularities in phase which result from interference between components of the event. The moveout is the systematic difference in the arrival time of an event from trace to trace.

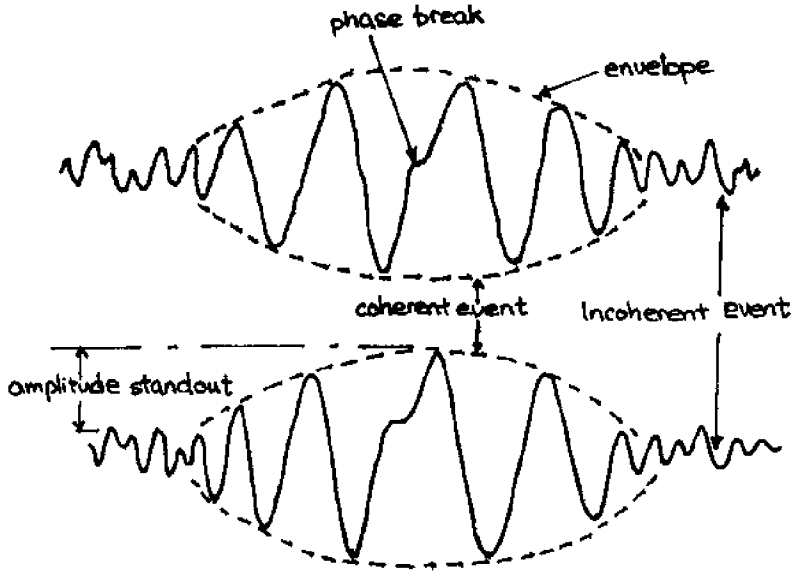

Figure 1.5 Characteristics of a Seismic Signal

1.4 Usefulness of Acoustic Reflection Method

The greatest advantage of acoustic reflection profiling over conventional methods is the continuity of the record. With an acoustic profile, sediment and rock units may be correlated from a few borehole data, eliminating the need for an extensive boring or coring program. Additional borings or cores can be taken in questionable areas or those requiring additional sediment analysis. Geologic features which may be delineated include slumping, large and small scale faulting, differential compaction of overburden, sediment erosion and deposition, eroded channels filled with unconsolidated sediments, etc. All of this information provides data from which a detailed geological map of a site can be constructed.

2. Theoretical Estimation of Depth and Dip of Sub-bottom Layers

This section examines theoretical methods of estimating the depth and dip of sub-bottom layers (the layer thickness can be deduced from the depth of adjoining layers). The velocity of sound in these media is the most important parameter in this estimation. The variation in sound speed in water and then in the sub-bottom layers is first examined. Then methods of estimating the depth and dip for the cases of horizontal reflector, single dipping reflector and two dipping reflectors are discussed.

2.1 Sound Velocity Variation in the Deep Sea

The speed of sound in water is approximately 1500 m/sec. The precise value is strongly dependent upon temperature, pressure and salinity, and its magnitude generally increases as these quantities increase. Typical vertical variations in the deep sea, in temperature and salinity are 25°C and 2ppt. These variations produce sound speed variations of about 80 m/sec and 3 m/sec, respectively. Velocity variation due to pressure is about 50 m/sec for 3000 m of water. Thus temperature and pressure are important variables in determining the vertical profile of sound speed.

Wilson (1960) provides an empirical formula relating sound velocity C to these three variables, as

$$C = 1449.14 + V_T + V_P + V_S + V_{STP} \qquad (2.1)$$

where

V_T is a fourth order polynomial of temperature T

V_P is a fourth order polynomial of pressure P

V_S is a second order polynominal of salinity S

V_{STP} is a polynomial involving cross-products of S,T, and P

(For the forms of V_T, V_P, V_S and U_{STP}, refer Wilson.)

Using equation [2.1] and field data for T,P and S, the speed of sound can be calculated to an accuracy of about ±0.3 m/sec.

In practice the velocity of sound is determined largely from temperature variations obtained by a bathythermograph from the shipboard. A direct method uses the 'sing-around velocimeter' which operates on the principle of timing the travel of an acoustic pulse between two points.

2.2 Sound Velocity Variation in Sea Sub-bottom

Birch (1966) showed that sound velocity V_p is a function of the mineral types of the medium. He obtained information on the variation of velocity with mineral type, as tabulated below.

Mineral Type	Sound Velocity (V_p) km/sec	Mean V_p km/sec
1. Alluvium, Clay, etc.	0.0 to 2.5	1.25
2. Sandstones, shales	0.6 to 4.2	2.40
3. Limestones, dolomites	2.0 to 6.0	4.00
4. Granites, metamorphics	3.0 to 7.0	5.00
5. Salt, Anhydrides	4.2 to 7.5	5.85

Various other researchers have produced empirical correlations which show a second-order polynomial relationship between sound velocity and porosity (discussed in Chapter 3). These results generally indicate decrease in velocity with increasing porosity. Therefore sediments or rocks subjected to greater overburdens (i.e. greater depths of burial) have lower porosities and hence greater velocities of sound propagation. Rapid velocity variation from area to area are observed in regions subjected to recent structural deformation and uplift such as California. Structural changes affect the overburden pressure and also change the porosity of the rocks, hence changing sound speed through the medium.

2.3 Adjustments to Account for Varying Velocity

i. Horizontal Variation:

The survey area is divided into small zones where the horizontal variations can be ignored and the same vertical velocity distribution used.

ii. Vertical Variation:

The constant velocity model is modified by replacing with the average velocity between the surface and the reflecting horizon. Thus a section is assigned a different velocity for each of the reflectors below it.

iii. Velocity Layering

The actual velocity distribution is approximated by a step distribution corresponding to a number of horizontal

layers of different velocities, the velocity being constant within each layer. A graphical method called the "Wave-front Chart", is used to find the depth and dip. This method replaces actual ray path with a series of line segments which are straight within each layer but undergo abrupt changes in direction at the boundaries between layers. Dix (1955) showed that the velocity-time function for this case can be written as

$$t = t_o^2 + x^2/U_{rms}^2 \qquad (2.2)$$

where

$$U_{rms} = \sqrt{\left(\sum_{i=1}^{n} V_i^2 t_i / \sum_{i}^{n} t_i\right)}$$

V_i, t_i are the average velocity in and travel time through the i^{th} layer.

t, t_o are two-way travel time; t_o is the time for normal reflection.

x is the offset, i.e. the distance between hydrophone and source.

2.4 Velocity Functions in Horizontal Reflectors

Acoustic profiles showed that actual velocity usually varies extremely rapidly over short intervals. If these changes are integrated over distances of a wavelength or so (30 m - 100 m), a function that is generally smooth except for discontinuities at marked lithological changes is obtained.

The path of a wave travelling in such a medium can be determined by two integral equations:

$$x = \int_{o}^{z} \frac{PV}{\{1-(PV)^2\}^{1/2}}\, dz \qquad (2.3)$$

$$t = \int_{o}^{z} \frac{dz}{V\{1-(PV)^2\}^{1/2}} \qquad (2.4)$$

where

$$P = \frac{\text{Sin } i_n}{V_n} = \frac{\text{Sin } i_o}{V_o} \quad \text{(i.e., Snell's Law)}$$

$V = V(z)$ where z is depth, $V(z)$ is the value of velocity at depth z.

i_o, i_n are the angles of incident in the 0 layer and the n^{th} layer, and

V_o, V_n are the velocity of sound in the 0 layer and the n^{th} layer (refer Figure 2.1).

Equations [2.3] and [2.4] assume that the medium is divided into a large number of thin beds, in each of which the velocity is a constant. Figure 2.1 illustrates this assumption.

A case of considerable importance is the case of linear increase in velocity with depth, i.e.

$$V_n = V_o + kZ_n \qquad (2.5)$$

where k is a constant whose values are generally in the range of 0.3 to 1.3 per sec.

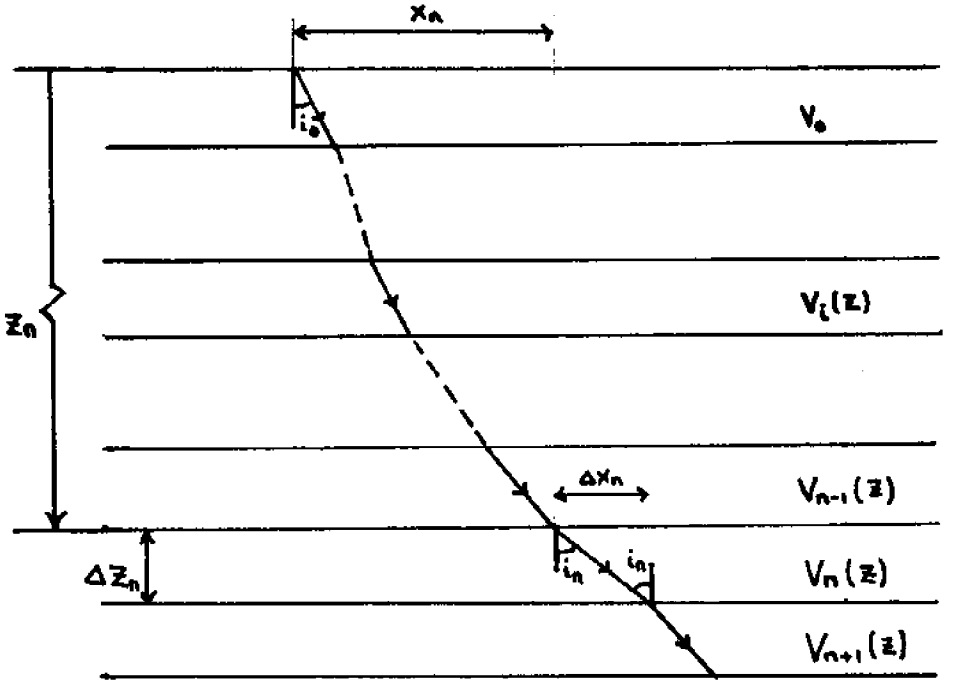

Figure 2.1 Raypath where velocity varies with depth.

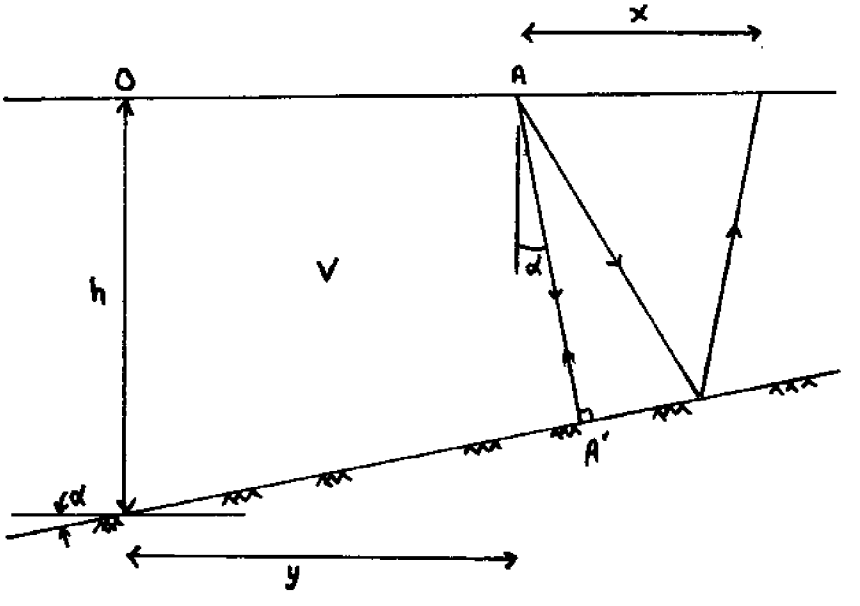

Figure 2.2 A single dipping reflector.

Substituting equation [2.5] in equations [2.3] and [2.4], we obtain

$$x = \frac{1}{Pk} (\text{Cos } i_o - \text{Cos } i) \tag{2.6}$$

$$t = \frac{1}{k} \log \left(\frac{\tan i/2}{\tan i_o/2}\right) \tag{2.7}$$

$$i = 2 \tan^{-1}(e^{kt} \tan i_o/2) \tag{2.8}$$

$$z = \frac{1}{k} (V-V_o) = \frac{1}{Pk} (\sin i - \sin i_o) \tag{2.9}$$

2.5 Parameter Estimation in a Single Dipping Reflector

Figure 2.2 illustrates a scheme for a single dipping reflector. The normal incidence time $t_o(y)$ and the normal moveout NMO(y) for point A at a distance y from an arbitrary reference point O is expressed as

$$t_o(y) = \frac{2(AA)}{V} = [2h \text{ Cos } \alpha - 2y \sin \alpha]/V$$

$$\text{NMO}(y) = [t_o^2(y) + x^2/V_s^2]^{1/2} - t_o(y)$$

where $V_s = V/\text{Cos } \alpha$ (x is the offset)

Making y = L = constant, we have

$$t_o(L) - 2h (\text{Cos } \alpha)/V - 2L(\sin \alpha)/V$$

$$t_o(O) = 2h (\text{Cos } \alpha)/V$$

$$\text{NMO}(O) = [t_o^2(O) + x^2/(V/\text{Cos } \alpha)^2]^{1/2} - t_o(O)$$

Solving the above equations give:

$$h = x\, t_o(0)/\{2\sqrt{[NMO(0) + t_o(0)]^2 - t_o^2(0)}\} \qquad (2.10)$$

$$\tan \alpha = h[t_o(0) - t_o(L)]/(Lt_o(0)] \qquad (2.11)$$

$$v = 2h/(t_o(0)\sqrt{1 + \tan^2 \alpha}) \qquad (2.12)$$

The parameters on the RHS of equations [2.10] to [2.12] can be measured. The direction of the dip can be determined from the signs

$$\text{Sign } (\alpha) - \text{Sign } [t_o(0) - t_o(L)] \qquad (2.13)$$

If Sign (α) > 0, then the slope is updip from point O, and similarly for Sign (α) < 0, the slope is down-dip from O.

2.6 Parameter Estimation in Two Dipping Reflectors

Sections 2.2 to 2.5 discuss the general variation of velocity in a sub-bottom section and methods to estimate the velocity parameter, depth and dip of a reflector. This section describes a more comprehensive and powerful theoretical method for estimating such parameters for the case of two dipping reflectors. This is the Virtual Image Algorithm (VIA).

The exact solution for velocity, depth and dip of a sub-bottom layer can only be obtained using iterations of the ray tracing method. The VIA method can be used to obtain approximate values of these parameters quickly and easily, thus enabling savings in time and acting as an effective decision tool for use on a site.

2.6.1 Basic Principles

The VIA technique for estimating reflection parameters requires the following to be satisfied:

(i) The reflectors are almost planes, at least over the length of the spread.

(ii) Relative velocity contrasts at the reflector planes are not large (i.e. $|V_i - V_{i+1}| / V_i \ll 1$)

(iii) The angles of incidence and dips of reflectors are not large, and the boundaries of reflectors must not intersect each other within the observed region.

When the above conditions are satisfied, the actual wavepath POR (Figure 2.3) through two media of velocities V_1 and V_2, can be replaced by a single wavepath P_VOR through a fictitious medium of velocity V_2 and delay T_p, starting from the virtual shotpoint P_V. T_p is derived below.

T_p = time to travel distance h_1 - time to travel distance h_2

$= h_1(1/V_1) = h_2(1/V_2)$

$$\frac{V_1}{V_2} = \frac{\text{Sin } \alpha_1}{\text{Sin } \alpha_2} \doteq \frac{\tan \alpha_1}{\tan \alpha_2} \doteq \frac{h_2}{h_1}$$

$$h_2 = h_1(V_1/V_2) \qquad (2.14)$$

Substituting h_2 in T_p,

$$T_p = h_1(1/V_1 - V_1/V_2^2) \qquad (2.15)$$

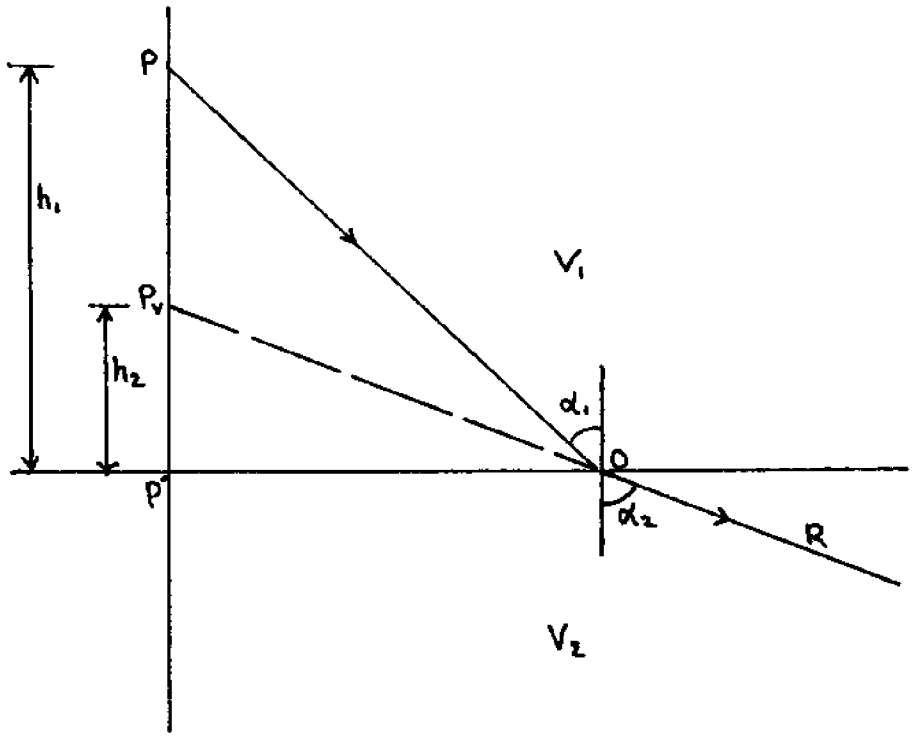

Figure 2.3 Schematic of a refracted ray and its 'virtual shotpoint' P_v .

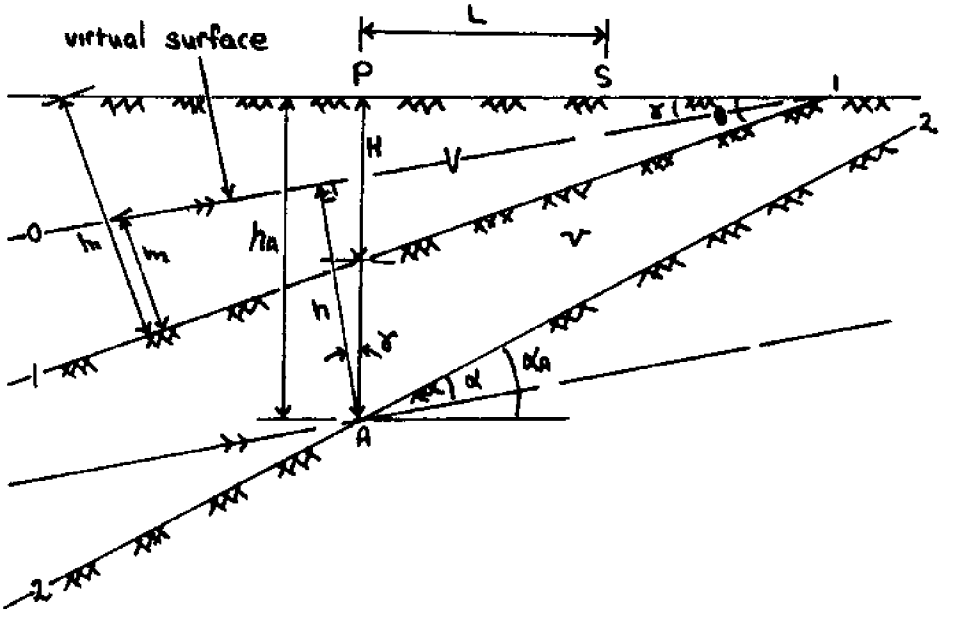

Figure 2.4 Schematic of the case of two dipping reflectors and their replacement by one homogeneous medium.

2.6.2 Solution for Two Dipping Reflectors

The VIA technique is used to determine solutions for the case of two dipping reflectors because the conventional ray path method is complicated and inaccurate. In the VIA method, the two different layers are replaced by one homogeneous medium with a virtual surface.

The parameters of the first reflector (and first layer) are determined as discussed in section 2.5, i.e. one can determine values of h_1, H,V,θ in figure 2.4 from equations 2.10 to 2.12. Then using the principles discussed in Section 2.6.1, the two layers (with their interface as the first reflector 1-1) are made into a single homogeneous layer, with the virtual surface located at 0-1. The problem is therefore reduced to a single reflector problem. Kesmarky (1977) produced solutions for h, α and v for the case of a second reflector given that similar values for the reflector above it are known. These solutions are:

$$\nu = \sqrt{\frac{4L^2x^2\mathrm{Cos}^2\theta - 4fL^2 - 2RQx^2}{R^2x^2 + 4eL^2}} \qquad (2.16)$$

$$\cos^2\alpha = \frac{eV^2 + f}{x^2(\mathrm{Cos}^2\theta + (V/\nu)^2\mathrm{Sin}^2\theta)} \qquad (2.17)$$

$$h = (c\nu^2 + d)/(2\nu\ \mathrm{Cos}\ \alpha) \qquad (2.18)$$

where $a = (1-L/H\ tg\theta)\ t_o(0) - t_o(L)$

$b = (L/H)\ t_g\theta$

$c = t_o(0) - 2H\ Cos\theta/V$

$d = 2HV\ Cos\theta$

$e = NMO^2(0) + 2NMO(0)[t_o(0) - 2H\ cos\theta/V]$

$f = 4NMO(0)\ HV\ Cos\theta$

$R = a + bc$

$Q = bd$

$t_o(0)$, $t_o(L)$ and $NMO(0)$ are measured quantities.

Equation 2.16 gives a value of v that can be used in equation 2.14 to determine the position of the virtual surface and the dip γ of this surface from the horizontal. The virtual dip α and virtual depth h (i.e. the dip and depth relative to the virtual surface) can be determined from equations 2.17 and 2.18. The value of the true depth h_A and true dip α_A at point A (where A is directly below point P) can then be determined as

$$h_A = (PQ)\ \tan\gamma + h/Cos\gamma \qquad (2.19)$$

$$\alpha_A = \alpha + \gamma \qquad (2.20)$$

The two top media whose parameters are now known, can be replaced by a single homogeneous medium with sound velocity equal to the velocity in the lower layer and the virtual surface can be found for the third reflector. The parameters for this reflector can then be similarly determined.

The procedure described above can be continued in the same

manner to estimate the parameters of deeper and deeper reflectors in a recursive fashion.

3. The Empirical Relationships between the Acoustical Properties and Geotechnical Properties of Marine Sediments

The ability to correlate accustical properties of soil sediments with their geotechnical properties would enable the geologist or geotechnical engineer to determine the engineering characteristics of an underlying geological structure and facilitates early planning for development of the offshore region. This chapter discusses empirical relationships between geotechnical and acoustical properties, based on laboratory investigations. These investigations indicate that no common relationship can be obtained for all regions, rather such relationships are specific to the region from which the soil samples used in the laboratory test are obtained. However, results can be useful in areas where past exploration records are available, or as an approximation, in areas where the regional geological trends and types are known to be similar to a region for which correlation equations have been developed.

3.1 Correlations between Geotechnical Properties and Porosity

Porosity was found to correlate strongly with density and elastic properties of marine sediments. Section 3.1.1 discusses the relationships between porosity and density and Section 3.1.2 examines the correlation of porosity with bulk modulus, shear modulus and poissons ratio.

3.1.1. Density and Porosity Relationships

The equation relating density and porosity in a saturated marine sediment was first given by Urick in 1947,

$$\rho = \rho_\omega \eta + \rho_s (1-\eta) \qquad (3.1)$$

where ρ is the saturated bulk density of the sediment

η is the porosity

ρ_ω is the density of seawater

ρ_s is the solid density of the sediment

In using this equation to predict porosity or density, given the other quantity, Hamilton (1974) suggested that it is usually better to assume values of ρ_s and ρ_ω and then compute the missing quantity. He recommended values for ρ_s and ρ_ω as follows

ρ_ω = 1.024 g/cm^3 at 23°C

ρ_s = 2.65 g/cm^3 for sands and silts

= 2.67 g/cm^3 for terrigeneous clay

= 2.70 g/cm^3 for deep-sea red clay

= 2.71 g/cm^3 for clay-calcareous ooze

= 2.45 g/cm^3 for clay-diatomaceous ooze

Hamilton (1970) has produced equations correlating porosity to density for three different marine physiographic regions. These regions are designated (τ) for the continental terrace, (H) for the abyssal hill, and (P) for the abyssal plane. These equations are shown below:

$$(T) \quad \eta = 1.554 - 0.565\,\rho \tag{3.2}$$

$$(H) \quad \eta = 1.548 - 0.550\,\rho \tag{3.3}$$

$$(P) \quad \eta = 1.629 - 0.614\,\rho \tag{3.4}$$

The standard deviations for equations (3.2), (3.3) and (3.4) are, respectively, 2.8, 0.8 and 1.3.

Akal (1972) produced results of relative density vs porosity for 15,124 samples. These results, shown in Figure 3.1, lead to the relation

$$\rho_r = 2.604 - 1.606\eta \tag{3.5}$$

where $\rho_r = \rho/\rho_\omega$

Equation (3.5) corresponds to equation (3.1) for $\rho_s = 2.66$. A similar plot produced by Buchan (1972) is shown in Figure 3.2. His results also indicate that the data generally fall between $\rho_s = 2.6$ and $\rho_s = 2.7$. Figure (3.3) shows comparative plots of equations (3.2) through (3.5) which correspond closely to each other.

3.1.2 Porosity and Elastic Properties

The elastic properties that geotechnical engineers are primarily interested in are bulk modulus, k, shear modulus G, and poisson's ratio μ. Hamilton (1971) proposed several equations which predict bulk modulus given porosity. These are

$$(T) \quad K = 215{\cdot}095 - 133{\cdot}101\ln\eta + 28{\cdot}287(\ln\eta)^2 \tag{3.6}$$

$$(H)+(P) \quad K = 128.991 - 72.048\ln\eta + 13.866(\ln\eta)^2 - 0.91(\ln\eta)^3 \tag{3.7}$$

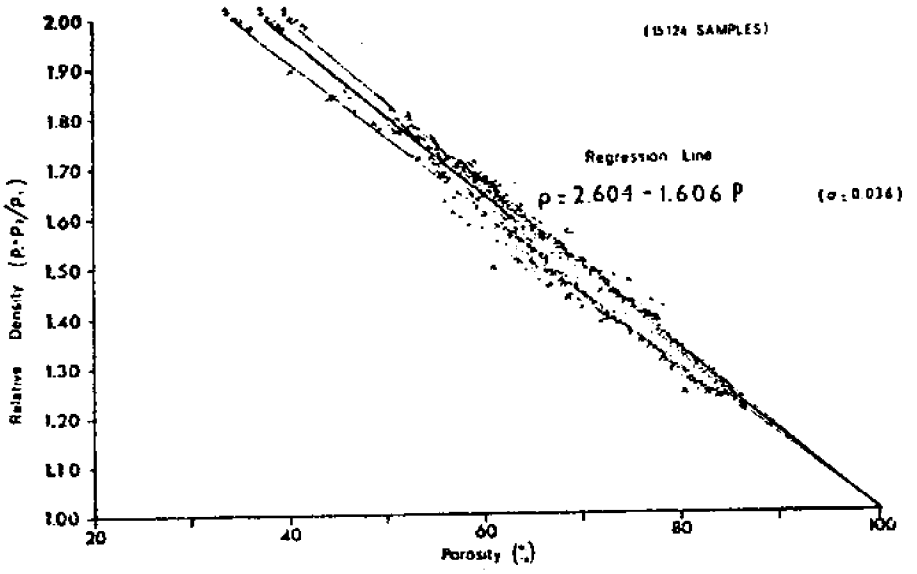

Figure 3.1 Correlation between relative density and porosity (Akal 1972)

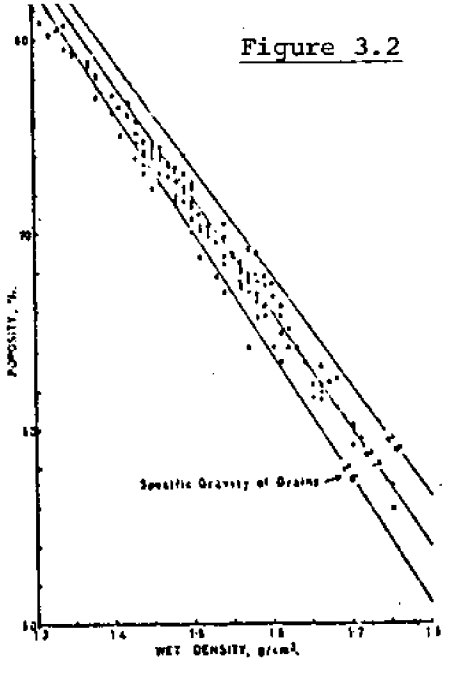

Figure 3.2 Porosity vs wet density (Buchan 1972)

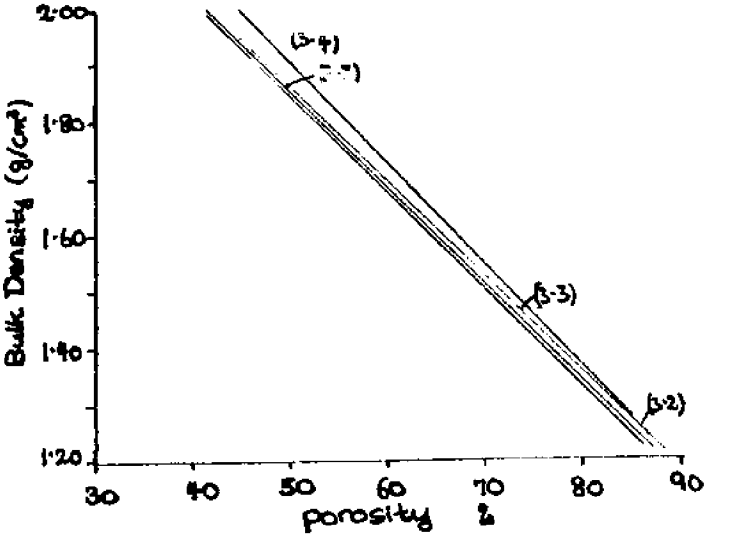

Figure 3.3 Comparative plots of Equations 3.2 to 3.5 .

where (T), (H) and (P) are physiographic regions having the same definitions as in Section 3.1.1.

The standard deviations for equations (3.6) and (3.7) are, respectively, 0.011 and 0.01 which are small, indicating good correlations. Figure 3.4 shows that the data points do actually fall into a very narrow band for all three regions.

The good correlation between bulk modulus and porosity allows us to predict the shear strength of the sediment. Hamilton listed the following steps to obtaining the shear modulus and Poisson's ratio from an acoustic reflection record:

Step

1. Obtain from acoustic record a relevant acoustic parameter (eg. velocity).
2. Use the responsive prediction equations and compute the porosity. (These equations will be discussed in Section 3.21 through 3.24)
3 Obtain estimates for the bulk modulus and density using equations (3.1) to (3.7).
4 Compute the Shear Modulus from equation (3.8)

$$V = \left(\frac{K + 4G/3}{\rho}\right)^{\frac{1}{2}} \qquad (3.8)$$

where V is the acoustic velocity

5. The shear velocity V_S can be obtained from equation (3.9)

$$V_S = (G/\rho)^{\frac{1}{2}} \qquad (3.9)$$

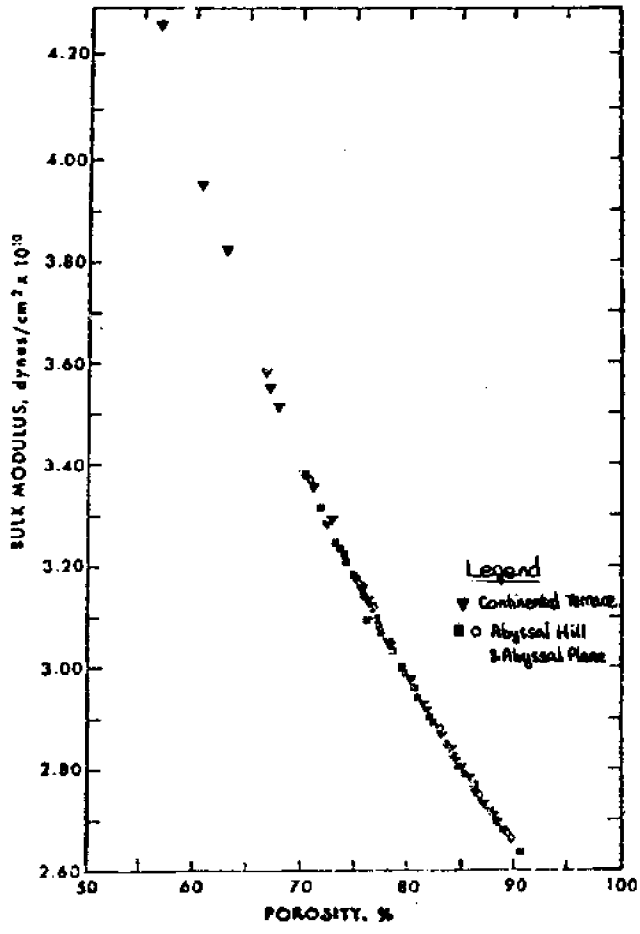

Figure 3.4 Porosity vs Bulk Modulus (Hamilton 1974).

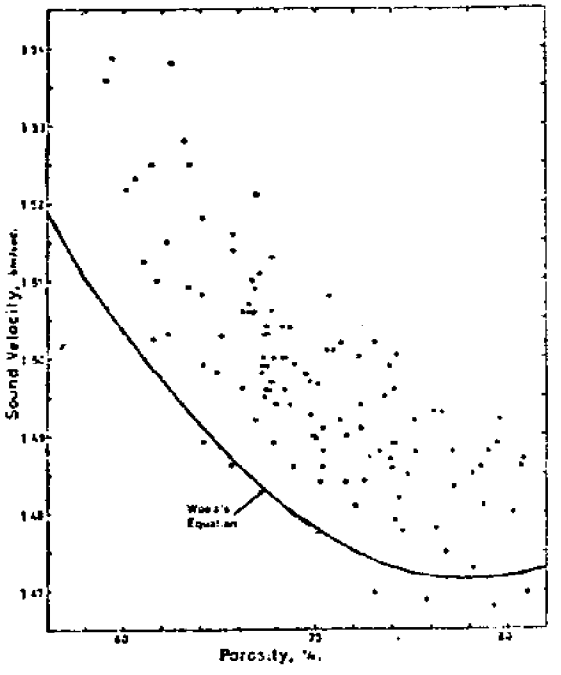

Figure 3.5 Velocity vs Porosity. (Buchan 1972)

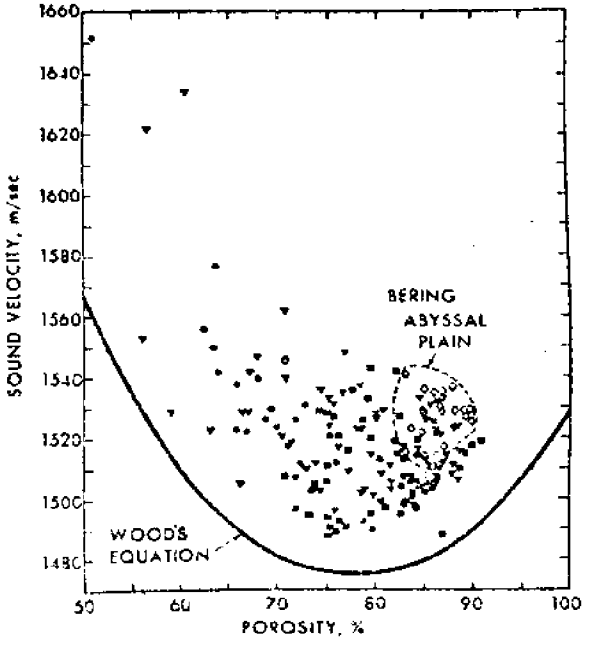

Figure 3.6 Velocity vs Porosity for Abyssal Hill & Abyssal Plain. (Hamilton 1974)

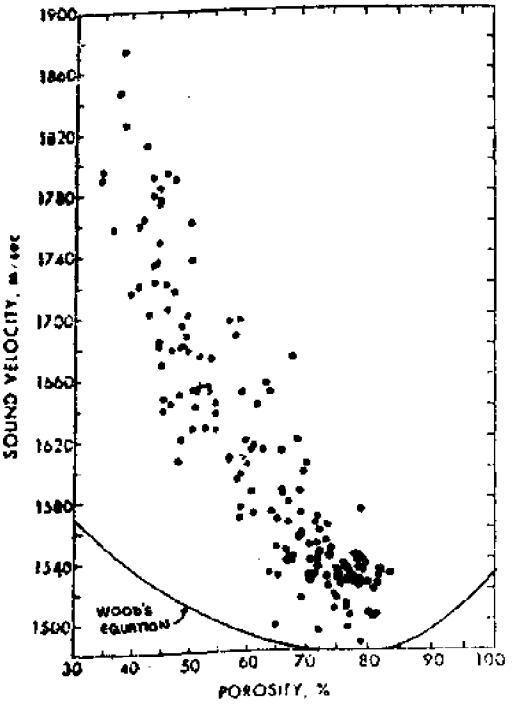

Figure 3.7 Velocity vs Porosity for Continental Terrace. (Hamilton 1974)

6. Poisson's ratio μ, can be obtained from equation (3.10)

$$\mu = \frac{3K - \rho V^2}{3K + \rho V^2} \qquad (3.10)$$

Equations (3.8), (3.9) and (3.10) only apply to an elastic, isotropic and homogenous material. These equations can, however, be used as a first approximation to the more complex and variable real relationships.

The stepwise approach to obtaining G and μ is inaccurate. This is because the bulk modulus is much larger (in magnitude) than the shear modulus G. Thus, small errors in estimating V can lead to large errors in G when estimated from equation (3.8). The approach can also lead to undesirable accumulation of errors. Equation (3.9) indicates that if V_s can be determined accurately then a more accurate estimate of G can be made, since the effect of K is absent. But to this date, no reliable or practical field estimate of V_s can be made.

3.2 Acoustical Properties and Physical Properties

In offshore exploration, the acoustical properties of the sub-seabottom sediments are the first known characteristics, since they are obtained from the preliminary acoustical soundings. It is therefore useful to be able to obtain estimates of the sediment's physical properties (such as porosity) from the acoustical records. The predicted physical parameters can then be used to estimate other geotechnical properties of the sediment, as disccused in Section 2.2.

Sections 3.2.1 through 3.2.4 discuss empirical results to correlate acoustical properties of soil with physical properties. The acoustic properties of interest are sound velocity (Section 3.2.1), acoustic independence (Section 3.2.2), reflectivity (Section 3.2.3) and attenuation (Section 3.2.4).

3.2.1 Sound Velocity and Physical Properties

Although acoustic sources generate both compressional waves and shear waves in subbottom sediment, only the compressional component is measured in conventional acoustical profiling and so will be referred to here merely as acoustic waves. The compressional wave velocity will be called the acoustic velocity.

The acoustic velocity is normally assumed in practice to be 1500m/s. This assumption is in order because acoustic velocity varies primarily with depth and only slightly with composition. Since density or porosity also varies with depth, it can be inferred that acoustic velocity and porosity may correlate well with each other. Section 3.2.1.2 shows that fair correlations do exist between acoustical properties and physical velocities of marine sediments.

To be able to estimate porosity from acoustical records, the acoustic velocity must be measured accurately. The Common Depth Point method (see Section 1.2.5) is one such method used to provide accurate measures of acoustic velocity. Section 3.2.1.1 examines the theoretical relationship between acoustic velocity and porosity or density while Section 3.2.1.2 discusses the empirical relationships.

3.2.1.1 Theoretical Relationship

The theoretical acoustic velocity V in an elastic, homogeneous isotropic solid is given by the equation

$$V = \frac{K + (4/3)r}{\rho}^{\frac{1}{2}} \tag{3.11}$$

where K is the bulk modulus of elasticity (equals $1/\beta$)

β is the compressibility

r is the rigidity modulus

Sediments down to a hundred feet below the seabottom are non-rigid, in which case r = 0 and we obtain Wood's Equation,

$$V = (1/\beta\rho)^{\frac{1}{2}} \tag{3.12}$$

Urick (1947) derives relationships for B and ρ as

$$\beta = \eta\beta_{\omega} + (1-\eta)\beta_{s} \tag{3.13}$$

$$\rho = \eta\rho_{\omega} + (1-\eta\ \rho_{s} \tag{3.14}$$

where $\beta_s = 2.33 \times 10^{-12}$ cm^2/dyne

$\beta_{\omega} = 43$ cm^2/dyne

$\rho_s = 2.65$ g/cm^3

$\rho_{\omega} = 1.024$ g/cm^3

The substitution of equations 3.13 and 3.14 into equation 3.12 produces a relationship between velocity and porosity. This relationship, called Woods Equation, forms a lower bound on the velocity vs porosity plot.

3.2.1.2 Empirical Correlations

It is generally accepted that the sound velocity increases as porosity decreases. However most researchers agree that porosity in itself is only a first approximation to a number of interrelated physical properties that affect the acoustic velocity to varying degrees. Some empirical correlations between velocity and porosity are discussed below.

Figure 3.5 shows empirical results obtained by Buchan (1972). The data points fall mostly above Woods' Equation which is the theoretical relationship between velocity and density (or porosity). Buchan correlates the sediment physical properties and sound velocity as follows:

$$V(m/sec) = 1336 + 92\mu_s + 1101\rho \quad (3.15)$$

$$V = 1616 + 90\mu_s + 2\eta \quad (3.16)$$

$$V = 1416 - 7\,M_{\phi} + 91\rho \quad (3.17)$$

where μ_s is the sand fraction with diameters greater than 62.5 microns,

M_{ϕ} is the mean diameter in phi units

The correlation coefficients of equations (3.15) to (3.17) are 0.789, 0.787 and 0.776 respectively, indicating fair correlation.

Figure 3.6 shows that Wood's Equation again forms the lower bound on data obtained for the abyssal hill and abyssal plain regions. The data in Figure 3.7 are obtained from the Continental Terrace. The prediction equations are

$$(T) \quad v(m/s) = 2456 - 21.7\eta + 0.126\eta^2 \tag{3.18}$$

$$(H) \quad v = 1483 + 0.32\eta \tag{3.19}$$

$$(P) \quad v = 1669 - 1.85\eta \tag{3.20}$$

where equation 3.18 is for figure 3.7 and equations 3.19 and 3.20 are for Figure 3.6. The standard deviations for equations (3.18) to (3.20) are respectively 34.9, 12.8 and 19.2.

Akal (1972) and Morgan (1969) also produced empirical correlations between sound velocity and porosity. Figure 3.8 shows results by Akal. The regression equation is

$$v/v_\omega = 1.631 - 1.78\eta + 1.2\eta^2 \tag{3.21}$$

where v_ω is the velocity of sound in water

v/v_ω is the relative sound velocity

The standard deviation of equation (3.21) is 0.039. Morgan's results are also indicated below

$$v(m/sec) = 2380 - (2197 \pm 1208)\eta + (1333 \pm 982)\eta^2 \tag{3.22}$$

$$v = 2232 - (1168 \pm 1103)\rho + (451 \pm 333)\rho^2 \tag{3.23}$$

Figure 3.9 summarizes the results of several researchers in correlating sound velocity with porosity. It is seen that for $\eta = 0.4$ to 0.8, the prediction curves from Shumway, Wood, Akal, Morgan and Hamilton (H) agree very well with each other. Figure 3.9 can be used as a reference or design curve. Field values of relative sound velocity can be used with the figure to obtain the corresponding value of porosity, the 90% confidence limits, and correlation results from other predictor equations can be checked against Figure 3.9 for compatibility.

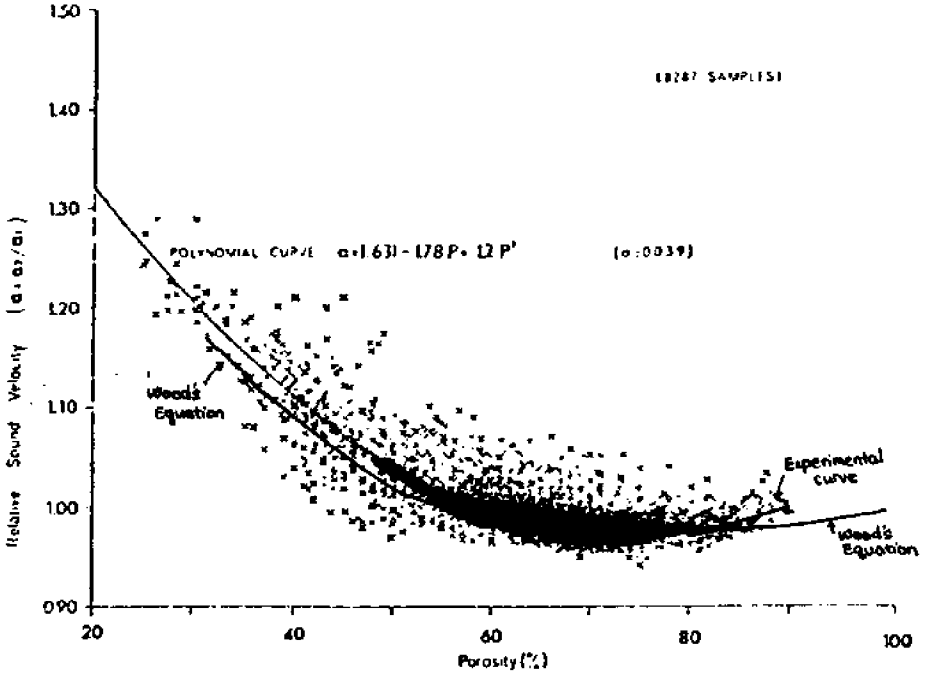

Figure 3.8 Relative sound velocity vs Porosity. (Akal 1972)

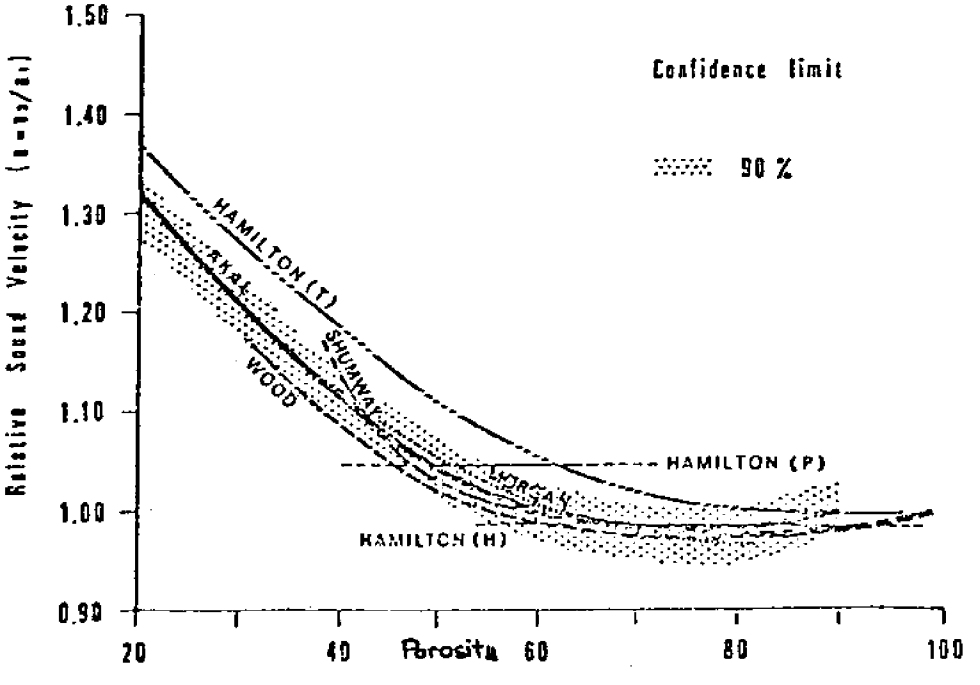

Figure 3.9 Comparison of curves of relative sound velocity vs porosity obtained by different researchers.

3.2.2 Acoustic Impedance and Porosity

The acoustic impedance is the energy change (loss) when sound propagates from one medium into a different medium in continuous reflection profiling records. The impedance difference between two sediment layers or at a discontinuity (such as faults and slips) produces a distinguishing image on the time-plot and therefore reveals the exact location of the sediment facies or discontinuities.

The acoustic impedance Z is defined as the product of the bulk density ρ and the acoustic velocity v.

$$Z = \rho v \tag{3.24}$$

Therefore, if we know the correlation between v and η (equations (3.18) to (3.22)), and between ρ and η (equations (3.1) to (3.5), we can deduce the correlation between z and η.

Buchan et al (1972) measured the acoustic impedance for samples of different porosities. Figure 3.10 shows his results. The correlation is very good. Equations (3.25) and (3.26) are the regression equations.

$$Z\left(\frac{Km}{sec}\ \frac{gm}{cm^3}\right) = 4.345 - 0.0294\eta \tag{3.25}$$

$$Z = -0.251 + 1.666\rho \tag{3.26}$$

The correlation coefficients for these equations are 0.979 and 0.990 respectively indicating very good correlations.

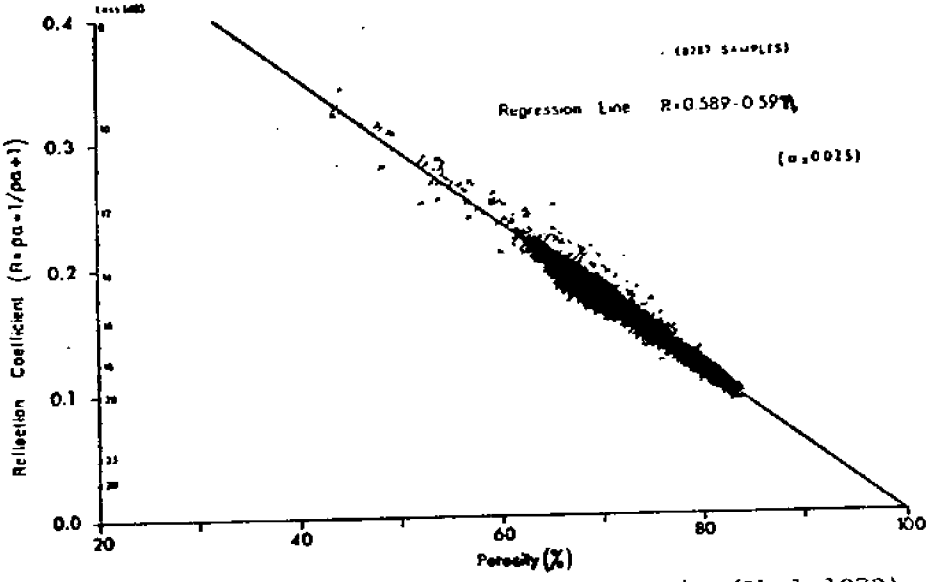

Figure 3.11 Reflection coeffient vs porosity(Akal 1972)

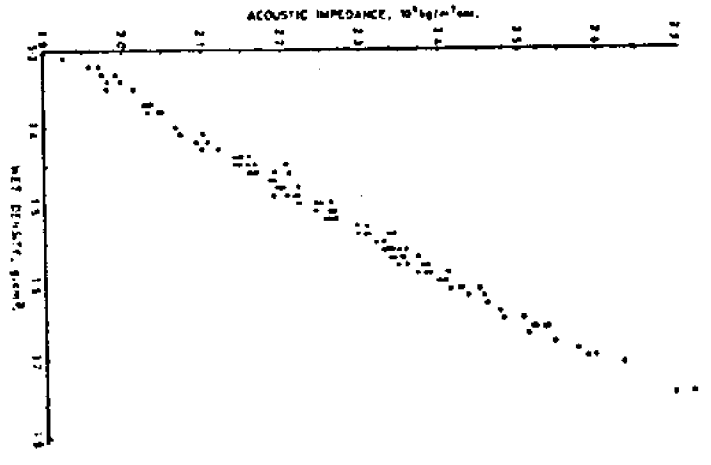

Figure 3.10 Acoustic impedance vs Bulk Density (Buchan 1972)

note: wet density = bulk density

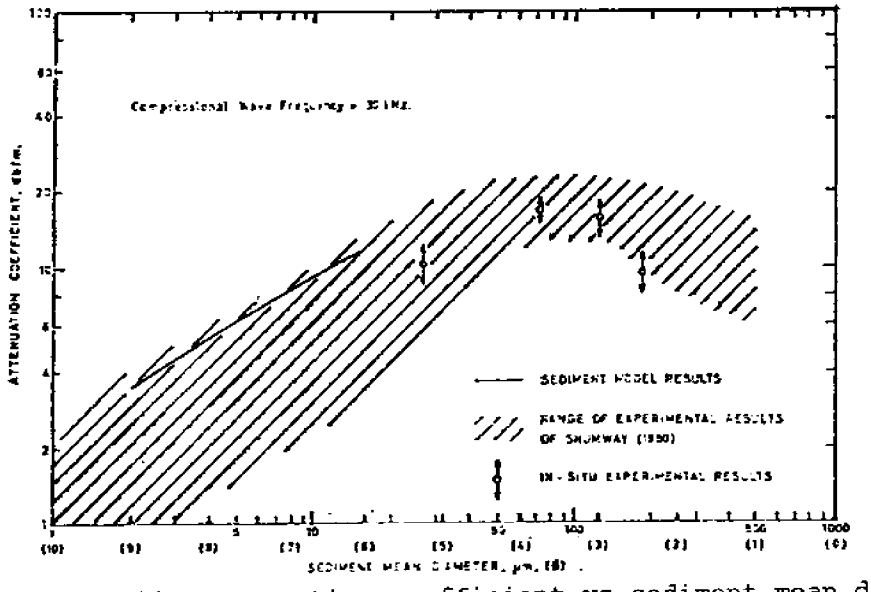

Figure 3.14 Attenuation coefficient vs sediment mean diameter (McCann & McCann 1969)

3.2.3 Reflectivity and Porosity

The reflectivity or reflection coefficient for normal incidence and reflection is defined as

$$R = \frac{Z_2 - Z_1}{Z_2 + Z_1} \tag{3.27}$$

where Z_2 = acoustic impedance in medium 2

Z_1 = acoustic impedance in medium 1

Since the acoustic impedance and porosity have been shown by Buchan to correlate fairly well with each other, it is expected from equation (3.27), that the reflectivity and porosity will also correlate well with each other. Akal (1972) measured the reflectivity for samples of sediments with different porosities and showed that a strong correlation exists between reflectivity and porosity as was expected. Figure 3.11 shows the plot of reflection coefficient vs. porosity. The linear regression line seems to fit the data points very well. The regression equation is

$$R = 0.589 - 0.59\eta \tag{3.28}$$

The standard deviation associated with equation (3.28) is 0.025.

Other researchers have also produced regression equations correlating reflectivity and porosity. These equations are given below:

Author		
Hamilton et al (1956)	$R = 0.6727 - 0.6961\eta$	(3.29)
Sutton et al (1957)	$R = 0.6636 - 0.6478\eta$	(3.30)
Shumway (1960)	$R = 0.6196 - 0.6277\eta$	(3.31)
Morgan (1964)	$R = 0.6634 - 0.6749\eta$	(3.32)
Faas (1969)	$R = 0.6468 - 0.6456\eta$	(3.33)

3.2.4 Attenuation and Physical Properties

The energy loss as sound waves propagated through a medium is of two types; spherical spreading loss and attenuation loss. The attenuation loss is proportional to $e^{-\alpha L}$ where L is the signal path length and α is the attenuation coefficient.

Buchan et al (1972) related the attenuation coefficient α to the wave frequency f

$$\alpha = Kf^{\eta} \qquad (3.34)$$

where K is a constant and $\eta \sim 1$. Using equation (3.34), Hamilton (1974) proposed the following steps for predicting the attenuation coefficient

Step	
1	Determine or predict the mean grain size or porosity of the sediment.
2	Enter the mean grain size or porosity vs K diagrams (Figures 3.12 and 3.13)
3	Determine a value of K and use this value in equation 35 to obtain α.

Buchan obtains good correlations of attenuation coefficient with the sand fraction μ_s and the graphic mean diameter M_Z (in phi units). The regression equations are given below

$$\alpha = 0.992 - 18.079\mu_s \tag{3.35}$$

$$\alpha = 16.002 - 1.534\ M_Z \tag{3.36}$$

Equations (3.35)and (3.36) have correlation coefficients of 0.901 and 0.895 respectively.

Figures 3.12 and 3.13 indicate that there is no direct correlation between k and n or between k and M_Z, therefore indicating no direct correlation between attenuation and porosity or mean grain size. Figure 3.14 is a plot of α vs M_Z for wave frequency f = 30kH_Z. This figure shows the range of experimental results of Shumway, insitu experimental results and sediment model results. Equation (3.36) will give an accepted value of α for a certain range of sediment mean diameter (shown in figure 3.14 as the sediment model results).

3.3 Conclusion

The porosity of a marine sediment correlates with both geotechnical and acoustical properties. This parameter can be estimated, using regression equations discussed above,once the sound velocity, acoustic impedance or reflectivity of the marine sediments are known. The estimated value for porosity can then be used to make rough estimates of engineering properties such as bulk modulus, poisson's ratio and shear modulus.

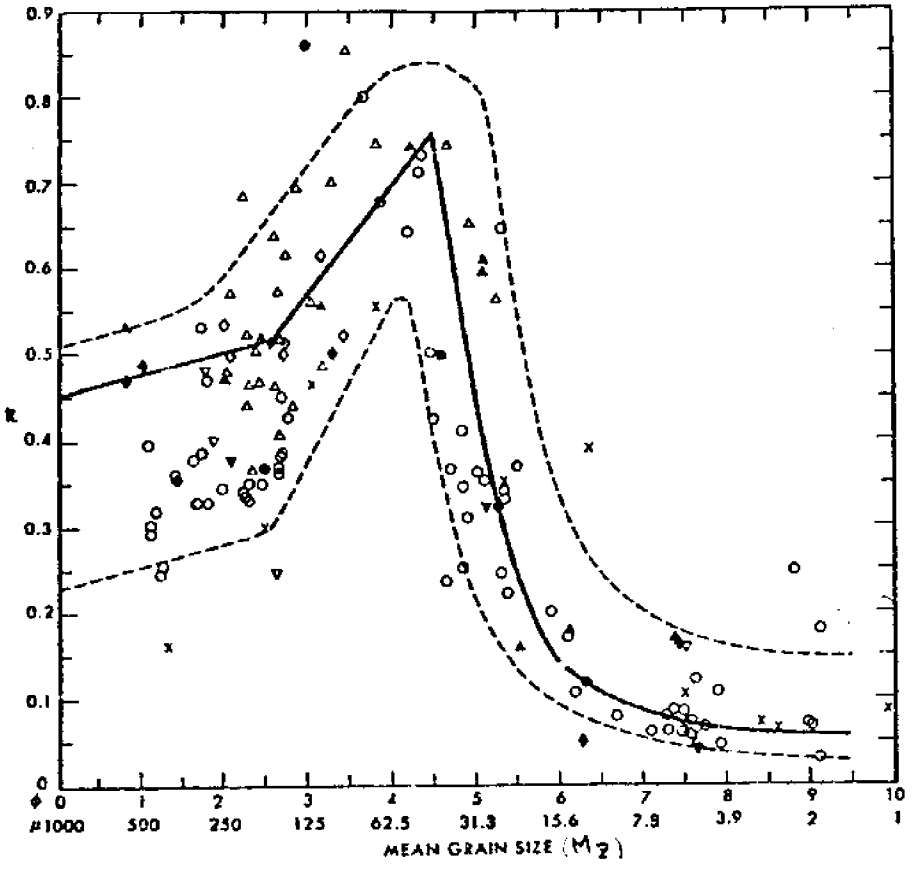

Figure 3.12 k vs mean grain size (Hamilton 1972).

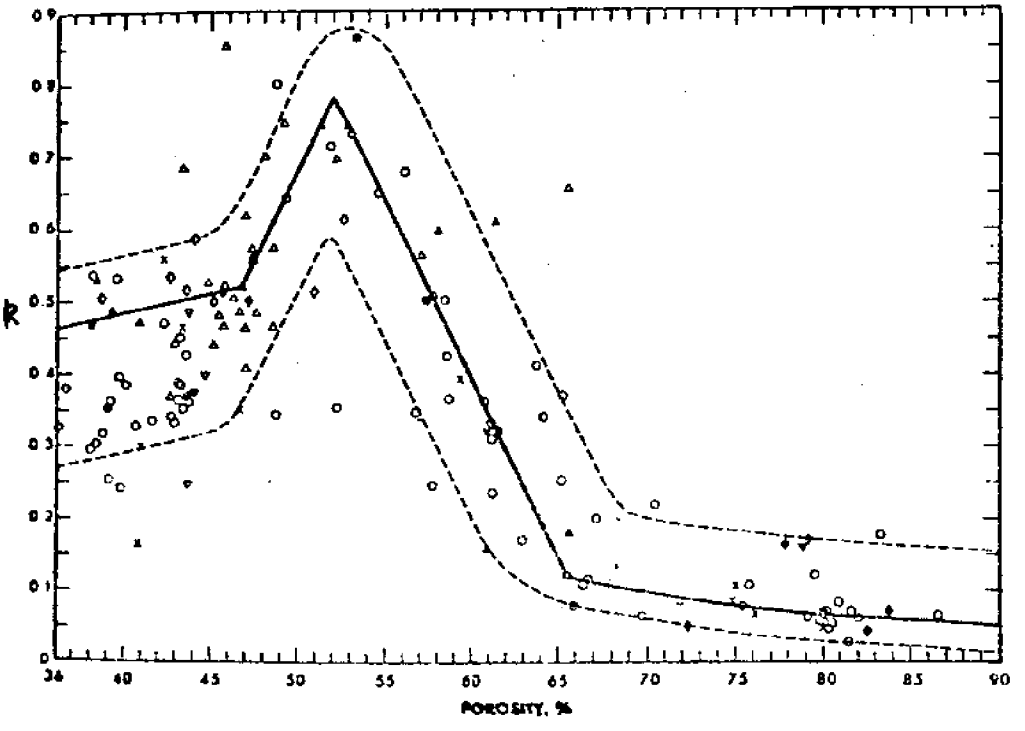

Figure 3.13 k vs porosity (Hamilton 1972)

Sound velocity and reflectivity can be determined fairly accurately from acoustic records. The reflectivity is obtained by taking the amplitude ratio of the return signal to the source signal while the velocity can be measured accurately using the CDP method. The correlations of porosity with sound velocity and with reflectivity is quite good. Therefore, it is recommended that in predicting the porosity of marine sediments, the relationships between porosity and sound velocity (equations (3.15) to (3.23) or between porosity and reflectivity (equations (3.27) to (3.33) should be used.

Thus knowing the acoustic properties of a marine sediment, we can arrive at preliminary estimates of the strength and load-bearing properties of a material. These estimates, however should not be used as design parameters for construction of offshore structures but as indicators of where more detailed investigations for siting purposes should be concentrated.

4. Other Sub-bottom Information from Acoustic Profiling Records

This chapter discusses other geological information that can be inferred from an acoustic profiling record. Section 4.1 examines the use of acoustic information in the recognition of depositional sequences and unconformities. Section 4.2 discusses the correlation of acoustic characteristics with some lithologic and physical characteristics of sediments, and Section 4.3 examines how acoustic records can be used to complement borehole data in refining sub-bottom information.

4.1 Recognition of Geological Depositional Sequences and Unconformities from Acoustic Records

When an acoustic wave propagates through an interface between materials of different acoustic impedance, the path of travel of the wave is deflected from its original path and some of the wave energy is reflected. This change in reflection characteristic is recorded in acoustic logs as distinct seismic events.

These seismic events can be used to distinguish two types of geological structures, i.e. strata surfaces and unconformities. The two media that form at the interface of a stratum surface or an unconformity surface, have different consolidation ages. The older medium will have a higher density. This change in density across the interface results in an impedance change as the acoustic wave propagates through the interface. Within these types of geological structures, four basic

reflection termination patterns can be recognized from the seismic section, i.e. onlap, downlap, toplap and erosional truncation (Ramsayer, 1979). Figure 4.1 shows the basic reflection termination patterns while Fig. 4.2 shows the stratigraphic and chronostratigraphic relationships.

Onlap occurs when a horizontal stratum laps out against an inclined surface. Figure 4.2 shows an onlapping pattern where successively younger strata (A,B,C,D) lap out against the nondepositional older strata. This type of pattern is common in marine environments. Downlap results when an inclined stratum terminates downdip against a horizontal or inclined surface. Figure 4.2 shows that both onlap and downlap have similar chronostratigraphic relationships. Toplap occurs when an inclined stratum terminates against an overlying surface. This termination pattern is common in marine environments. An erosional truncation is formed when a stratum is terminated as a result of erosion.

Using the discordant reflection termination patterns in Fig. 4.1, unconformity surfaces can be recognized on a seismic section and can be extrapolated into areas where the reflectors become concordant because of strata conformity. Major shifts and changes in deposition can then be recognized and depositional sequences defined.

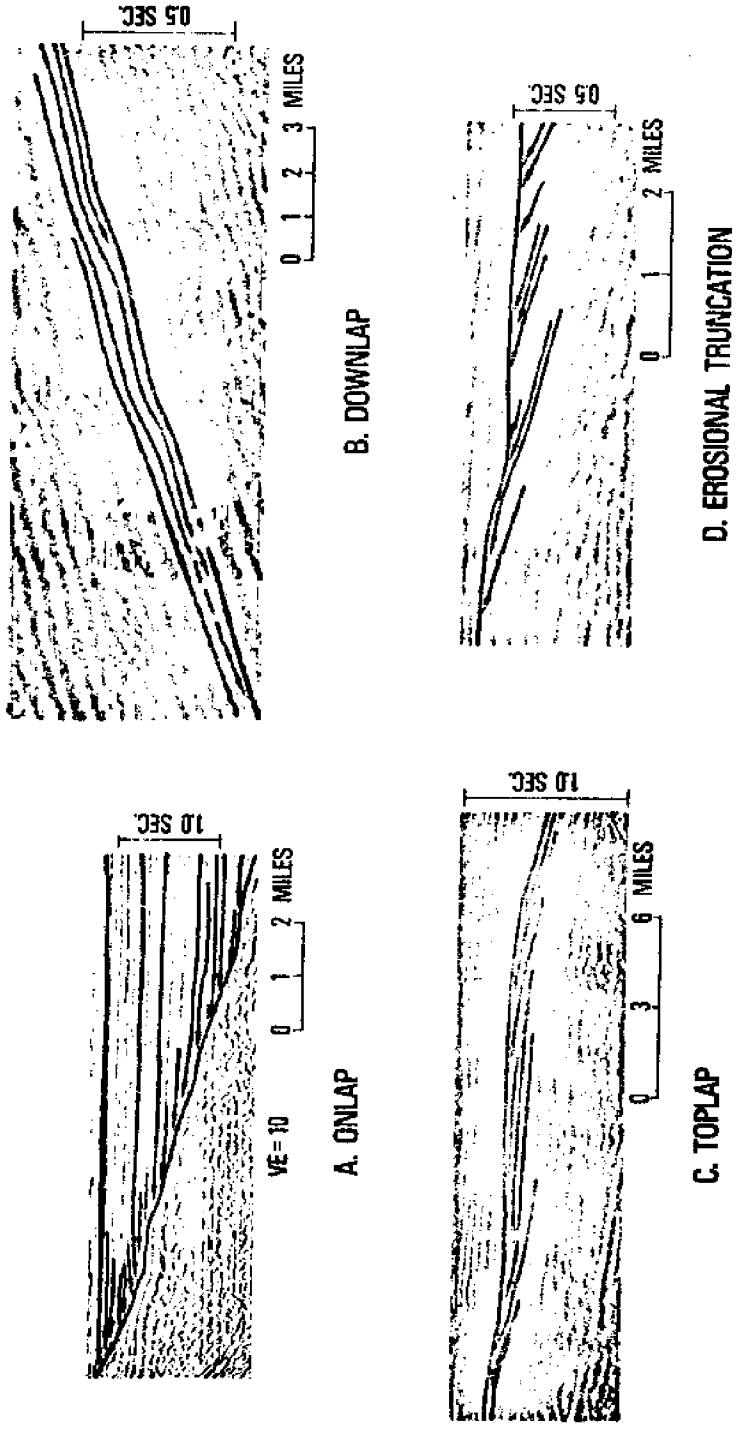

Figure 4.1 Basic reflection termination patterns. (Ramsayer 1979)

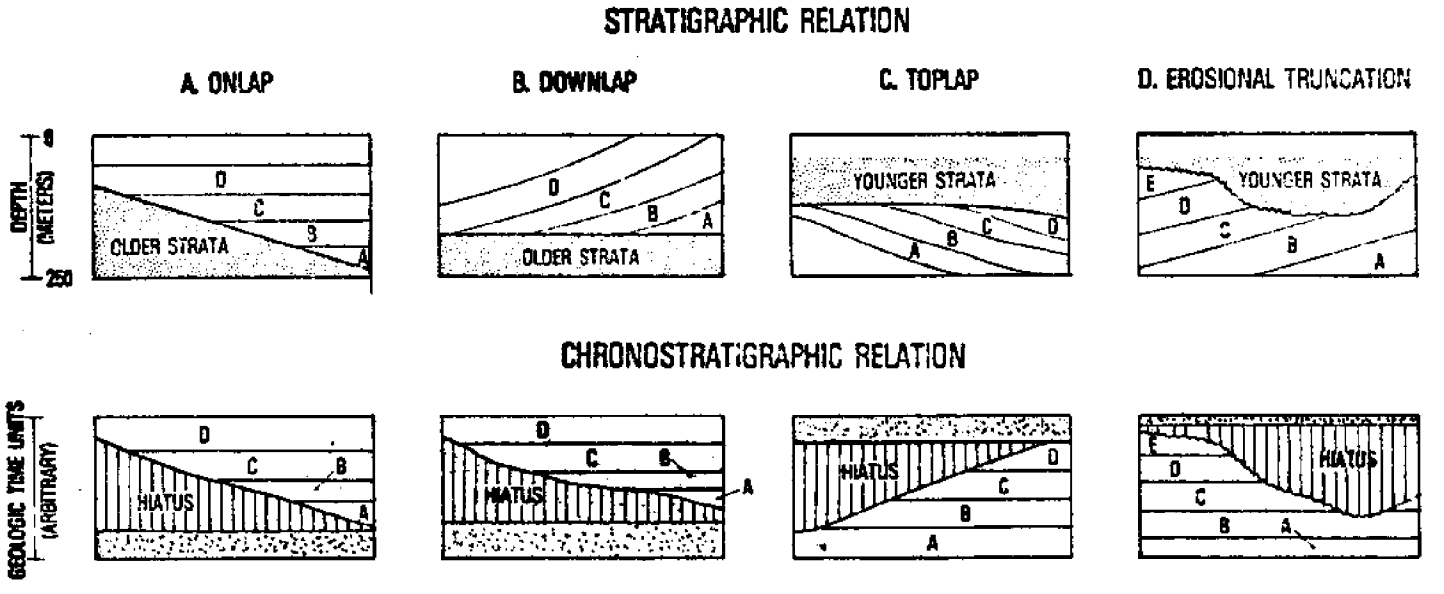

Figure 4.2 Stratigraphic & chronostratigraphic relations of onlap, downlap, toplap & erosional truncation (Ramsayer 1979).

4.2 Correlation of Acoustic Characteristics with Some Lithologic and Physical Characteristics of Sediments

Self and Mahmood (1978) presented a survey of the Alaskan Kodiak Shelf in Fig. 4.3 to illustrate the applicability of acoustic profiles in identifying instability in the sea bottom . Table 4.1 is a summary of the soil and rock units and their qualitative acoustic characteristics as observed by Self and Mahmood.

Addy, Behren and Haines (1979) obtained 3800 km of 3.5 kHz reflection profiles and 77 piston core samples from 25,000 square km of the upper continental shelf off Panama City, Florida. They classified the acoustic profiles into eight reflection types (Fig. 4.4). Type I to Type V consist of distinct reflections, while Type VI to Type VII are of indistinct reflections. The descriptions of these various reflection types are given below:

Reflection Type	Characteristics
Type I	Distinct and sharp bottom echo with numerous parallel sub-bottom reflectors continuous for tens of kms. Depth of penetration of sound energy varies from 25 m to 70 m.
Type II	This type is most widespread. It consists of distinct and sharp bottom echos with

GENERAL DESCRIPTION OF SEDIMENTS	CHARACTERISTICS ON HIGH-RESOLUTION GEOPHYSICAL RECORDS
Possible slide or turbidity current deposits	Hummocky upper surface; no internal bedding; located at base of fairly steep slope.
Migrating, Quaternary age sand and gravel (?) deposits	Undulating, dune-shaped, or rippled upper surface; faint or no internal reflectors (coarse-grained?); poor acoustic penetration; apparent localized migration indicated on duplicate lines.
Unconsolidated, Quaternary age, very sandy, silts or clays; silty or clayey sands	Smooth upper surface; internal reflectors vary from strong to faint, general : parallel (marine deposits?); fair acoustic penetration.
Unconsolidated, Quaternary age, sandy silts or clays with occasional sand layers	Smooth upper surface; strong and numerous parallel internal reflectors (marine deposit); good acoustic penetration (fine-grained and soft?); variations in thickness are generally gradual.
Unconsolidated, Quaternary age, glacial or glacio-fluvial sand and gravel deposits with occasional clay layers	Upper surface varies from smooth to irregular; scattered internal reflectors; channelling and X-bedding common; poor acoustic penetration (coarse-grained?); very irregular unconformity forms lower surface; abrupt lateral variations in thickness; overlies Tertiary deposits.
Hard/very dense, Tertiary age bedrock	Angular unconformity forms irregular upper surface; strong to faint internal reflectors; moderate structural deformation common; faulting and fracturing common in places.

Table 4.1 Summary of soil & rock units observed & their qualitative acoustic characteristics (Self & Mahmood 1978).

Properties	Reflection Types I	IV	VI	VIIa	VIIb	VIIc	VIII
wet bulk density (g/cc)*	1.40	1.43	1.57	1.68	1.68	na	1.66
in situ velocity (m/s)*	1435	1447	1482	na	1520	na	1536
average porosity (%)*	74	73	65	57	57	na	59
% gravel	--	--	--	--	--	13	13
% sand	2	5	24	63	97	85	80
% silt	20	28	47	25	2	2	5
% clay	78	68	30	12	1	0	2
% carbonate	28	37	70	76	25	95	90
mean grain size (Φ)	9.9	9.4	6.6	4.2	2.3	0.7	1.2
standard deviation (Φ)	2.5	2.8	3.2	2.7	1.0	1.6	2.0
skewness	-0.5	-0.3	0.7	1.8	2.4	0.1	1.2
kurtosis	-0.2	-0.7	-0.4	4.1	12.8	0.7	4.7

*for top two meters of cores.

Table 4.2 Average physical properties of sediments in each reflection type (Addy, Behren & Haines 1979)

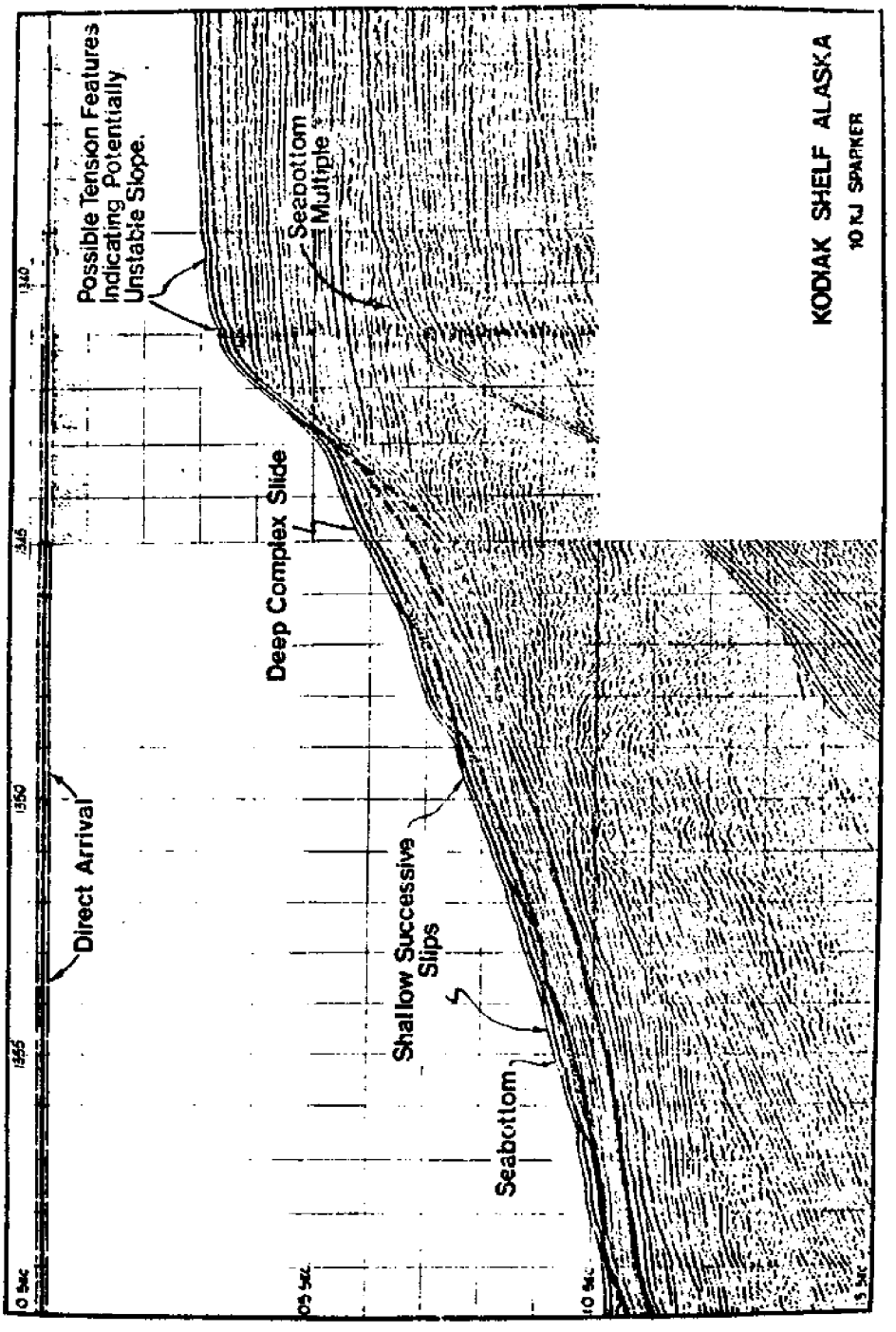

Figure 4.3 Example of regional slope stability survey, Kodiak Shelf, Alaska. (Self & Mahmood 1978)

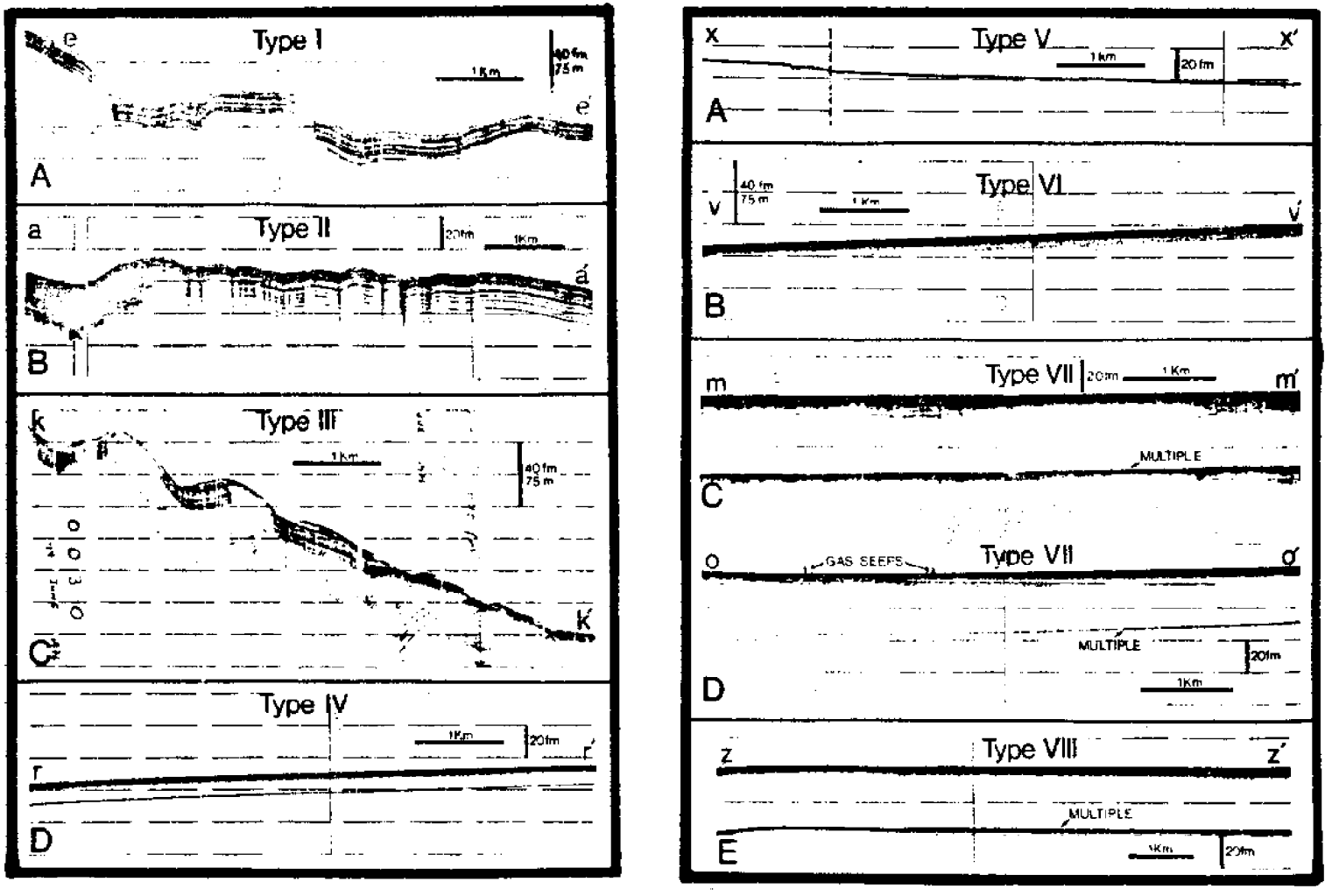

Figure 4.4 Examples of reflection types I to VIII (Addy, Behren & Haines 1979)

	numerous draping sub-bottom reflectors looking like broad hyperbolas. Depth of penetration similar to Type I.
Type III	Characterized by acoustically transparent zones, mixed with Type I reflections. Shown presence of subsurface faults, uplifted blocks and depressions.
Type IV	Distinct and sharp bottom echos with fewer sub-bottom reflectors. Most areas with this reflection type have an acoustically transparent zone above the deepest visible reflector. Depth of penetration is 15 m to 35 m.
Type V	Distinct sharp bottom echos with no apparent sub-bottom reflectors.
Type VI	Indistinct and semi-prolonged initial bottom echo with faint sub-bottoms. Semi-prolonged image due to a continuous and fuzzy echo from the surface to depth of about 12 m. Depth of penetration is about 15 m to 25 m.
Type VII	Indistinct, semi-prolonged initial bottom echos with 'mushy' or intermittent sub-bottoms, alternate occasionally with

prolonged bottom echos with no sub-bottom.

Type VIII — Indistinct, prolonged, bottom echo with no sub-bottom. All sound energy is reflected from upper few meters of the sediments.

Type I sediments consist primarily of terrigenous clay (lutite) laminated with carbonate. Foraminiferal sand parallels carbonate content, varying from 1% to 11% in carbonate rich layers. Differences between Types I, II and III are mainly due to morphological differences on the ocean floor.

Type IV reflections are associated with foraminiferal silty clay. Most samples collected for this type are nearly completely homogeneous in structure. Sediments consist mainly of terrigenous clay with carbonate content of about 10%.

Type VI sediments consist chiefly of carbonate silt, with considerable carbonate sand and clay. 10 cm to 70 cm thick beds of fine to coarse, muddy shells are present.

Type VII(a) have sediments of muddy, calcareous sands corresponding to fine sand or coarse silt. Type VII(b) sediments are medium to fine sand, usually of quartzose, with less than 25% carbonate present. Type VII(c) sediments are gravelly, coarse sand, made from mainly algal debris with some shell and minor quartz.

Type VIII sediments are gravelly, coarse to medium algal

sand with secondary amounts of shell and foraminiferal.

Tables 4.2 to 4.4 give the physical and acoustic properties of various reflection types, as measured in the laboratory.

Using either method discussed above, the type and characteristics of sub-bottom sediments can be estimated from acoustic records. The reflection type method of Addy et al. is probably the better method because visual distinction of reflection type is usually more accurate than obtainable from word descriptions of acoustic characteristics. From Table 4.2 one can obtain estimates of important physical properties of the various reflection types illustrated in Fig. 4.4.

4.3 Extrapolation of Boreholes with Acoustic Data

Borehole measurements are capable of defining earth strata precisely. However, boreholes are usually so sparsely spaced horizontally that it is very difficult to identify layers from one well site to the next.

Acoustical methods sample the earth relatively well horizontally but vertical resolution is limited by the band-width of the received acoustic signal. Widness (1973) ascribed this maximum bandwidth to be one-eight cycle of the dominant frequency. In practice, because of noise and other environmental factors, such resolution is rarely achieved. However, the seismic response is sensitive to lateral change even below the Widness limit.

Reflection Types	R_v[1]	Bottom Loss[3]	Rp[2]	Bottom Loss[3]
Type I	0.15	16.5	0.15	16.5
Type IV	0.15	16.5	0.15	16.5
Type VI	0.20	14.0	0.21	13.5
Type VII	0.26 (one core)	11.7	0.25	12.0
Type VIII	0.24	12.4	0.24	12.4

[1] R_v (Reflection coefficient) = $\frac{Vsρs - Vwρw}{Vsρs + Vwρw}$, where Vs, Vw, ρs and ρw are compressional wave velocities and densities in the upper 2 meters of the sediment column and in the bottom water.

[2] Rp = reflection coefficient as determined from porosity[7] (Rp = 0.589 - 0.59P).

[3] Bottom loss in dB = $-20 \log_{10} R$.

Table 4.3 Reflection coefficient & bottom losses at normal incidence in areas of various reflection types.

Reflection Types	Attenuation in dB/m[1] derived from mean grain size	Attenuation in dB/m[1] derived from mean porosity
Type I	2.1	3.4
Type IV	2.6	3.6
Type VI	4.3	7.3
Type VII a	31.3	22.9
VII b	21.4	26.2
VII c	20.2	8.9
Type VIII	20.6	17.2

[1] Attenuation in dB/m for the upper 2 m of sediment has been calculated from empirical relationships between attenuation and mean grain size, and attenuation and mean porosity.[4]

Table 4.4 Attenuation of compressional waves in the sediments of areas of various reflection types.

Combination of acoustic data and borehole data is attractive because of their complementary nature. Acoustic data act as transfer functions for the borehole logs in evaluating lateral change between adjacent boreholes. The acoustic trace corresponding to the borehole location is the pilot signal. Seismic responses to the same layers away from the borehole are compared with the pilot signal by statistical methods such as least squares, pattern recognition, maximum entropy, etc. The borehole data are extrapolated along the seismic section with the seismic data determining the applicability of the logs at each location.

Figure 4.5 shows the soil conditions as obtained with acoustical profiling at a site in the Gulf of Alaska. Table 4.5 shows the corresponding borehole profile. The double reflections at the sea floor and at 25 ft penetration are due to the source signature and are not geologic in nature. The boundary at 25 ft is marked by large amplitude reflection as would be expected from the lower porosity and higher density in the gravel as compared to the soft clay above it. The gravel-sandy clay interface at 37 ft penetration is more difficult to discern. It is recognized because it marks an unconformity with the Yakataga Formation near the left hand edge of the figure.

Figure 4.6 gives the acoustical profile at a Gulf of Mexico site. Table 4.6 shows the borehole profile. The silt and clay seams within the upper sand layer probably account

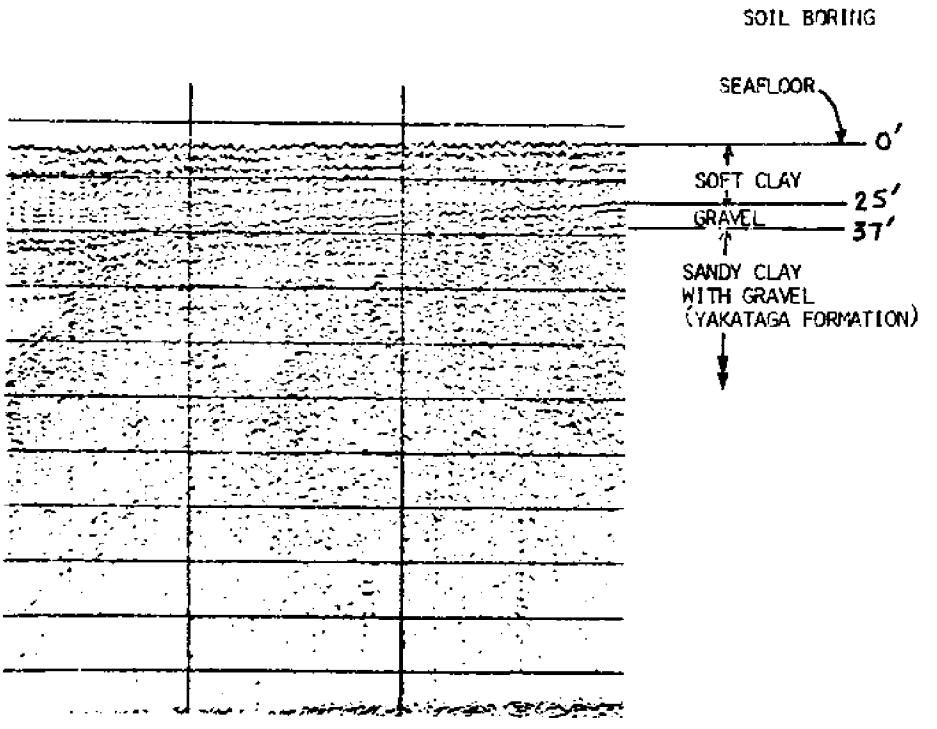

Figure 4.5 Seismic profile of Gulf of Alaska Site.

	Water Depth = 251 ft	
	Penetration Below Seafloor = 130 ft	
Stratum I	0-25 ft	Very Soft Gray Clay with Silt Seams
		Undrained Shear Strength, Average = 0.15 tons/ft^2 (3 Samples)
		Range = .04 to 0.32 tons/ft^2
		Typical Plasticity Values
		LL = 40, PL = 18
		w = 50%
Stratum II	25-37 ft	Coarse Sand and Gravel with Cobbles
		Poor Recoveries
Stratum III	37-130 ft	Very Stiff Gray Silty and Sandy Clay with Gravel
		Undrained Shear Strength, Average = 2.5 tons/ft^2
		Range = 1.1 to 5 tons/ft^2
		Typical Plasticity Values
		LL = 25, PL = 15
		w = 16%

Table 4.5 Summary of soil properties of Gulf of Alaska Site.

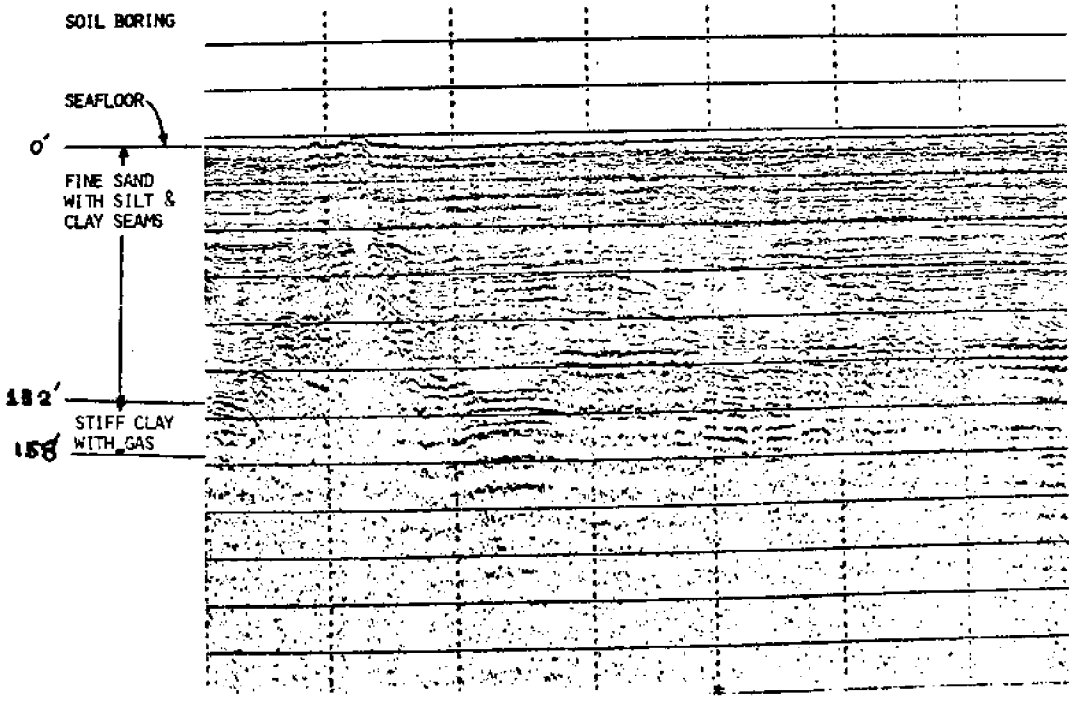

Figure 4.6 Seismic profile of Gulf of Mexico Site

	Water Depth = 332 ft	
	Penetration Below Seafloor = 450 ft	
Stratum I	0-132 ft	Medium Gray Silty Fine Sand, with Silt and Clay Seams, Shell Fragments
Stratum II	132-158 ft	Stiff Light Gray Clay with Gas
		Undrained Shear Strength, Average = 0.6 tons/ft^2
		Range = 0.25 to 0.76 tons/ft^2 (6 Samples)
Stratum III	158-178 ft	Medium Gray Sandy Silt
Stratum IV	178-238 ft	Stiff Medium Gray Clay with Silt Partings and Seams

Table 4.6 Summary of soil properties of Gulf of Mexico Site.

for the numerous horizontal reflections, while those areas with an apparent lack of reflections (below 150 ft) probably represent zones of homogeneous fine sand. The fine sand-stiff clay boundary at 132 ft is clearly discernable as an interface of large amplitude reflections. The presence of gas in the clay increases the acoustic contrast across this interface.

5. Mapping From Parallel Traverse Lines

5.1 Introduction

The ability to obtain a complete picture of the subsurface is useful to the geologist, engineer and policy-maker. The geologist needs this information to understand geological processes and to determine mineral potential. The engineer needs this information to determine foundation strength and to predict the behavior of site formations under changing loads. The policy-maker needs this information to make decisions regarding land use and mineral leasing.

Generally, a complete picture of the subsurface is economically unobtainable. Such a picture requires massive data collection which is time-consuming, technology-constrained and expensive. As a result, subsurface maps are created from a limited data, and considerable effort has gone into the development of mapping techniques. These include among many others, nearest neighbor analysis, trend surface analysis and fourier analysis.

Probability theory and statistics are used in the present study to evaluate the accuracy of maps produced from point or line data. The term "mapping error" will be taken to mean the percent of the map area misclassified. Since in practice the true distribution of materials in the subsurface is generally unknown, surface maps of geological features have been used to generate data, and various mapping methods -- or

algorithms -- used to reconstruct an estimated map. The estimated map is then compared to the original map, and the mapping error is calculated. An analysis of the mapping error serves both to indicate the accuracy of various mapping techniques and also the gains of accuracy with increased sampling effort.

In this study the sample data consist of parallel lines simulating acoustic traverses on a horizontal plane. The spacing between lines is varied (thereby changing the number of known lines over the map region) to determine the variations in the estimated maps with changing spacings. Increasing the number of known lines over the entire region increases the accuracy of the estimated map. However the marginal value of each extra line decreases with increasing data. To make rational decisions regarding investments in data collection, it is necessary to quantify the error expected to arise from given amounts and patterns of data, and to estimate the reduction of error with the addition of more data. The relationship between mapping accuracy and degree of control is illustrated in Fig. 5.1 (Dahlberg, 1975).

The maps investigated in this study are taken to comprise two mutually exclusive and cumulatively exhaustic regions (i.e. 2-color maps). Examples of such maps are soil and geologic maps. Although the predicted map quality can be enhanced by augmenting the data base with geological theory, the examination here considers only spatial information. The

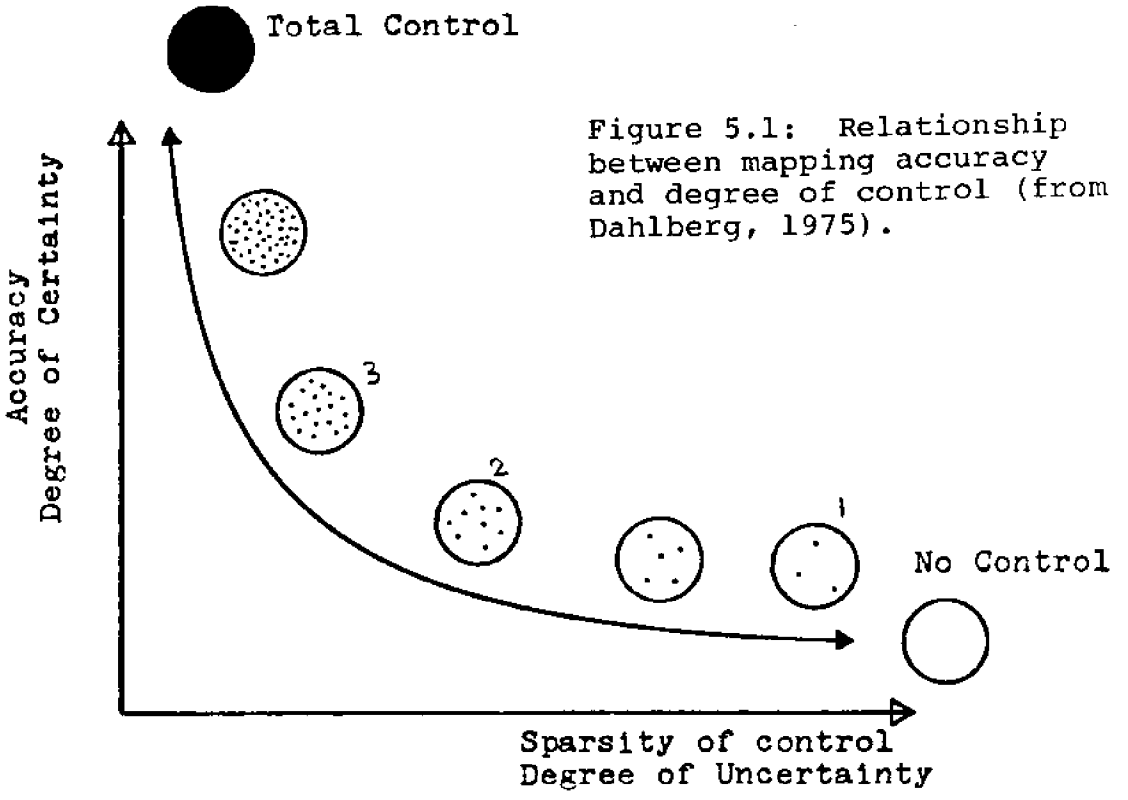

Figure 5.1: Relationship between mapping accuracy and degree of control (from Dahlberg, 1975).

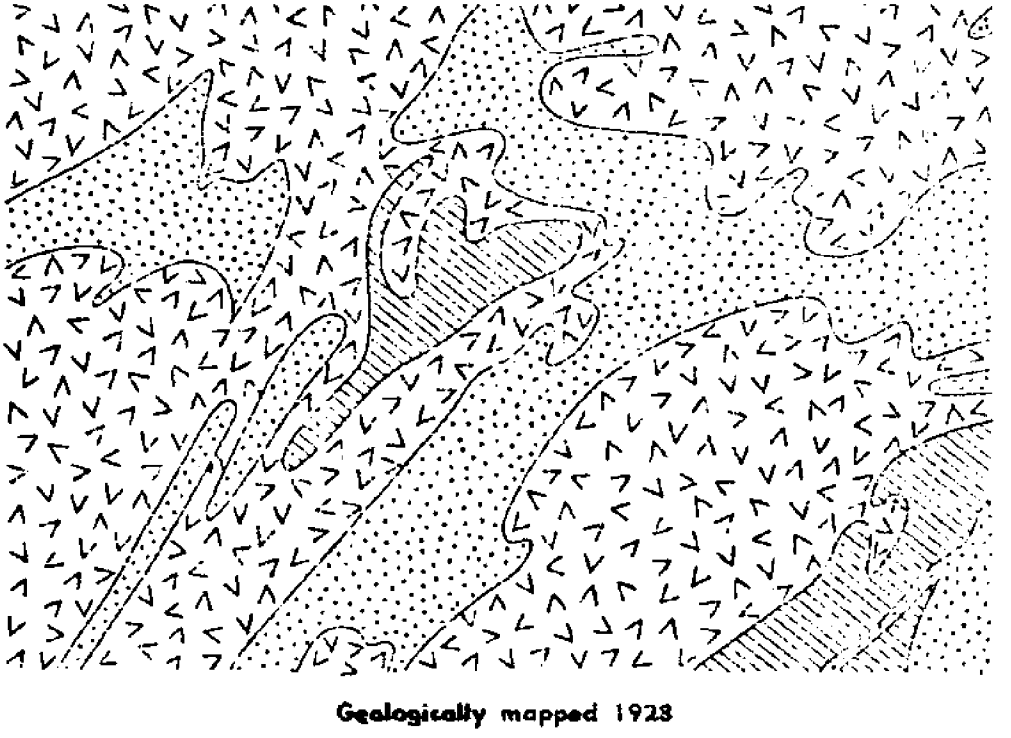

Figure 5.2(a) Change in geological map from using different trending theory (from Harrison, 1963).

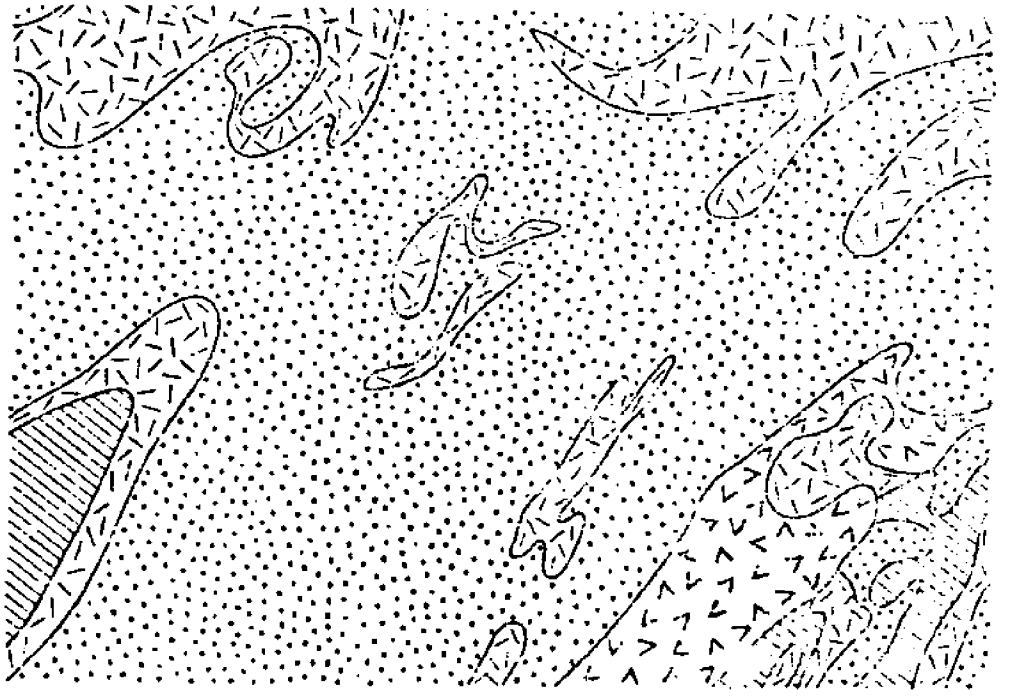

Geologically mapped 1958

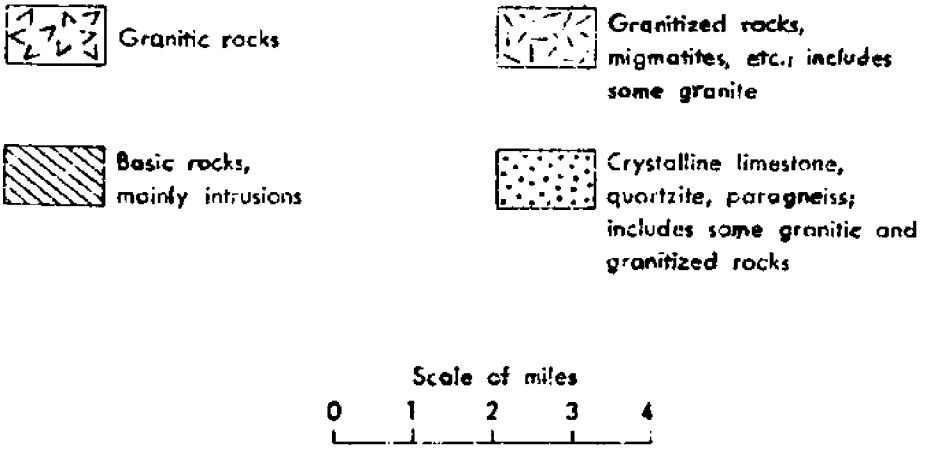

Figure 5.2(b) Change in geological map from using different trending theory (from Harrison, 1963).

influences of geological theory on map construction is clearly shown by Figs. 5.2(a) and 5.2(b), which have been reconstructed from the same data base using differing concepts of geological processes (Harrison, 1963).

This study first examines the prediction of map classifications at points of various distances from a known line and between two known lines. Using these results, a technique is developed to optimally contour a map from point or line data. Section 5.2 examines certain aspects of mapping theory, and presents previous results from Nucci (1979), based on discrete point data. Section 5.3 describes the mathematic model used to map from profile lines. Section 5.4 gives results of the applications.

5.2 Mapping From Discrete Points

Recent statistical and probabilistic analyses of map reconstruction from observed point data are discussed below. Subsection 5.2.1 examines mapping theory while Subsection 5.2.2 presents results of mapping from discrete points.

5.2.1 Mapping Theory

In geological mapping a generalized pattern is typically reconstructed from sample data by freehand or by the "nearest neighbor (NN) rule". The NN rule assigns an unobserved point to the same class as the nearest observed point. The accuracy of this reconstructed map is indicated by the value of the misclassification error, i.e. the ratio of the area misclassi-

fied to the total map area. Obviously the smaller the misclassification error, the more accurate the predicted map.

Two assumptions are made in estimating errors associated with the nearest neighbor rule:

(1) For all points in the mapped area, the probability of the observed point being of class i is the underlying spatial frequency of class i in the true map.

(2) For all pairs of points, S_1 and S_2, with a given distance between them, there is a definite probability function $P_{ij}(r)$, indicating the probability of S_2 being of a different class than S_1 for any distance r.

The expected error is then given by Switzer (1967):

$$\text{Expected Error} = P_i[1-n \int_{S_o} P_{ii}(|s|)] \, ds \qquad [5.1]$$

where P_i is the spatial frequency of class i;

n is the number of observations;

S is the distance between any sample point and its nearest observation point;

ds is the areal size of each sampling location;

P_{ii} is the probability of a point at distance r from an observation point of class i, is of class i

Points close to an observation point are likely to be of the same class as the observation point. As the spacing increases, the probability of an arbitrary point being of the same class i as the observation point decreases to the

frequency P_i. Therefore

$$P_{ii}(0) = 1.0 \tag{5.2}$$

$$P_{ii}(r) = P_i \quad \text{as } r \to \infty \tag{5.3}$$

Switzer (1967) suggested that a decay term of the form $e^{-\gamma r}$, where γ is the decay parameter, can be used to model this decay. The decay function is then described as,

$$P_{ii}(r) = P_i + (1-P_i)\, e^{-\gamma r} \tag{5.4}$$

This decay function, if interpreted in light of discrete random field theory, impies an exponential autocovariance function. For a two color map of major class i and minor class j, and with areas A_i and A_j respectively, the spatial frequency is denoted as the percentage of the total area occupied by each class, i.e.,

$$P_i = A_i/A \tag{5.5}$$

$$P_j = A_j/A \tag{5.6}$$

$$P_j + P_j = 1.0 \tag{5.7}$$

$$P_i \geq P_j \tag{5.8}$$

Equation (5.4) suggests that as the distance r between an unknown point and an observation point increases, the probability of the unknown point being of the same class i as the observation point decreases from 1.0 for r = 0 to P_i for large r, obtaining equations (5.2) and (5.3). Other variations

of equation (5.4) are

$$P_{ij}(r) = P_j(1-e^{-\gamma r}) \tag{5.9}$$

$$P_{ji}(r) = P_i(1-e^{-\gamma r}) \tag{5.10}$$

$$P_{jj}(r) = P_j + (1-P_j)\ e^{-\gamma r} \tag{5.11}$$

where $P_{ij}(r)$ is the probability of a point at distance r from an observation point of class i, is of class j. Figure 5.3 shows the characteristics of decay functions, equations (5.4), (5.9), (5.10) and (5.11). Note that P_{ii} and P_{ji}, P_{jj} and P_{ij} are non-intersecting functions, while P_{jj} and P_{ji} intersect at $r = r_c$ and probability = 0.5. For distances greater than r_c, the probability of the unknown point being of the major class is greater than the probability of it being of the minor class.

Decay parameters are influenced by size and general shape of the map pattern. Smaller individual bodies and uneven shape increase the value of this parameter. Two methods, direct and indirect, can be used to obtain an estimated value of γ. The direct method uses a finite number of data points and requires knowledge of the true map. The indirect method does not require a knowledge of the true map.

The direct method involves selecting sampling points on the map and drawing a series of concentrate circles about each point (Baecher, 1972, Fig. 5.4). For each circle, the

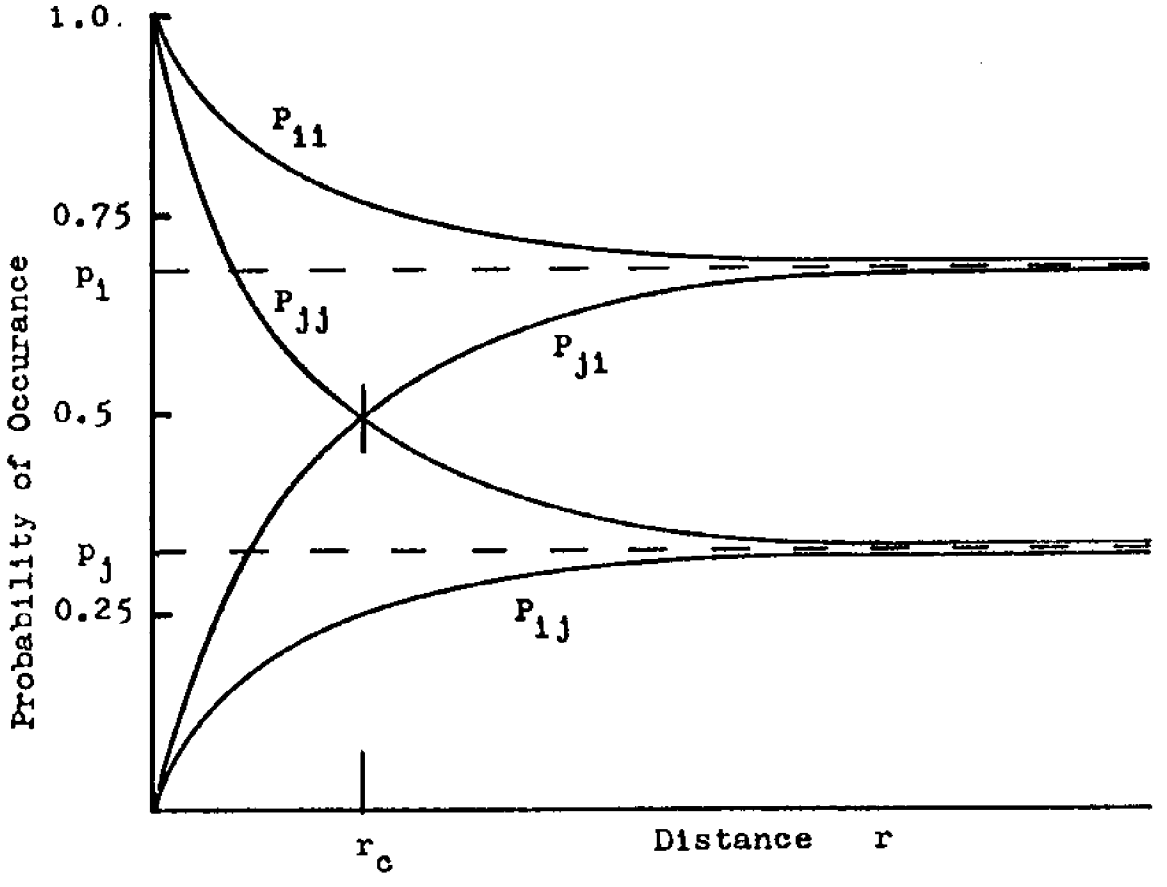

Figure 5.3 Probability Decay Functions (from Nucci, 1979)

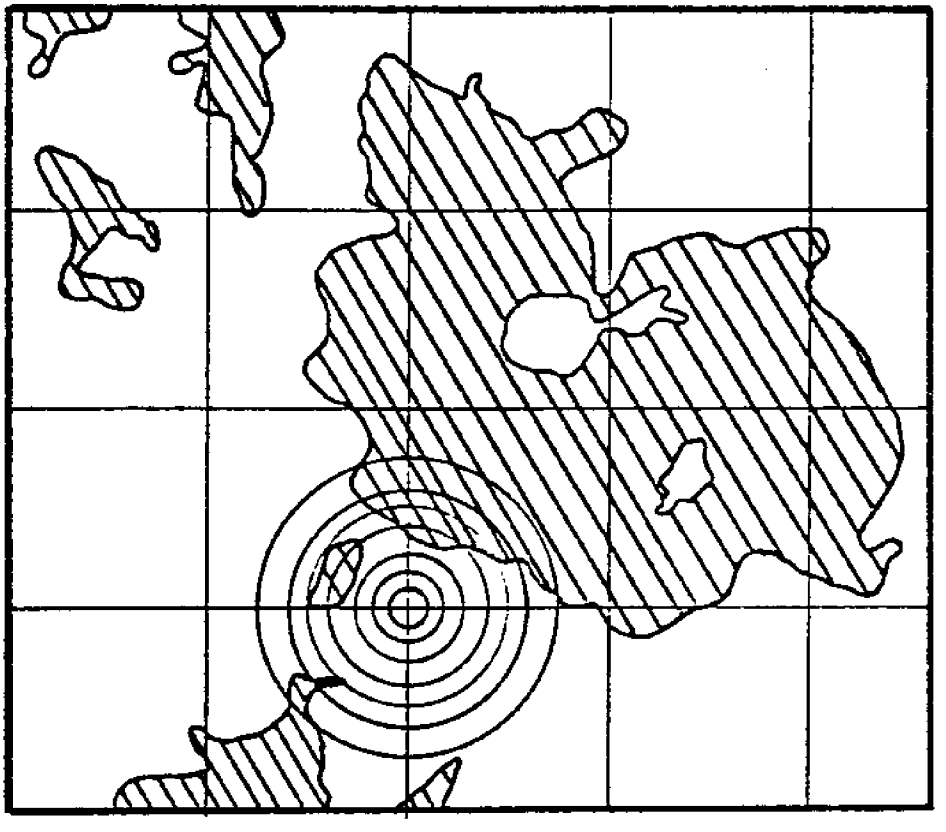

Figure 5.4 Direct Method of Evaluation of Decay Parameter

percentage of the circumference which intersects class i, is determined and a set of frequency distribution compiled for each radius r of the circles. Figure 5.5 shows a sample plot of frequency distribution against radius r. The value of γ can then be determined from equation (5.9). Similar plots can be made of $P_{ii}(r)$, $P_{ji}(r)$ and $P_{jj}(r)$ and the best value of γ can be obtained by regression.

The indirect method is based on statistical estimation using the finite number of observed data points. This is discussed by Nucci (1979).

5.2.2 Mapping from Discrete Points - Results (Nucci, 1979)

Nucci (1979) reconstructed maps from a number of geological regions using the nearest neighbor algorithm. Results from three of these maps are presented below. In Section 5.4, these results are compared to maps reconstructed using a new mapping technique (discussed in Section 5.3). These maps are:

Map 1 (Map 2 in Nucci): Engineering Geology of the Katalla Area, Alaska USGS Map I-308;

Map 2 (Map 3 in Nucci): Geology of the Bridgewater Quadrangle, Mass. USGS Map GQ-127;

Map 3 (Map 6 in Nucci): Pre-Quaternary Geology of the Brown's Mill Quadrangle, NJ, USGS Map GQ-264.

These maps were chosen because the regions are approximately of isotropic shape, so as to avoid any major trends. The

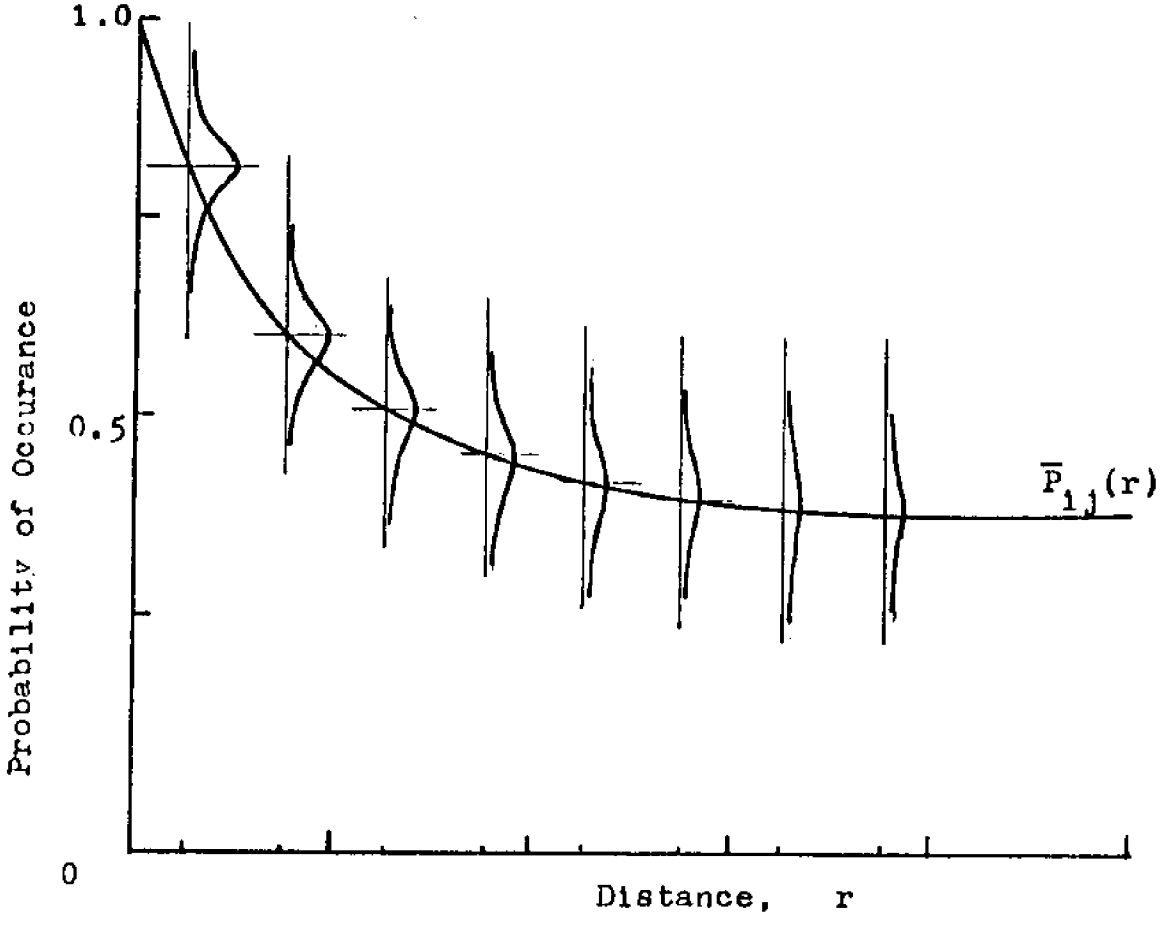

Figure 5.5 Direct Method Probability Decay Function

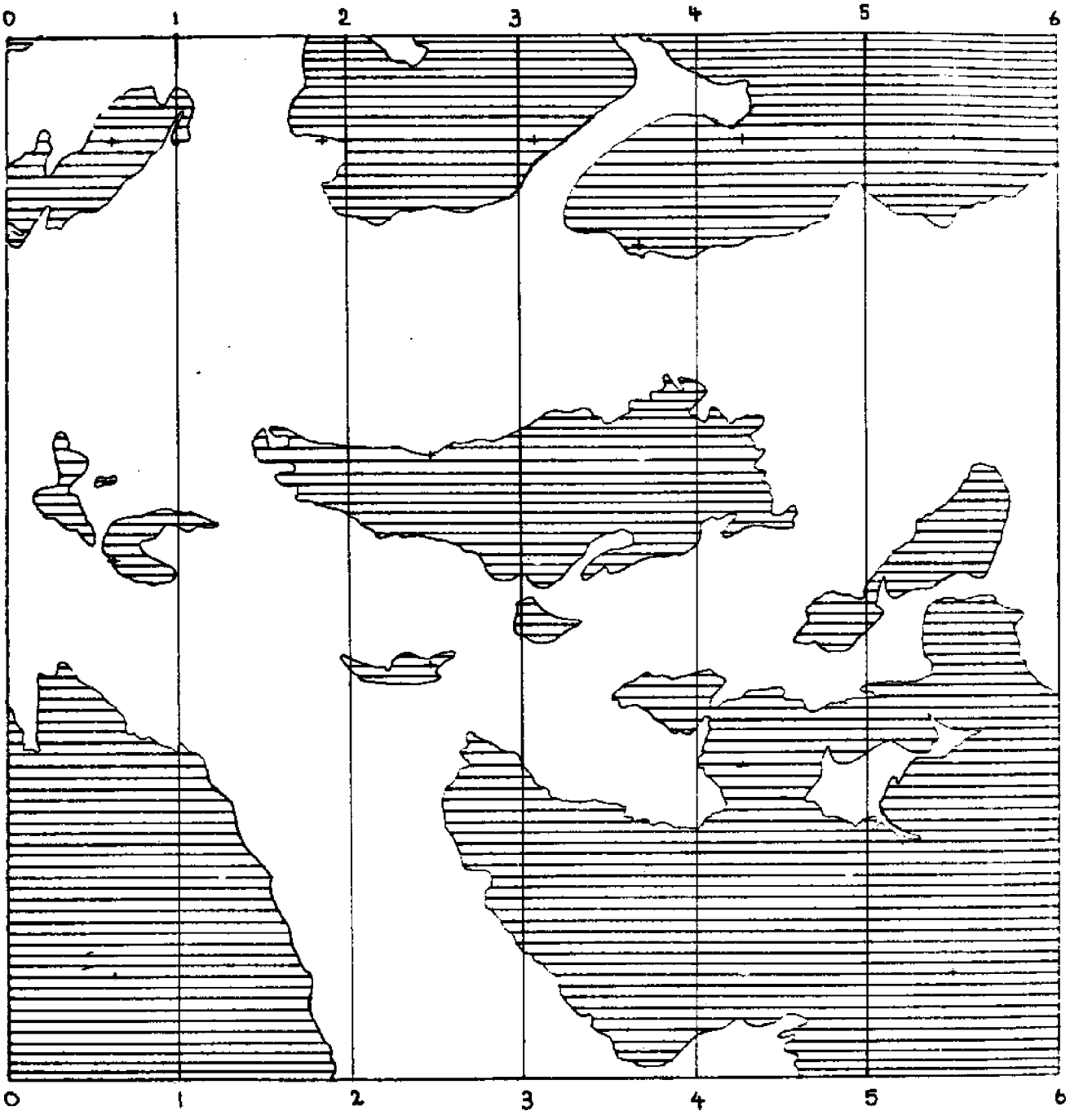

Figure 5.6 Map 1; showing lines 0-0, 1-1, 2-2, 3-3, 4-4, 5-5 & 6-6, spaced at 1/6 unit apart. δ= 15.15, p_1=0.46

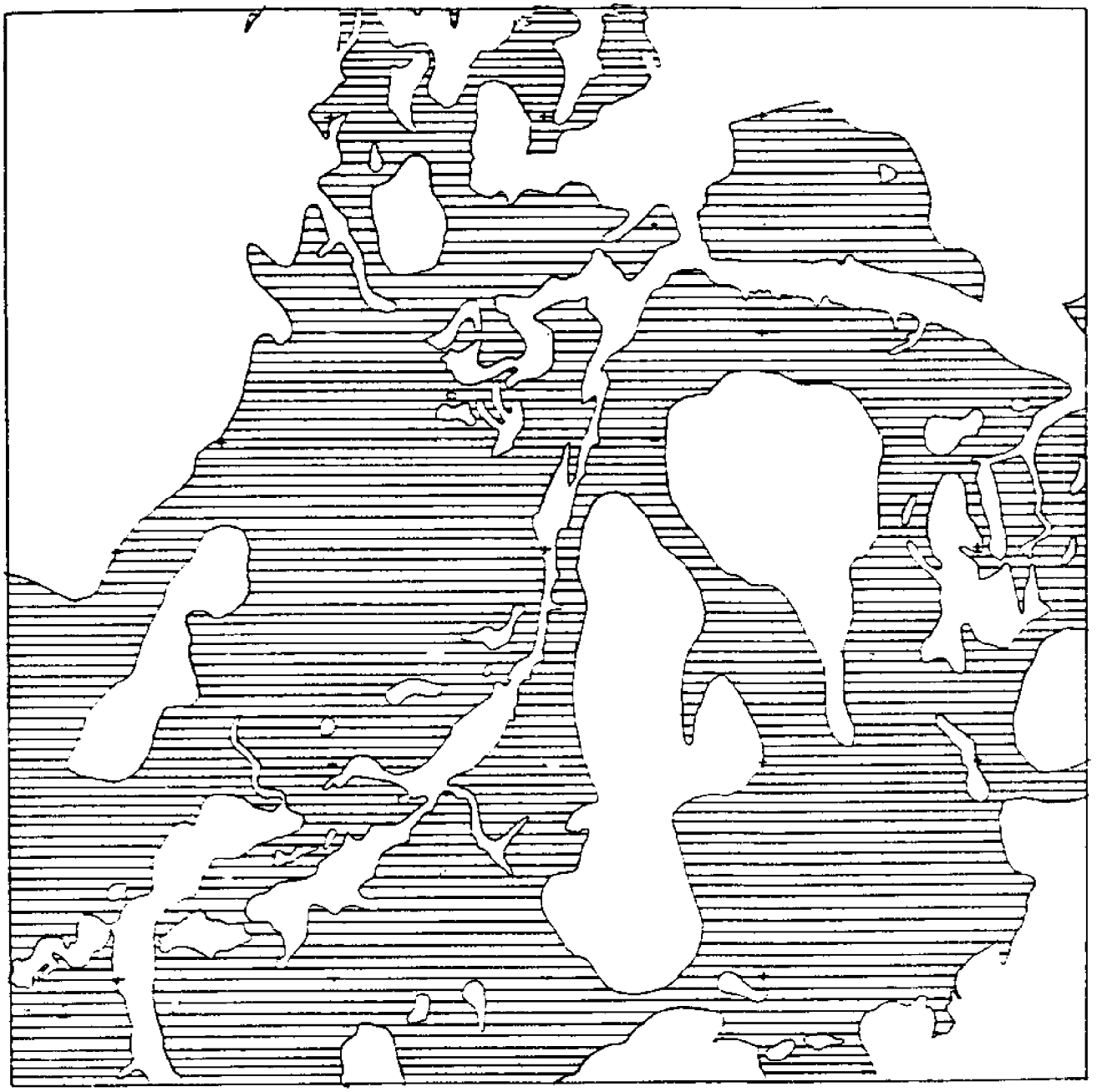

Figure 5.7 Map 2, γ = 12.41.

Figure 5.8 Map 3, γ = 8.88.

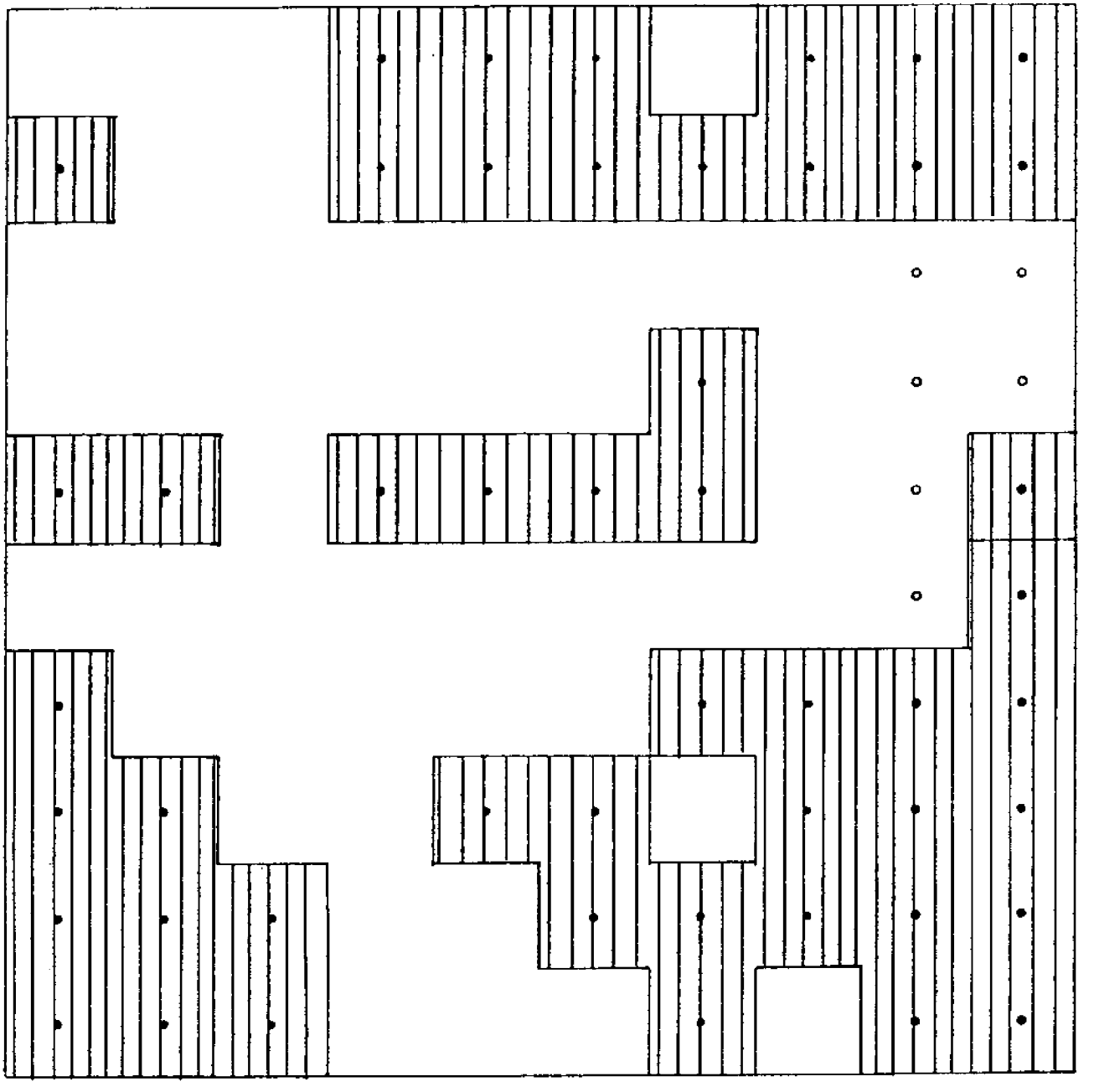

Figure 5.9 Estimated Map 1 for 10 x 10 gridded observations, Error = 13.6%.

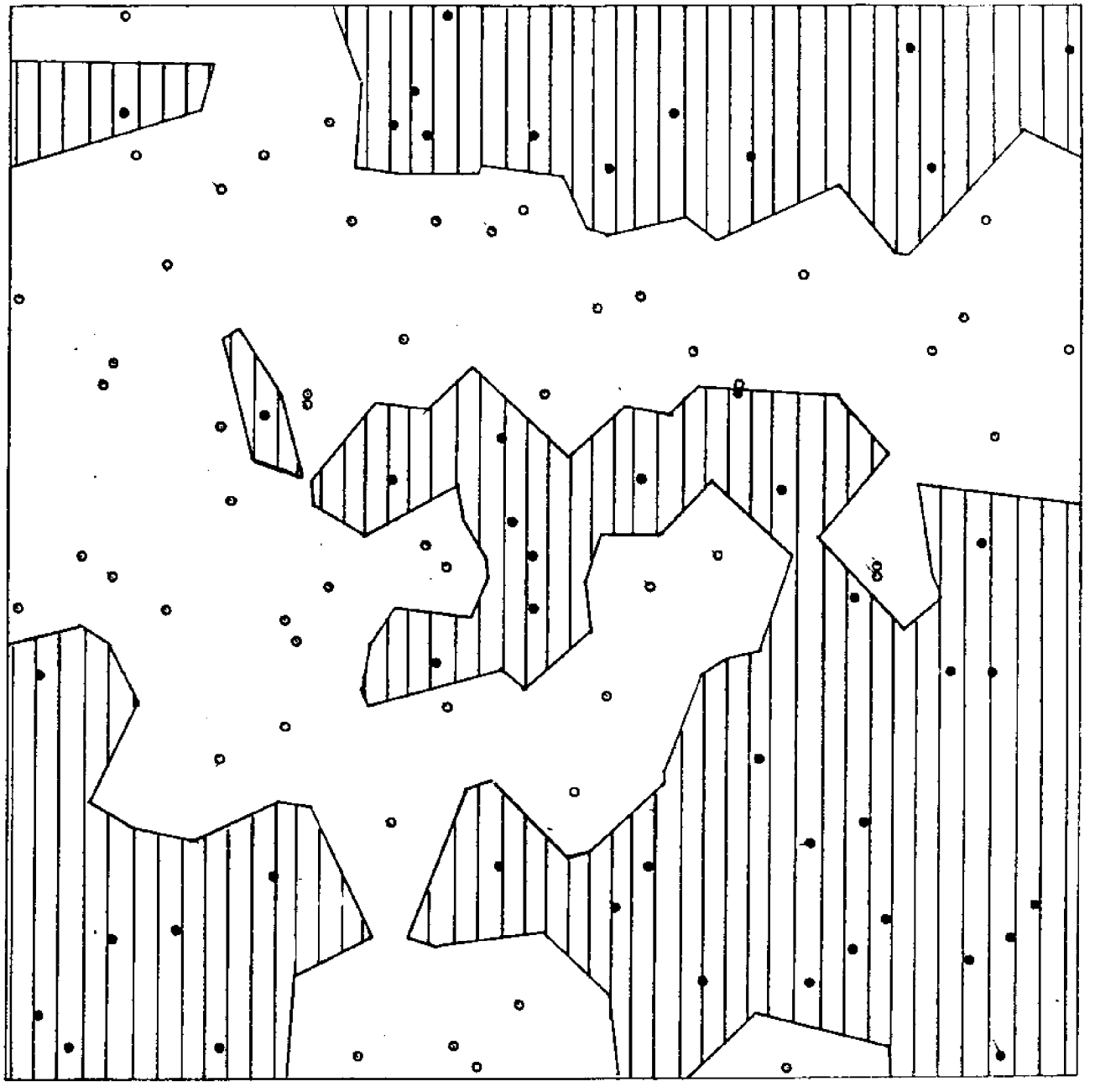

Figure 5.10 Estimated Map 1, 100 random observations, Error = 15.4%.

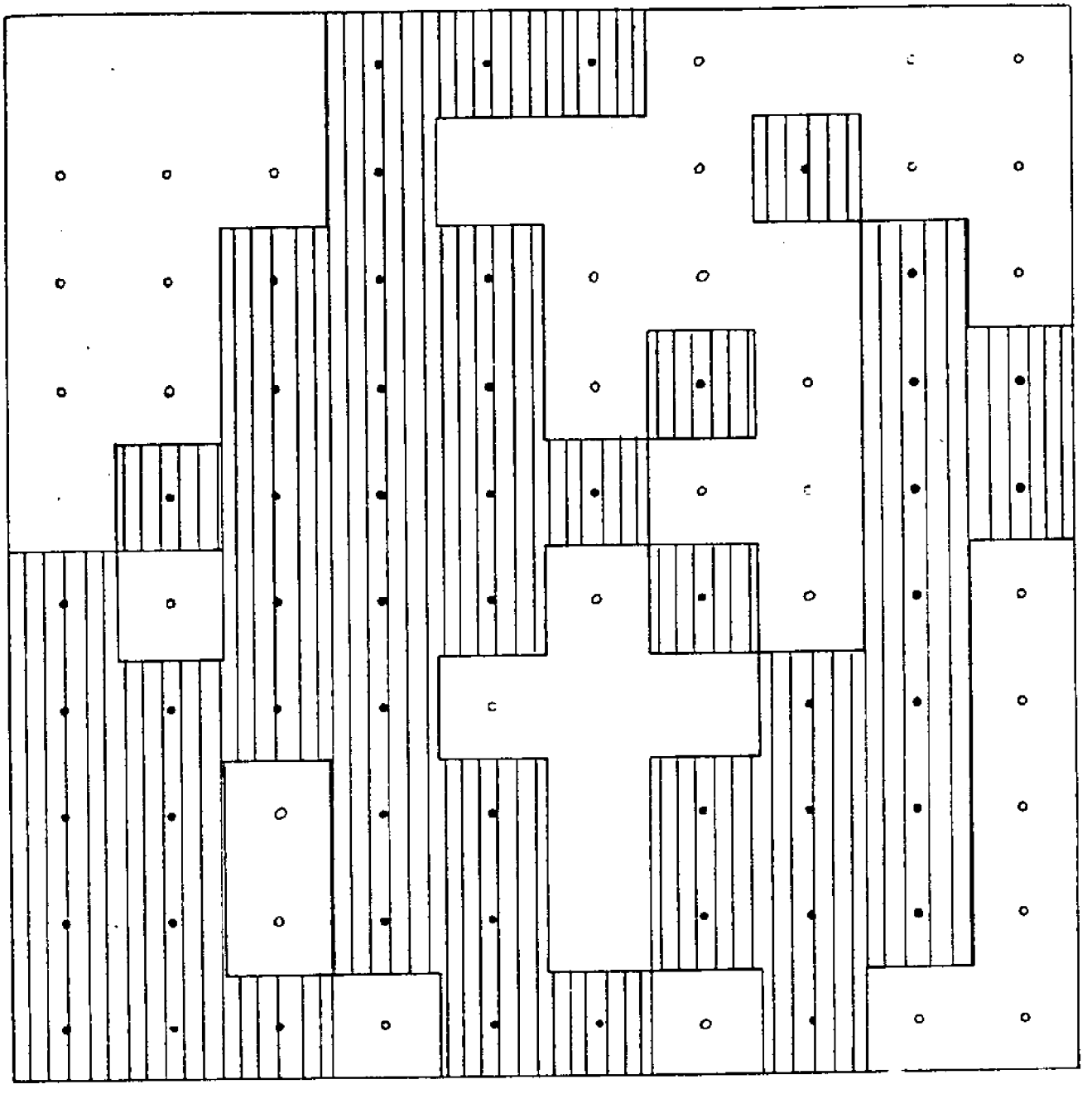

Figure 5.11 Estimated Map 2, 10 x 10 gridded observations, Error = 20.0%.

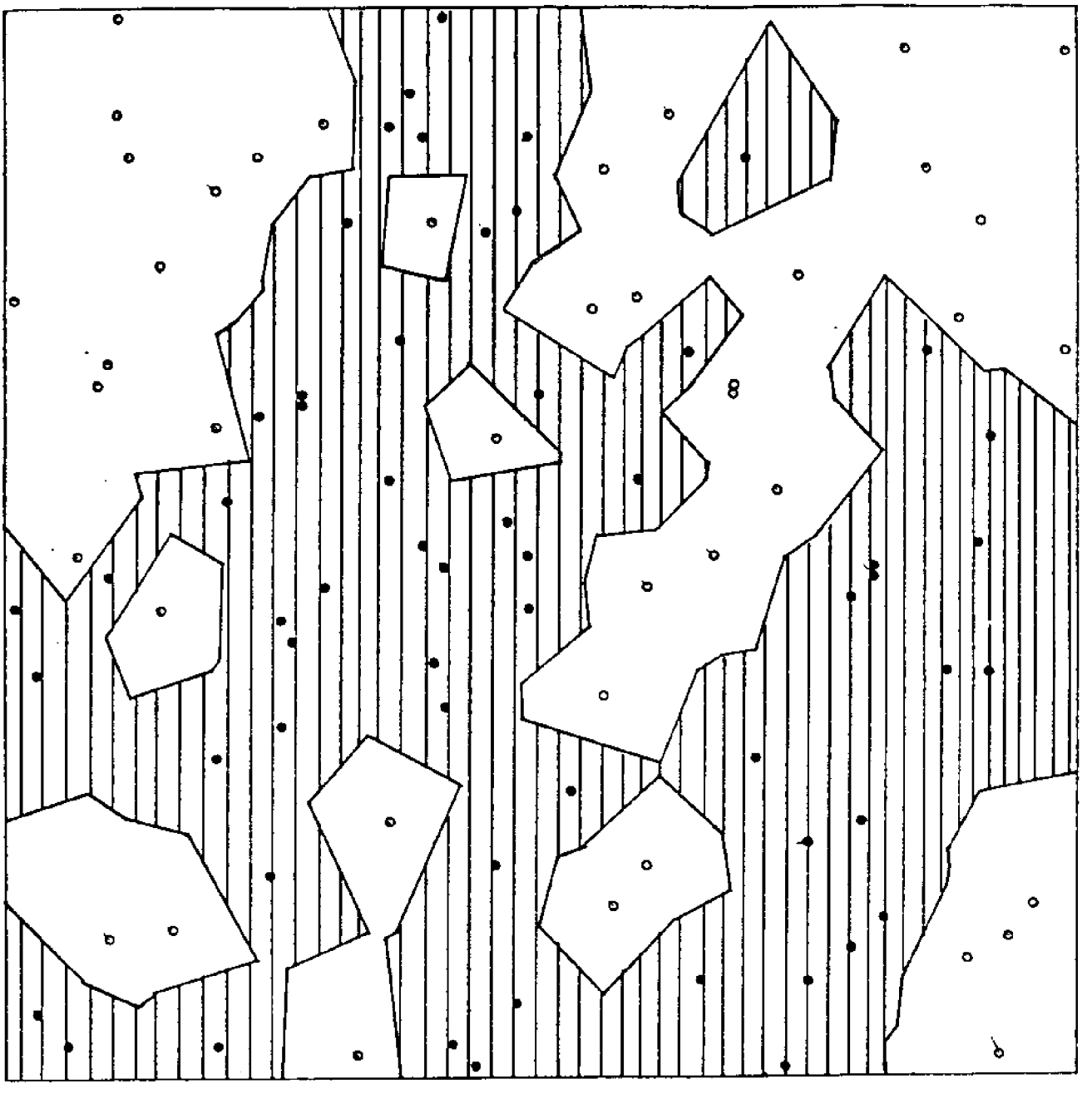

Figure 5.12 Estimated Map 2, 100 random observations, Error 17.8%.

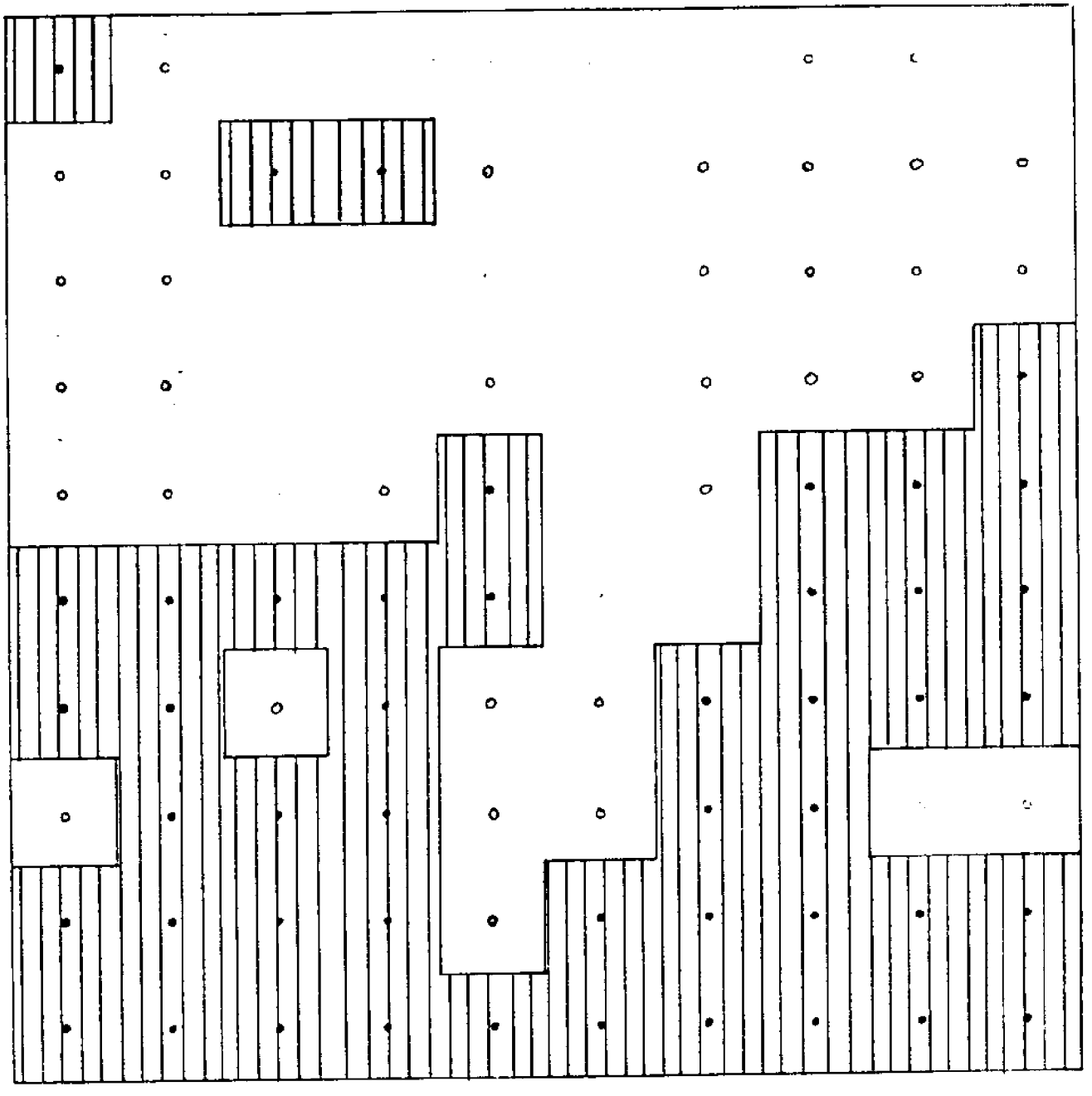

Figure 5.13 Estimated Map 3, 10 x 10 gridded observations, Error = 11.1%.

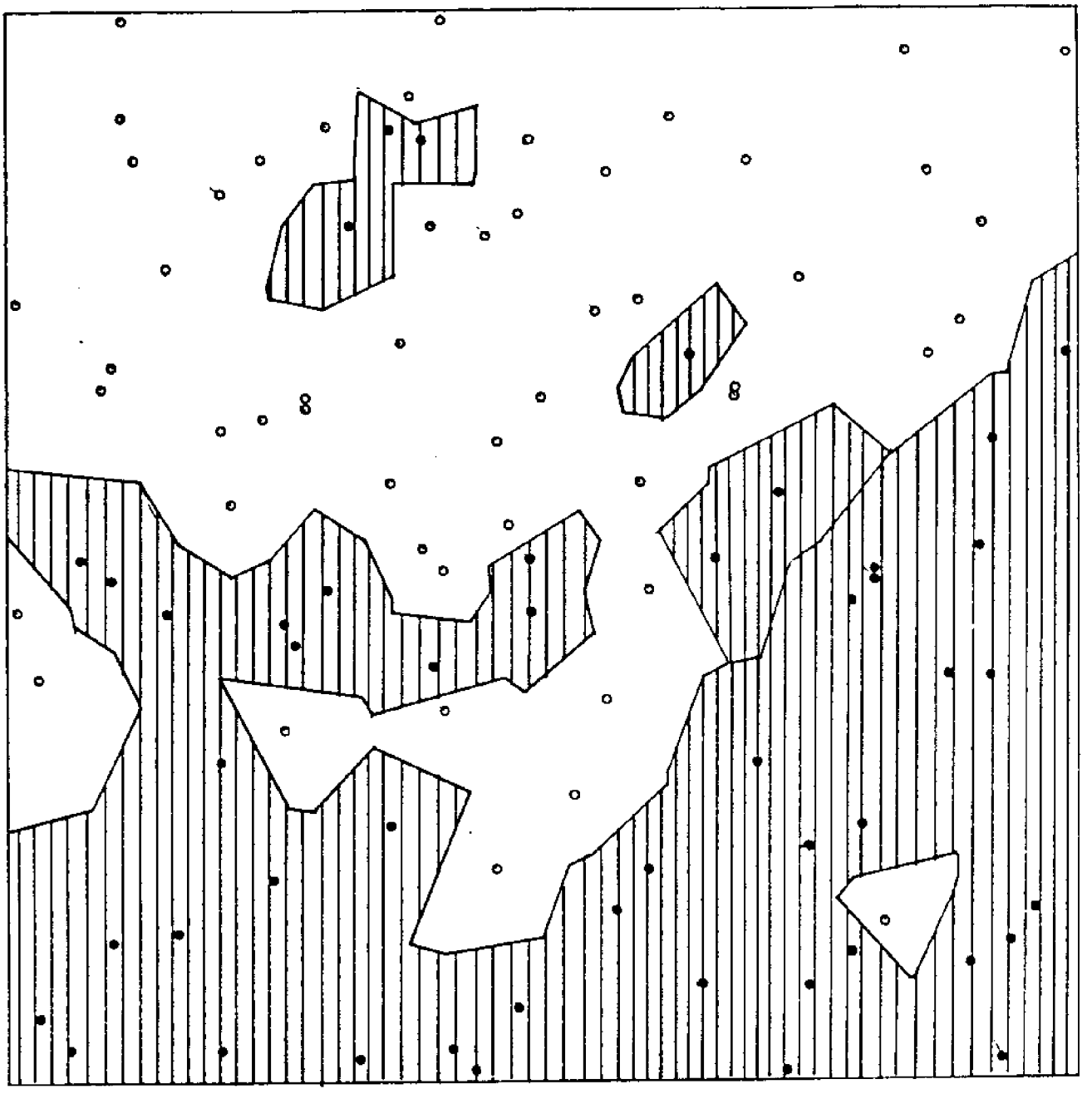

Figure 5.14 Estimated Map 3, 100 random observations, Error = 9.0%.

decay parameters were determined using the direct method to be

	Decay Parameter	90% Confidence Limits
Map 1	15.15	± 4.84
Map 2	12.41	± 2.70
Map 3	8.88	± 1.06

Map 1, Map 2 and Map 3, and their spatial frequencies and decay parameters are shown in Figures 5.6 to 5.8 respectively. The reconstructed maps were derived from discrete random points and from points arranged in a square grid.

The results of these analyses are presented in Figures 5.9 to 5.14 for 100 random observation points and for 10 x 10 gridded observations. Only results from the 100 observations and 10 x 10 gridded points are presented because these form the largest size of Nucci's analyses and are also the most accurate.

5.3 The Mathematical Model

This section describes the derivation of the mathematical model for predicting states of unobserved location between two parallel profile lines. Subsection 5.3.1 describes the notation, subsection 5.3.2 describes the basic equations used in this derivation, subsection 5.3.3 describes the derivation of the model and subsection 5.3.4 presents the computer program describing the model.

5.3.1 Notation

A two color map of isotropic regions i and j is assumed, with x_1, x_2 and x_3 three arbitrary points on the map. Event x_{1_i} is the event of x_1 being of state i, x_{1_j} is the event of x_1 being of state j. Similar definitions are made for x_2 and x_3.

5.3.2 Basic Equations

Two points (x_1, x_2)

Of the spatial frequency of region i is P, and the points x_1 and x_2 are distributed in a Poisson manner, then the assumed prior probability is

$$P(x_{1_i}) = P \tag{5.12}$$

$$P(x_{1_j}) = q = 1-P \tag{5.13}$$

The probability that a point, say x_2 is of state i, given that x_1 is of state i is given by

$$P(x_{2_i}/x_{1_i}) = P + qe^{-\gamma r_{12}}$$

where r_{12} is the linear distance of x_2 from x_1 on the map. The probability of x_1 and x_2 being both of state i is then determined,

$$P(x_{1_i},x_{2_i}) = P(x_{1_i})\ P(x_{2_i}/x_{1_i}) = P(P+q\ e^{-\gamma r_{12}}) \tag{5.14}$$

or

$$= P(P+q\ e^{-\frac{\rho_2 r_{12}}{\pi}}) \tag{5.15}$$

where $\rho = \frac{\pi\gamma}{2}$

Similarly,

$$P(x_{1_i},x_{2_j}) = P(x_{1_i})\ P(x_{2_j}/x_{1_i})$$

$$= P[1-P(x_{2_i}/x_{1_i})]$$

$$= Pq(1 - e^{-\frac{\rho_2 r_{12}}{\pi}}) \tag{5.16}$$

$$P(x_{1_j},x_{2_i}) = Pq(1 - e^{-\frac{\rho_2 r_{12}}{\pi}}) \tag{5.17}$$

$$P(x_{1_j},x_{2_j}) = q(q + Pe^{-\frac{\rho_2 r_{12}}{\pi}}) \tag{5.18}$$

Three Points (x_1, x_2, x_3)

A triangle with vertices at x_1, x_2 and x_3, lengths r_{12}, r_2 and r_1, is considered, as indicated below

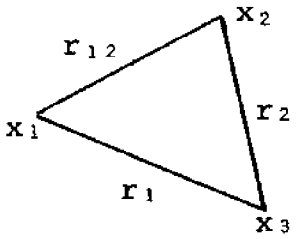

r* is the mean apparent diameter (i.e. mean 1-D projection) of the triangle and can be defined as a particular case of Minkowski's formula in the plane (Matheron, 1971, page 42), i.e.

$$r^* = (r_1 + r_2 + r_{12})/\pi \tag{5.19}$$

The probability that all three points (x_1, x_2, x_3) belong to the same class is derived by Veneziano (personal communication) as

$$P(X_{1_i},X_{2_i},X_{3_i}) = P^3 + (P-3p^2+2P^3)\, e^{-\rho r^*} + (P^2-P^3) \sum_{r=r_1,r_2,r_{12}} e^{-\frac{\rho_2 r}{\pi}} \qquad (5.20)$$

$$P(x_{1_j},x_{2_j},x_{3_j}) = q^3 + (q-3q^2+2q^3)\, e^{-\rho r^*} + (q^2-q^3) \sum_{r=r_1,r_2,r_{12}} e^{-\frac{\rho_2 r}{\pi}} \qquad (5.21)$$

5.3.3 Model Derivation

Using equations (5.12) to (5.21) derived above, the basic elements of the model can be established. In acoustic mapping we are given acoustic profile lines of finite length. These lines are usually parallel to each other and provide only a 1-dimensional vertical profile of the subsurface. In this derivation, the profile line is taken to consist of numerous equal segments and traces of regions i and j occur on the line (see figure below). The point y is

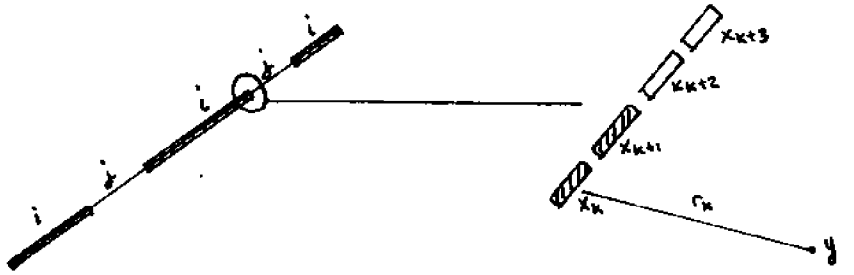

unknown and the model attempts to determine the state (region) of y given one profile line and then given two profile lines, one on either side of y.

Bayesian theory forms the structure of this model, i.e. the purpose is to determine the posterior probability of the

point y being of state i or of state j. The posterior probability of y is given by

$$P[y_i/\text{data (i.e. line)}] = \frac{P(y_i)\ P(\text{data}/y_i)}{P(\text{data})} \qquad (5.22)$$

$$\text{or } P(y_i/x_1,x_2,\ldots x_n) = \frac{P(y_i)\ L(x_1,x_2,\ldots x_n/y_i)}{p(y_i)\ L(x_1,\ldots x_n/y_i)+P(y_j)\ L(x_1,\ldots x_n/y_j)} \qquad (5.23)$$

$$P'(y_i) + P'(y_j) = 1.0 \qquad (5.24)$$

where $L(\text{data}/y_i)$ is the likelihood function of the line given that y is of state i

$P'(y_i) = P(y_i/\text{data})$ i.e. posterior probability of y_i

$P'(y_j) = P(y_j/\text{data})$ i.e. posterior probability of y_j

$P(y_i)$ and $P(y_j)$ are the prior probabilities of states i and j, which is the spatial frequency of i and j on the known line (s), $P(y_i) = 1 - P(y_j)$.

The unknown factor in Equation (5.23) is the likelihood function which will be derived below.

$$L(\text{data}/y_i) = P(x_1/x_2,\ \ldots,\ x_n,y_i)\ P(x_2/x_3,\ldots,x_n,y_i) \ldots P(x_n/y_i) \qquad (5.25)$$

To solve the term $P(x_1/x_2,\ldots,x_n,y_i)$ and other similar terms the segments that compose the known line are assumed to exhibit Markov dependence. This is a major assumption and provides

a solution of equation (5.25) although it approximates the solution a great deal. Hence

$$L(\text{data}/y_i) = P(x_1/x_2,y_i)\ P(X_2/x_3,y_i)\ldots P(x_{n-1}/x_n,y_i)\ P(x_n/y_i) \quad (5.26)$$

$$L(\text{data}/y_j) = P(x_1/x_2,y_j)\ P(x_2/x_3,y_j)\ldots P(x_{n-1}/x_n,y_j)\ P(x_n/y_j) \quad (5.27)$$

or in logarithm form,

$$\text{Log}[L(\text{data}/y_i)] = \text{Log}(P(x_1/x_2,y_i)] + \text{Log}[P(x_2/x_3,y_i)] + \ldots \text{Log}[P(x_n/y_i)] \quad (5.28)$$

$$\text{Log}(L(\text{data}/y_j)] = \text{Log}[P(x_1/x_2,y_j)] + \text{Log}[P(x_2/x_3,y_j)] + \ldots \text{Log}[P(x_n/y_j)] \quad (5.29)$$

To solve equations (5.28) and (5.29), the eight conditions illustrated below have to be considered.

States

x_i	x_{i+1}	Y
i	i	i
i	j	i
j	i	i
j	j	i
i	i	j
i	j	j
j	i	j
j	j	j

Therefore the following set of equations will have to be solved,

$$P(x_{ki}/x_{k+1}{}^{i},y_i) \tag{5.30}$$

$$P(x_{kj}/x_{k+1}{}^{i},y_i) \tag{5.31}$$

$$P(x_{ki}/x_{k+1}{}^{i},y_j) \tag{5.32}$$

$$P(x_{kj}/x_{k+1}{}^{i},y_j) \tag{5.33}$$

$$P(x_{ki}/x_{k+1}{}^{j},y_i) \tag{5.34}$$

$$P(x_{kj}/x_{k+1}{}^{j},y_i) \tag{5.35}$$

$$P(x_{ki}/x_{k+1}{}^{j},y_j) \tag{5.36}$$

$$P(X_{kj}/x_{k+1}{}^{j},y_i) \tag{5.37}$$

For computation simplicity, allow k=1, k+1 = 2, then

Equation (5.30)

$$P(x_{1_i}/x_{2_i},y_i) = \frac{P(x_{1_i},x_{2_i},y_i)}{P(x_{2_i},y_i)} = \frac{\text{Equation (5.20)}}{P(P+q\ e^{-\frac{\rho 2r_1}{\pi}})}$$

Equation (5.31)

$$P(x_{1_j}/x_{2_i},y_i) = 1 - \text{equation (5.30)}$$

Equation 5.32)

$$P(x_{1_i}/x_{2_i},y_j) = \frac{P(x_{1_i},x_{2_i},y_j)}{P(x_{2_i},y_j)} = \frac{P(x_{1_i},x_{2_i},y_j)}{pq(1 - e^{-\frac{\rho 2r_1}{\pi}})}$$

where $P(x_{1_i},x_{2_i},y_j) = P(y_j/x_{1_i},x_{2_i})\ P(x_{1_i},x_{2_i})$

$$= \left[1 - \frac{P\ (x_{1_i}, x_{2_i}, y_i)}{P(x_{1_i}, x_{2_i})}\right] P(x_{1_i}, x_{2_i})$$

$$= P(x_{1_i}, x_{2_i}) - P(x_{1_i}, x_{2_i}, y_i)$$

$$= (5.15) - (5.20)$$

Equation (5.33)

$$P(x_{1_j}/x_{2_i}, y_j) = 1 - (5.32)$$

Equation (5.34)

$$P(x_{1_i}/x_{2_j}, y_i) = \frac{P\ (x_{1_i}, x_{2_j}, y_i)}{pq(1 - e^{-\frac{\rho 2 r_1}{\pi}})}$$

where $P(x_{1_i}, x_{2_j}, y_i) = P(x_{2_j}/x_{1_i}, y_i)\ P(x_{1_i}, y_i)$

$$= [1 - P(x_{2_i}/x_{1_i}, y_i)]\ P(x_{1_i}, y_i)$$

$$= P(x_{1_i}, y_i) - P(x_{1_i}, x_{2_i}, y_i)$$

$$= P(p + q\ e^{-\rho 2 r_1/\pi}) - (5.20)$$

Equation (5.35)

$$P(x_{1_j}/x_{2_j}, y_i) = 1 - (5.34)$$

Equation (5.37)

$$P(x_{1_j}/x_{2_j}, y_j) = \frac{P(x_{1_j}, x_{2_j}, y_i)}{P(X_{2_j}, y_j)} = \frac{(5.21)}{q(q + p\ e^{-\frac{\rho 2 r_2}{\pi}}}$$

Equation (5.36)

$$P(x_{1_i}/x_{2_j}, y_j) = 1 - \quad (5.37)$$

5.3.4 The Computer Model

The acoustic profiling line is divided into 66 segments (the choice of 66 is for programming convenience). Initially the reliability of estimating the state of the point y, given only one line, is examined, then in a modified program, the case of two known lines is studied. The line(s) and the map have unit dimensions. For states i and j, the identifications 1 and 0 have been substituted.

5.3.4.1 Single Line

Definitions

GAMA = $\gamma = 2\rho/\pi$

S is the distance perpendicular to line, over which the model is to be extrapolated;

TL is the length of the known line (i.e. = 1 unit);

P is the prior probability of state 1;

[M(I), I = 1,66] denotes the states of the 66 segments along the line. If M(I) =1, then the segment J is of state 1; if M(J) = 0, then the segment I is of state O.

(x,y) denotes the unknown point;

x is the distance parallel to line, y is the distance perpendicular to the line (see Fig. 5.15).

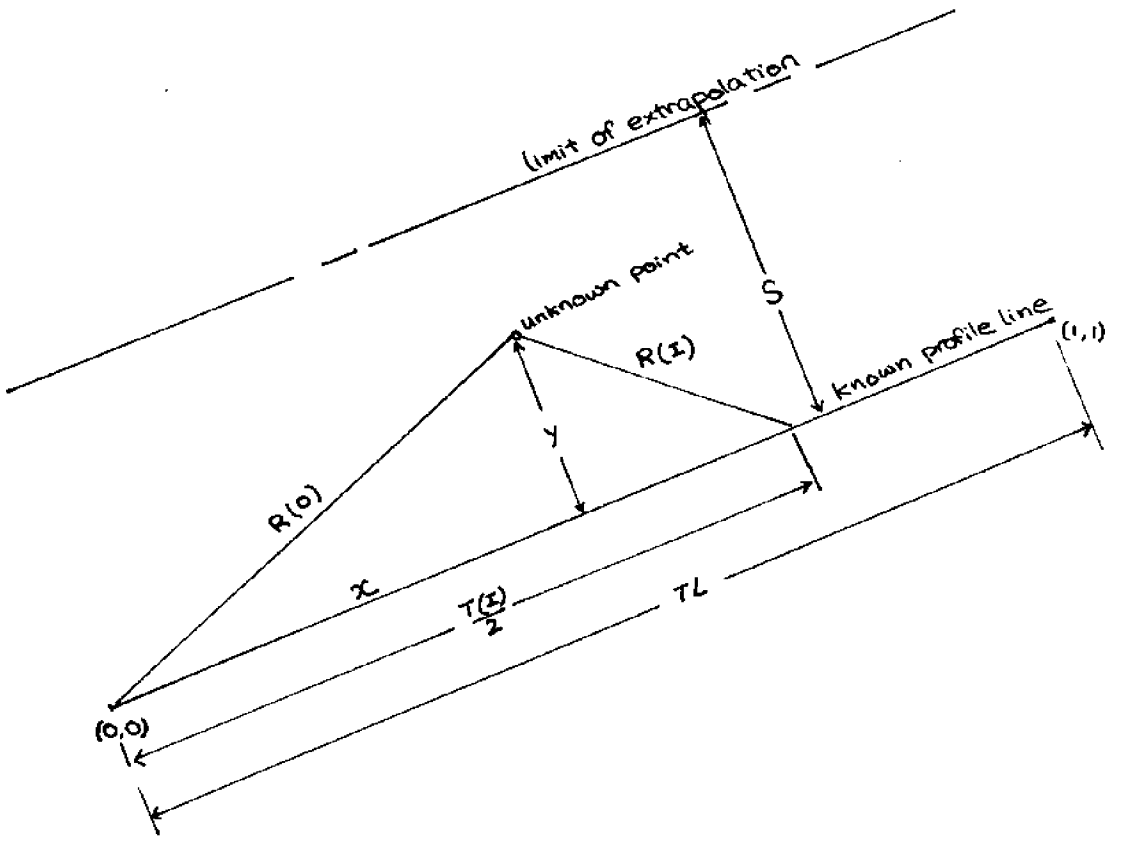

Figure 5.15 Dimensions in model definition.

T(I)/2 is the distance along the line from the origin (0,0) to the mid point of the Ith segment, i.e.

$$T(I)/2 = (I - 1/2)TL/66$$

R(I) is the distance of the unknown point from the Ith segment of the line, i.e.

$$R(I) = \sqrt{[x(I) - T(I)/2]^2 + y(J)^2}$$

$$A1 = [R(I-1) + R(I) + T(1)]/\pi$$

$$A2 = \exp(-\rho 2R(I-1)/\pi)$$

$$A3 = \exp(-\rho 2R(I)/\pi)$$

$$A4 = \exp(-\rho 2T(1)/\pi)$$

$$A = p^2 + (1-3p+2p^2)\exp(-\rho A1) + (p-p^2)(A2 + A3 + A4)$$

$$B = p + q(A3)$$

$$C = p + q(A4)$$

$$D = p + q(A2)$$

$$E = q^2 + (1-3q + 2q^2)\exp(-\rho A1) + (q-q^2)(A2 + A3 + A4)$$

$$F = q + p(A3)$$

FY1 is the term $P(x_k/x_{k+1}, y_1)$

FY0 is the term $P(x_k/x_{k+1}, y_o)$

FLOWCHART

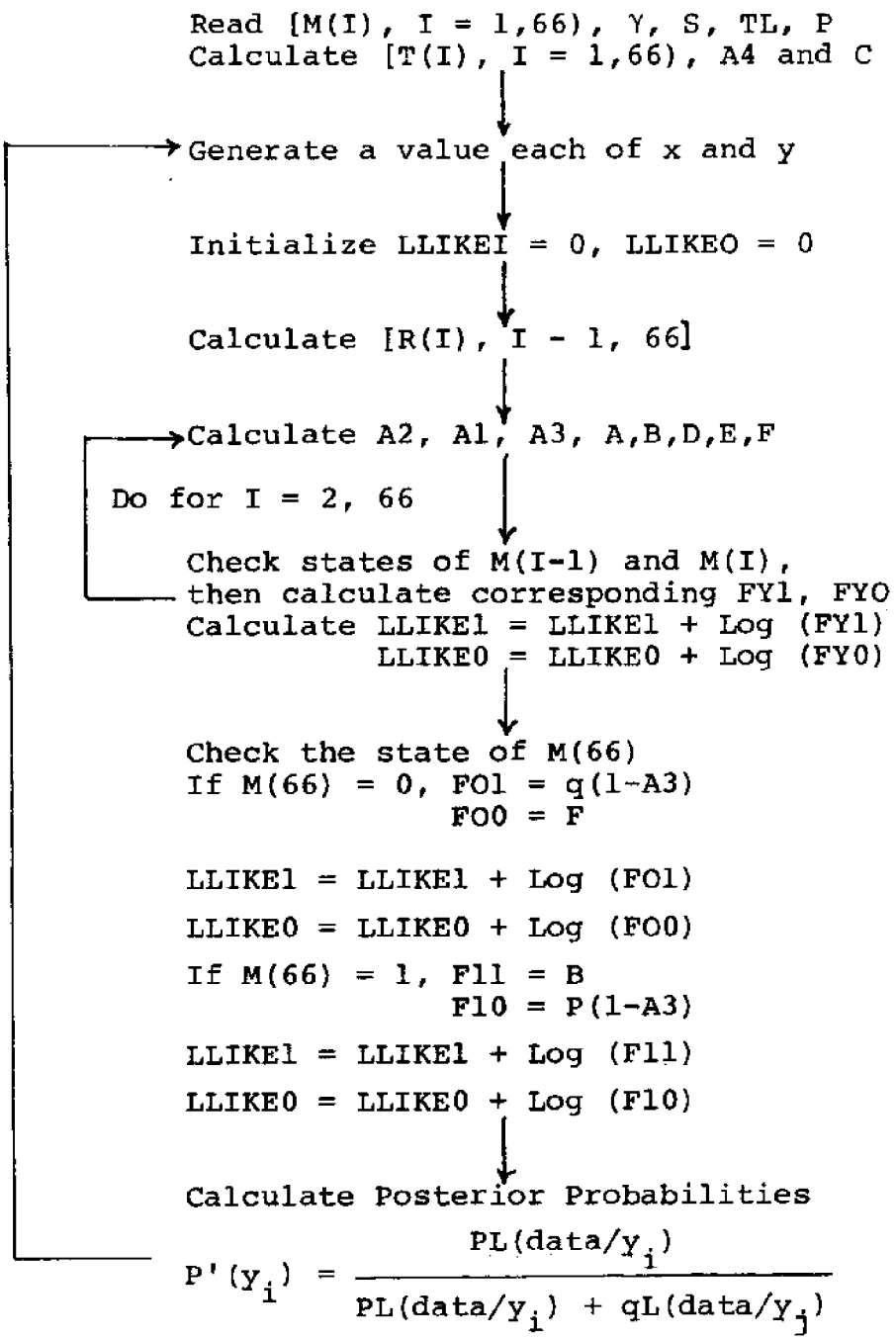

The program is written in Fortran IV and is given in Appendix Al.

If M(I-1) = 1, M(I) = 1, then FY1 = A/B, FYO = (C-A)/(1-B)

If M(I-1) = 0, M(I) = 0, then FY1 = 1-(D-A)/(1-B), FYO = E/F

If M(I-1) = 1, M(I) = 0, then FY1 = (D-A)/(1-B), FYO = 1-E/F

If M(I-1) = 0, M(I) = 1, then FY1 = 1-A/B, FYO = 1-(C-A)/(1-B)

LLIKE 1 = Logarithm form of likelihood function for state 1.

LLIKE 0 = Logarithm form of likelihood function for state 0.

5.3.4.2 Two Lines

In this case, S is defined as the distance between the two parallel lines in Fig. 5.15. The unknown point (x,y) lies between these two lines. In estimating the posterior probability of the point (x,y), the likelihood functions, equations (5.28) and (5.29), are solved first for one line and then for the other. The two likelihood functions (in logarithmic form) are then summed to obtain the final likelihood function. This involves a major assumption that the two lines are independent and do not intersect, i.e.

$$L(\text{line 1, line 2}/y_i) = L(\text{line 1}/y_i)\ L(\text{line 2}/y_i)$$

The program in Appendix A1 is modified to account for this change, and to allow two different data sets to be read. The modified program is shown in Appendix A2.

5.4 Results

In this section, various experimental results of the model are presented. Subsection 5.4.1 discusses the probability

variation from a line; subsection 5.4.2, the probability variation with varying decay parameter; subsection 5.4.3, checking the applicability of the model; subsection 5.4.4, the probability variation between two parallel lines; and subsection 5.4.5 discusses the estimated maps.

5.4.1 Probability Variation from a Line

The line chosen for this analysis is line OP in Map 4*, Figure 5.16. This line was divided into 66 segments and used with the model to estimate the posterior probabilities of state 1 (shaded region) away from the line. Figure 5.17 shows the probability variation for state 1 along a line parallel to line OP and at increasing distance from OP (y is the perpendicular distance from the line OP). Appendix B tabulates these probabilities for various values of x (distance parallel to OP) and y.

It is seen that at close distances to the line OP, there is significant variation in the estimated probabilities. These variations quickly decay down to the spatial frequency value at y = 0.4 or greater. The spatial frequency for state 1 used for this case is 0.3788 (note that state 1 is the minor state) and was estimated from lines OP, QR, ST and UV.

Figure 5.17 also indicates that at y = 0.2, the posterior probability of (x,y) being of state 1 has already dropped below 0.5 (i.e. the extrapolation distance r_c is short).

* Map 4 shows the engineering geology of Southern California.

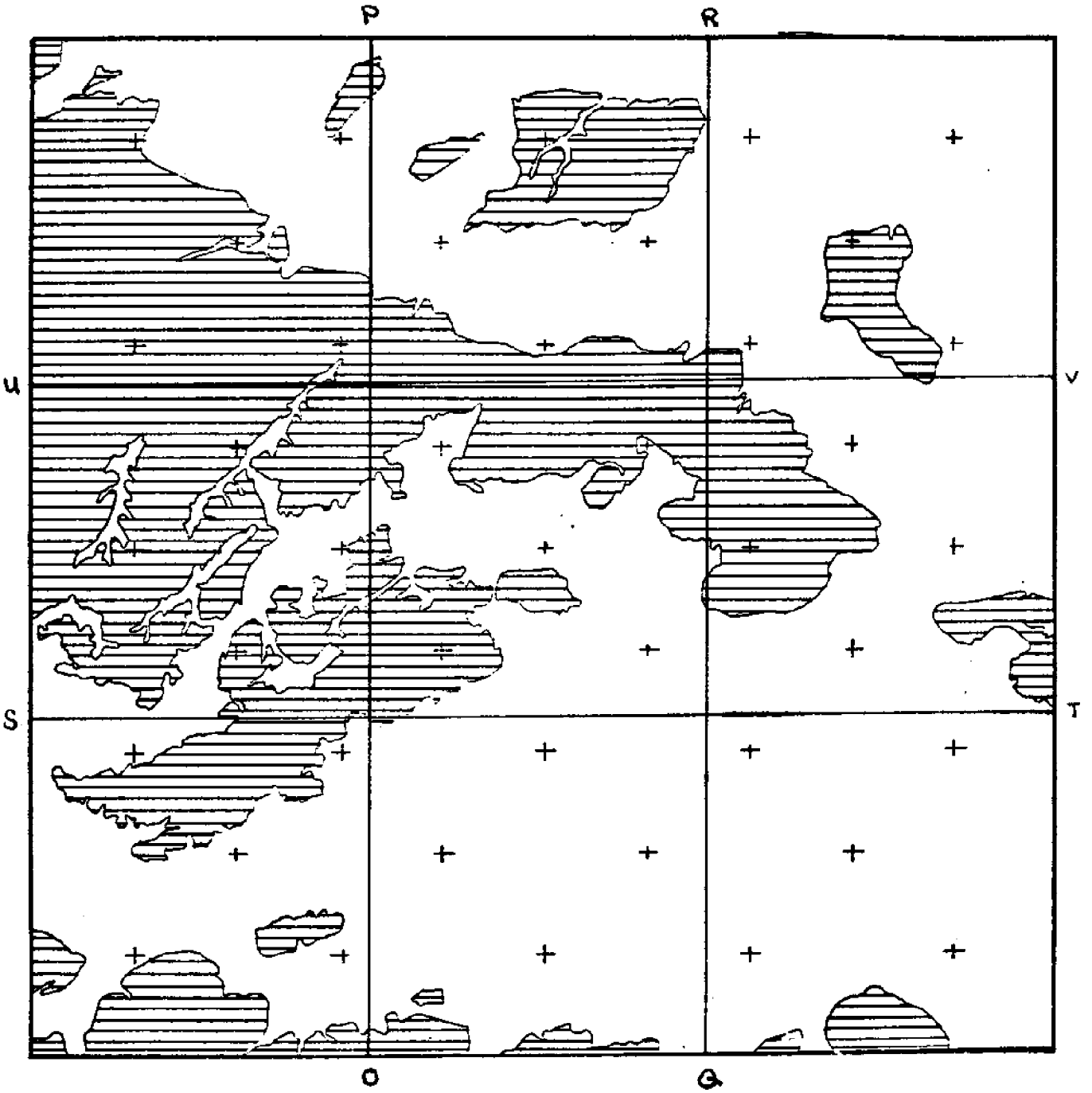

Figure 5.16 Map 4; Engineering Geology of Southern California, γ = 11.76

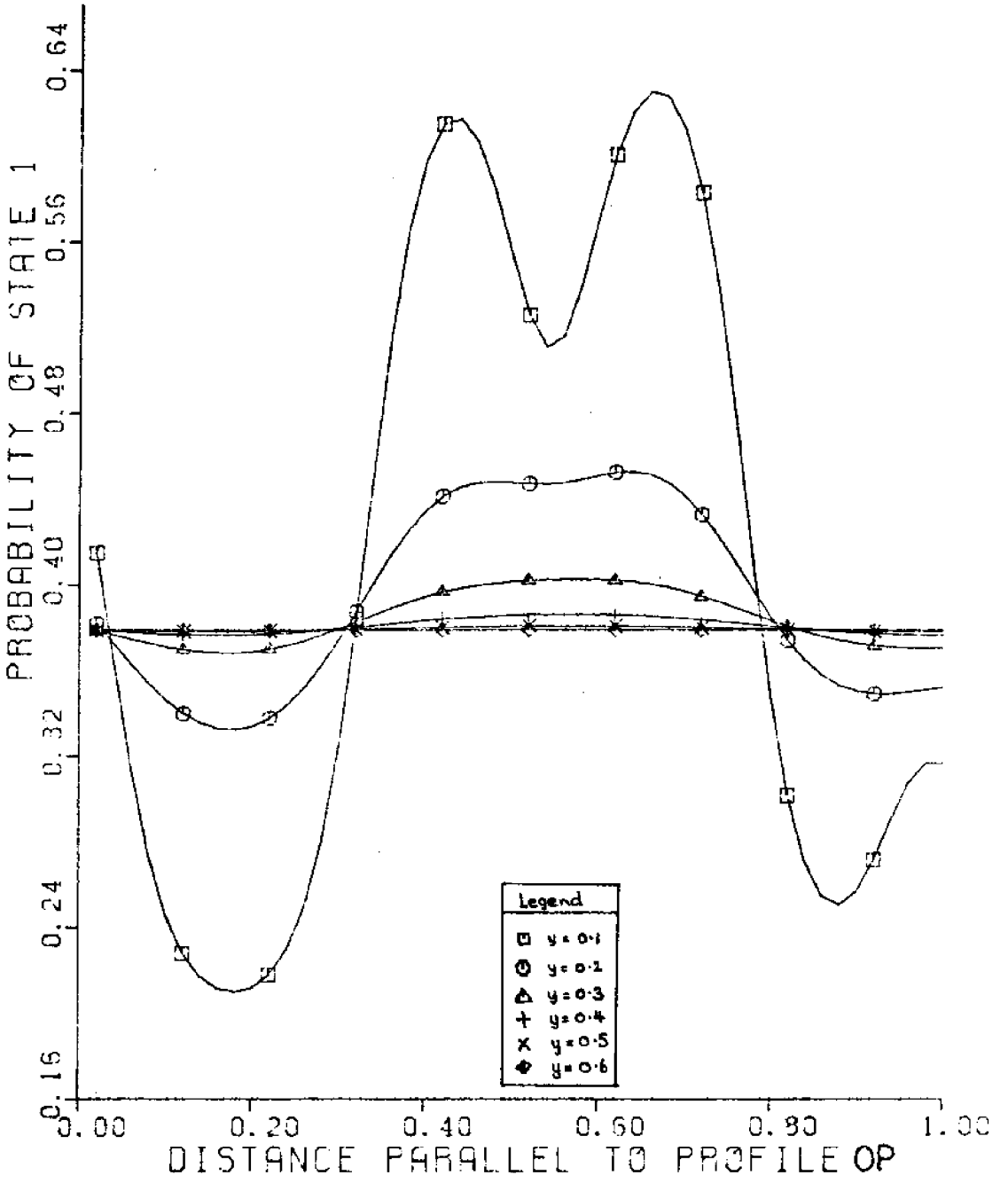

Figure 5.17 Probability distribution along lines parallel to line OP in Map 4, Figure 5.15.

This shows a rapid decay. Therefore at $y \geq 0.2$, the predicted state would have been state 0 throughout. A comparison with Map 4 (Fig. 5.16) shows that the model is ineffective in mapping beyond the distance of $y = 0.2$

Figures 5.18 and 5.19 show two different 3-D plots of the probability variation away from line OP. The z-axis is the probability axis, the x and y axes are as defined earlier. These plots indicate the rapid decay of the estimated posterior probability of state 1 to the spatial frequency value.

Figures 5.20 to 5.26 show the probability variation for lines 0-0, 1-1, 2-2, 3-3, 4-4, 5-5 and 6-6 of Map 1 (Fig. 5.6). The prior probability used here is 0.5 and γ is 15.15. The extrapolation distance for Map 1 is seen from figures 5.20 to 5.26 to be larger than for Map 4. This is because the prior probability is larger for Map 1 than for Map 4. Also by virtue of its larger decay parameter, the probability variation of Map 1 decays more rapidly to the prior probability value than in Map 4, as can be seen from the Figures 5.20 to 5.27.

5.4.2 Probability Variation with Varying Decay Parameter

The decay parameter for Map 4 was reduced from the true value of 11.76 to 7.64, 4.46 and 1.91 (i.e. ρ was reduced from 18.47 to 12,7 and 3). Figure 5.27 to 5.30 shows plots for $\rho = 18.47$, 12,7 and 3 respectively. (Figure 5.27 is a reproduction of Fig. 5.17.)

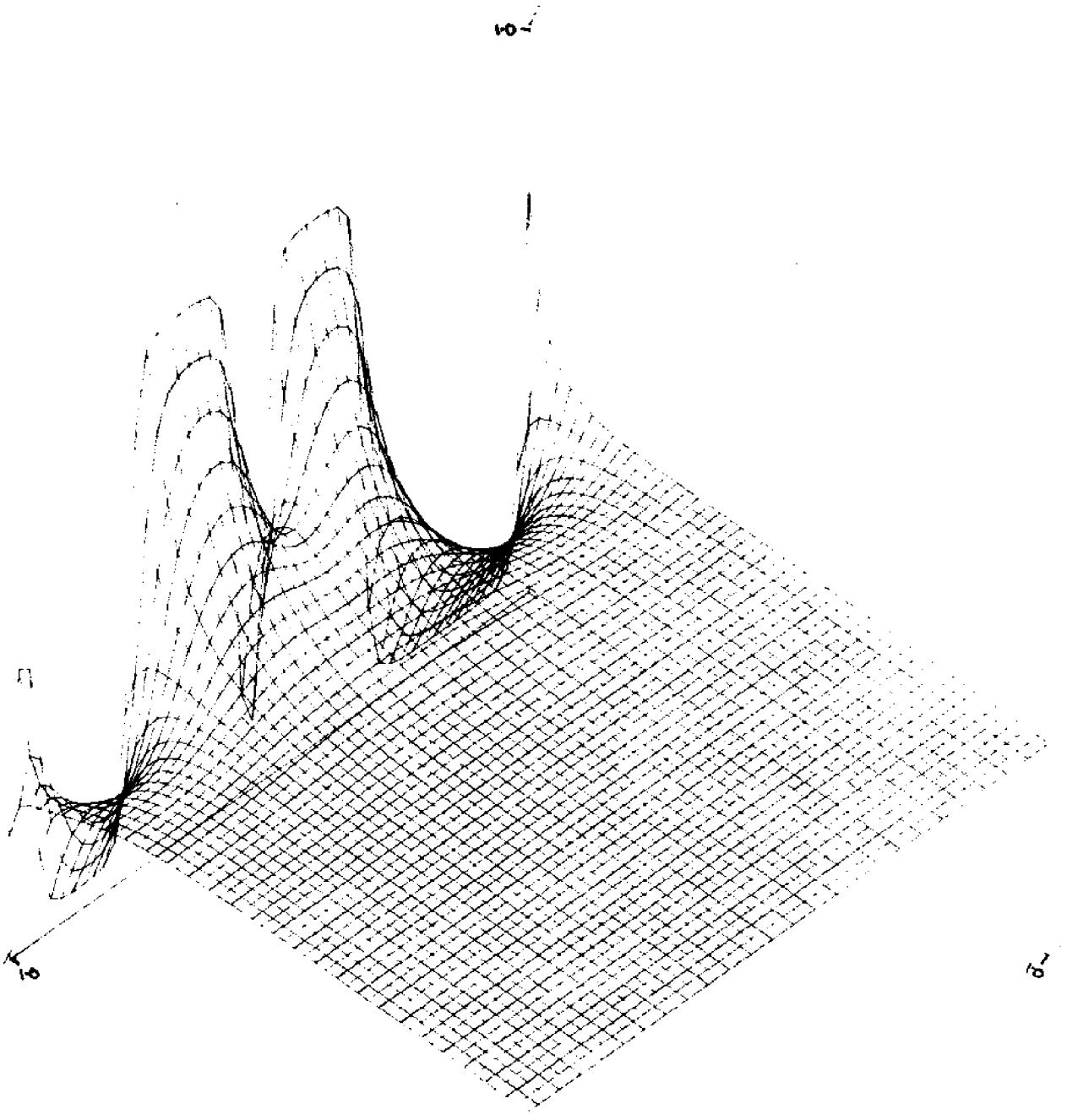

Figure 5.18 3-D representation of probability variation from line OP, Map 4.

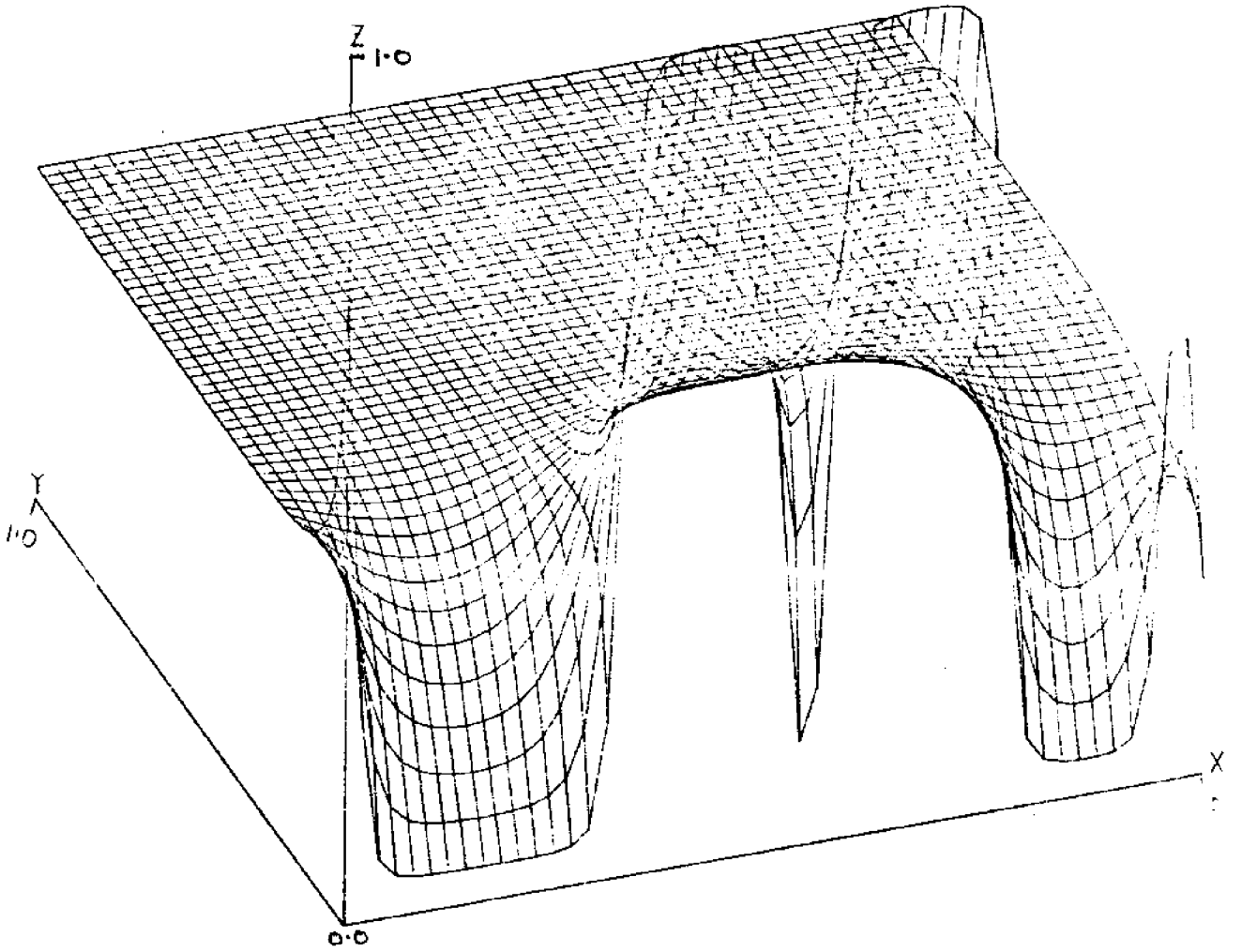

Figure 5.19 3-D representation of probability variation from line OP, Map 4.

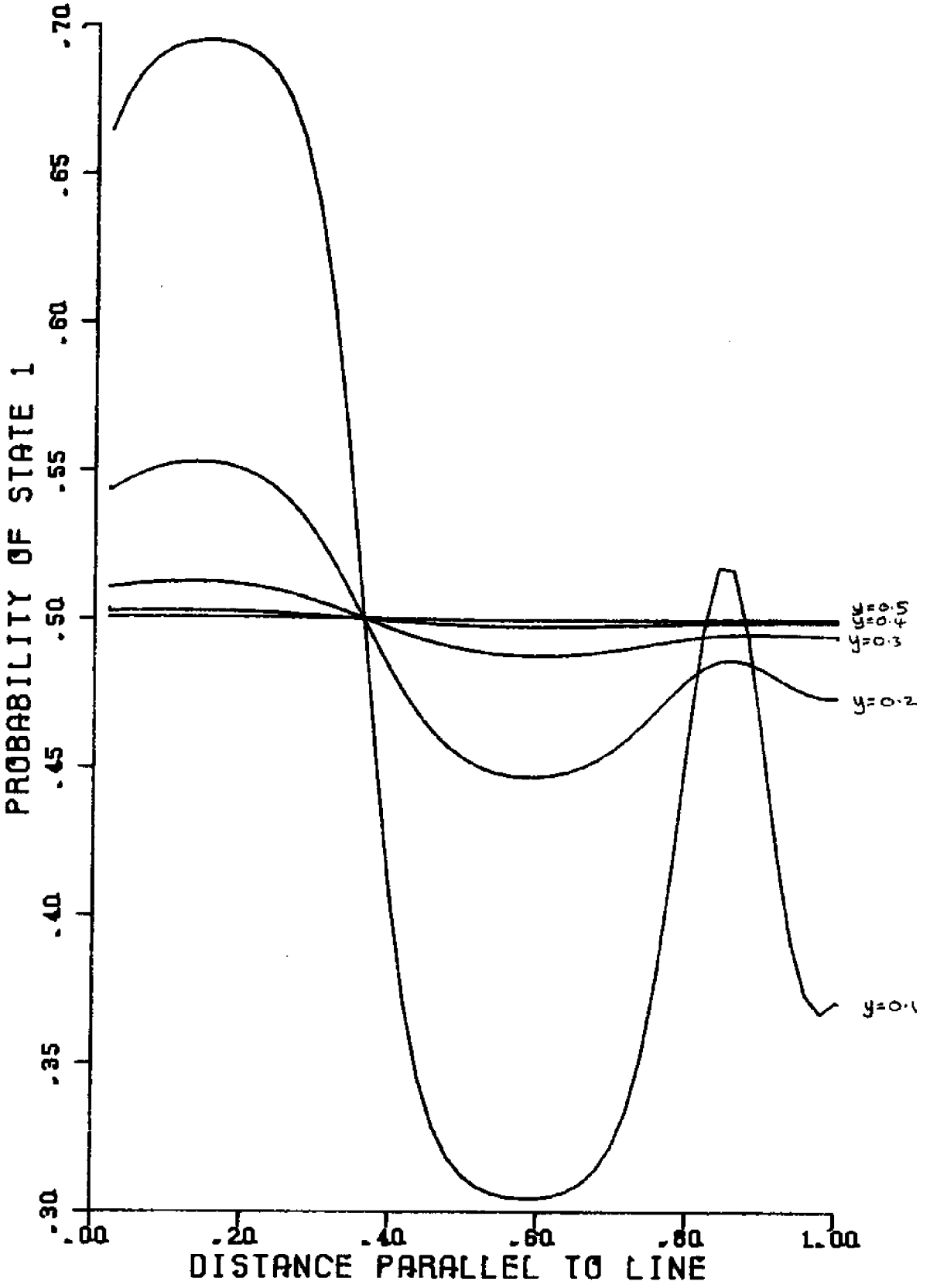

Figure 5.20 Probability variation from line 0-0, Map 1.

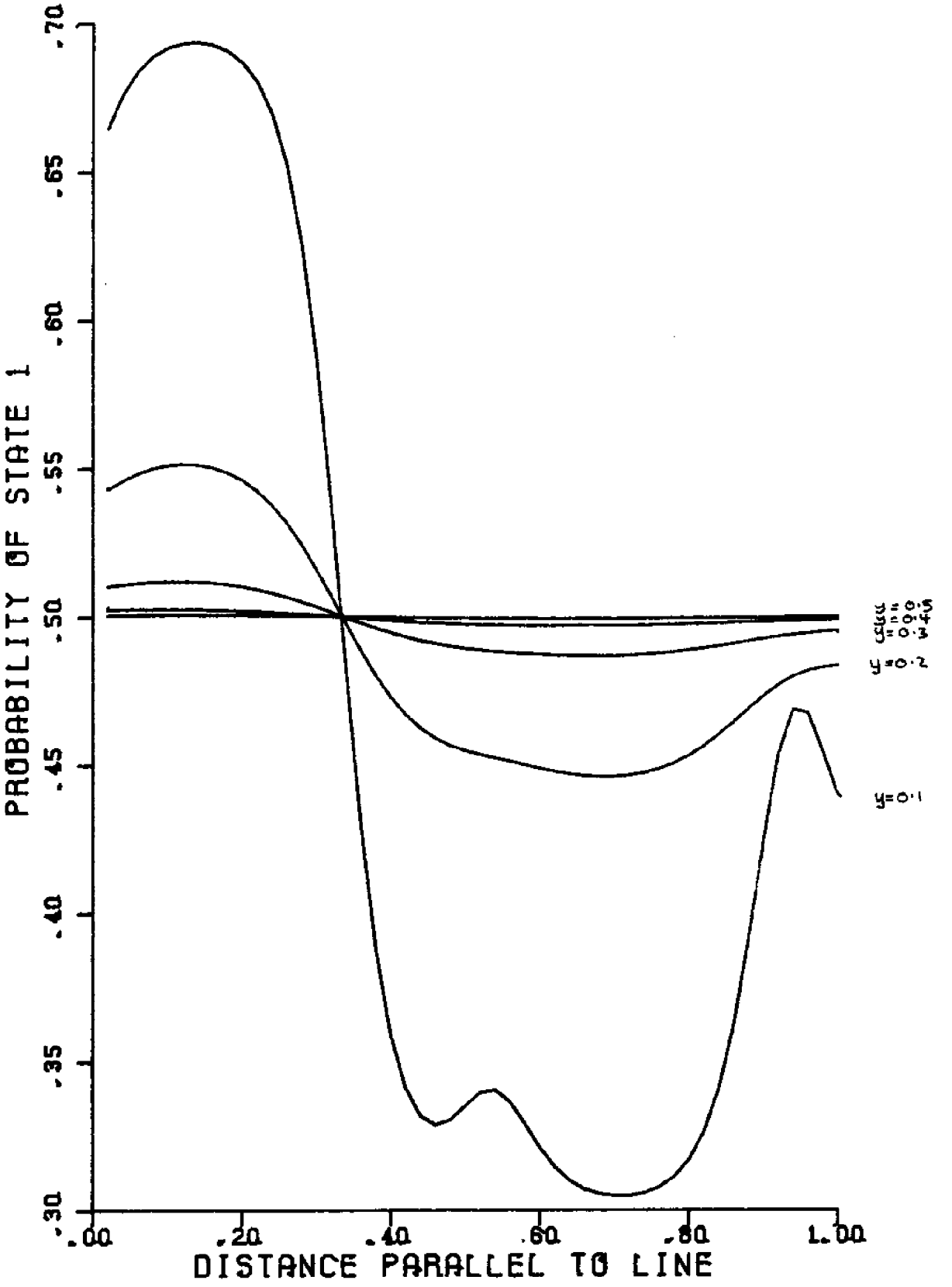

Figure 5.21 Probability variation from line 1-1, Map 1.

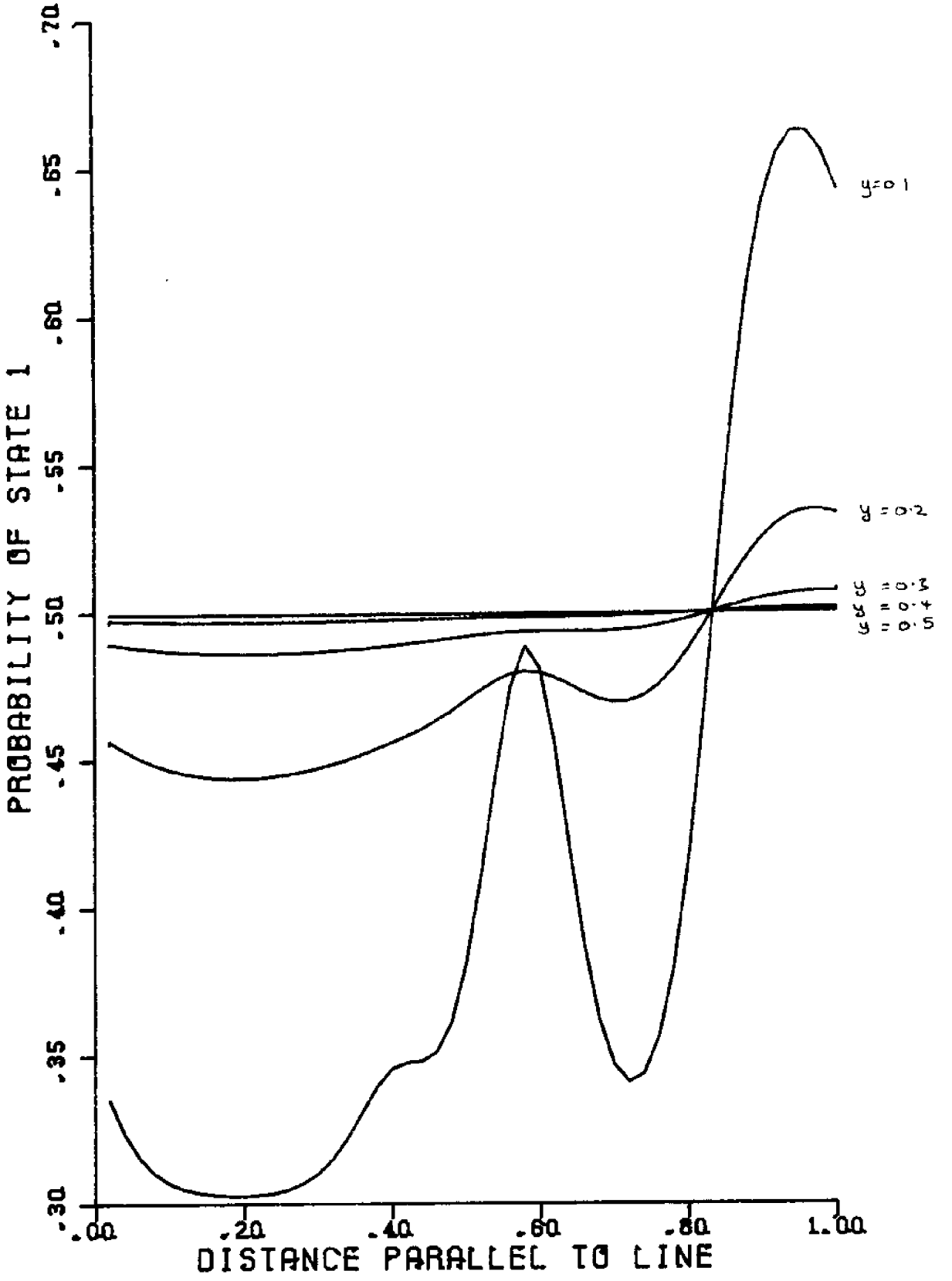

Figure 5.22 Probability variation from line 2-2, Map 1.

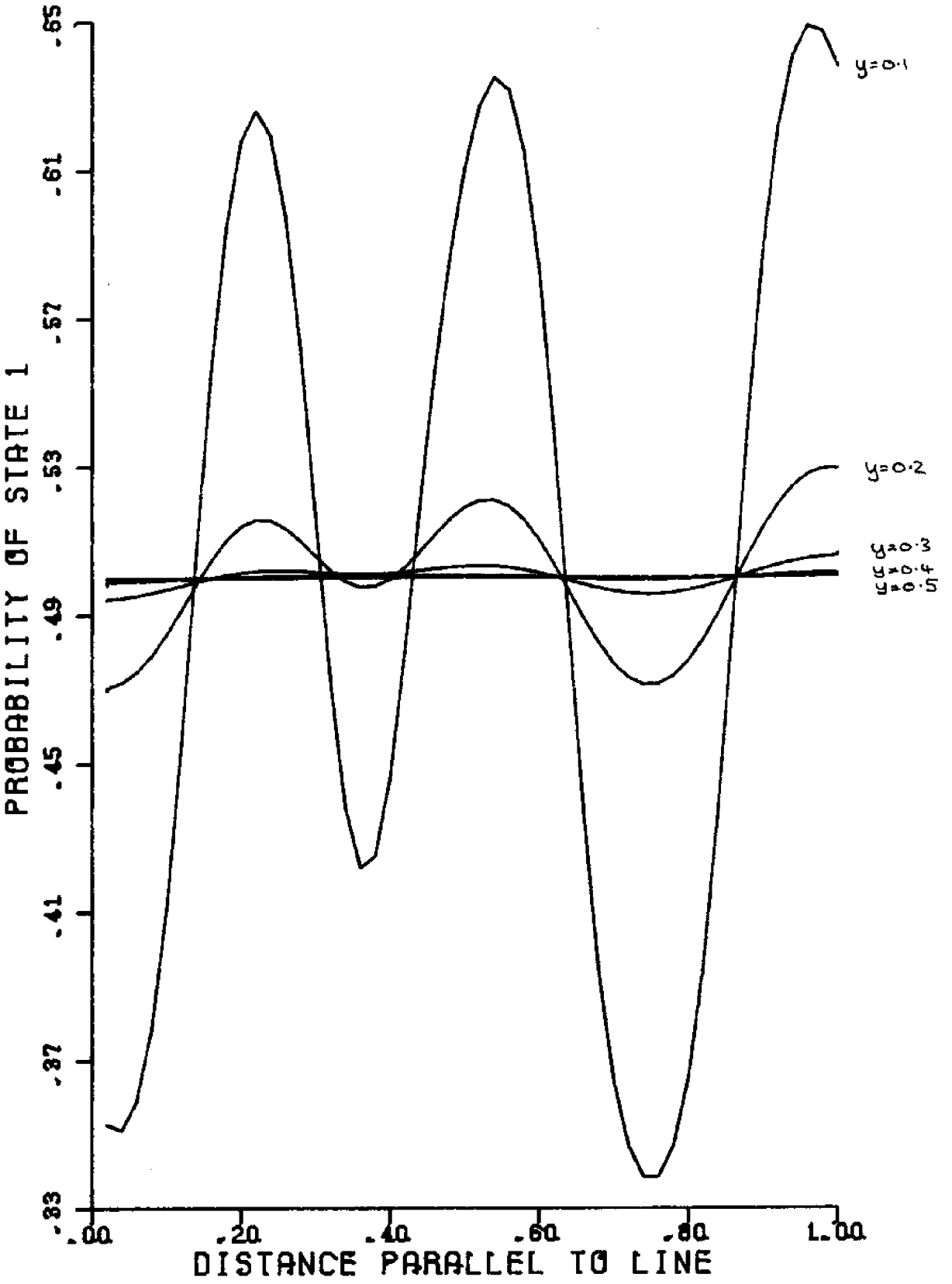

Figure 5.23 Probability variation from line 3-3, Map1 .

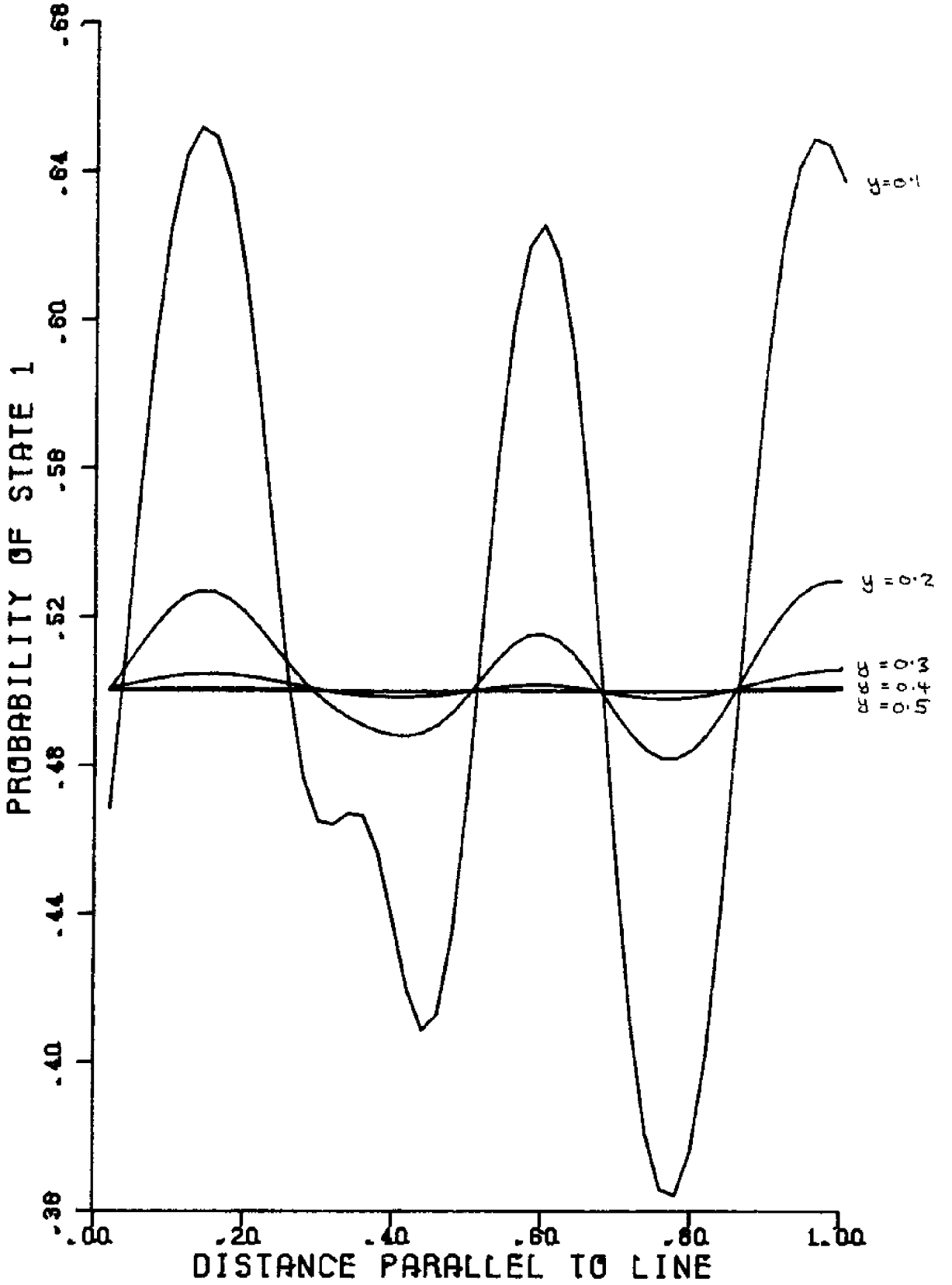

Figure 5.24 Probability variation from line 4-4, Map 1.

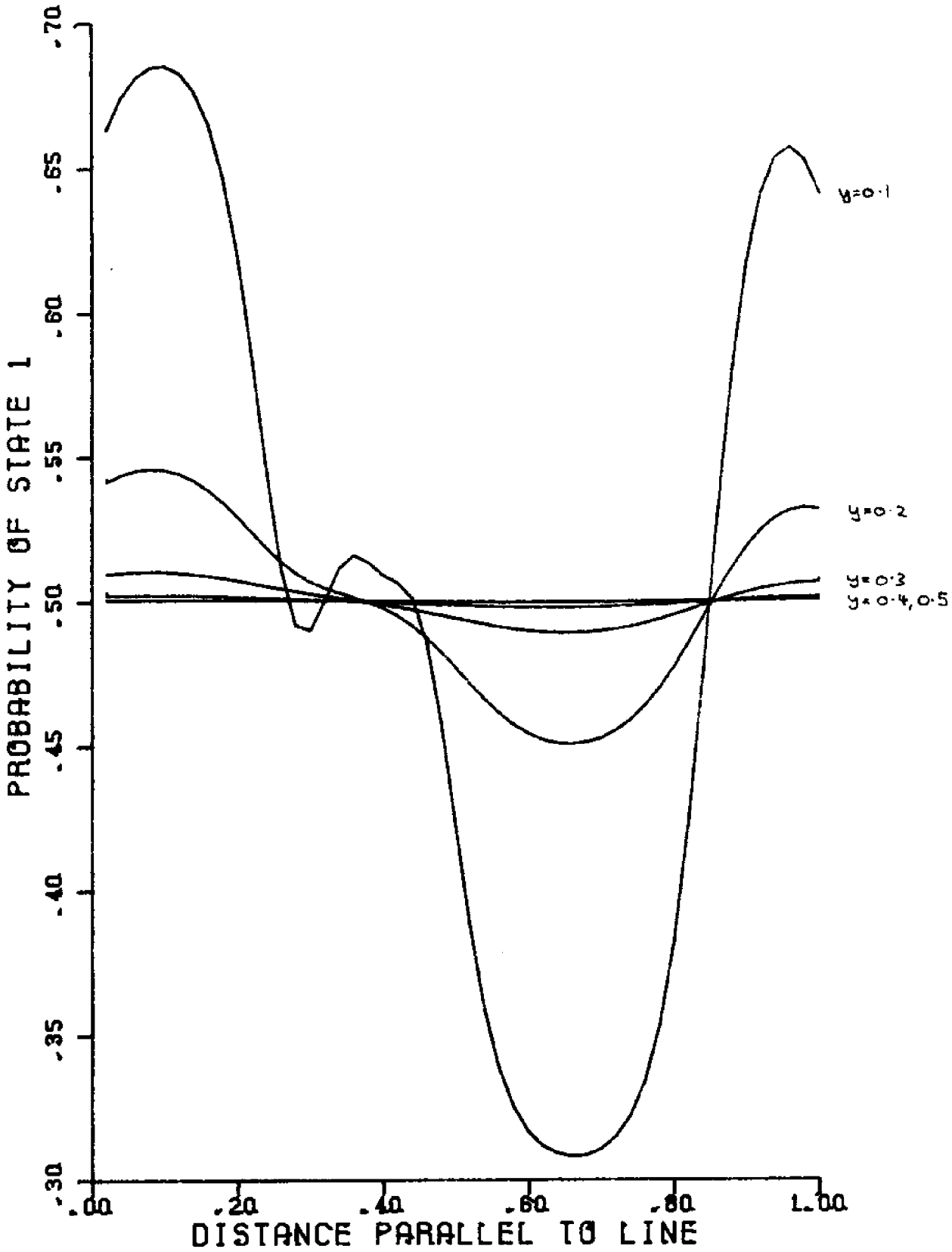

Figure 5.25 Probability variation from line 5-5, Map 1.

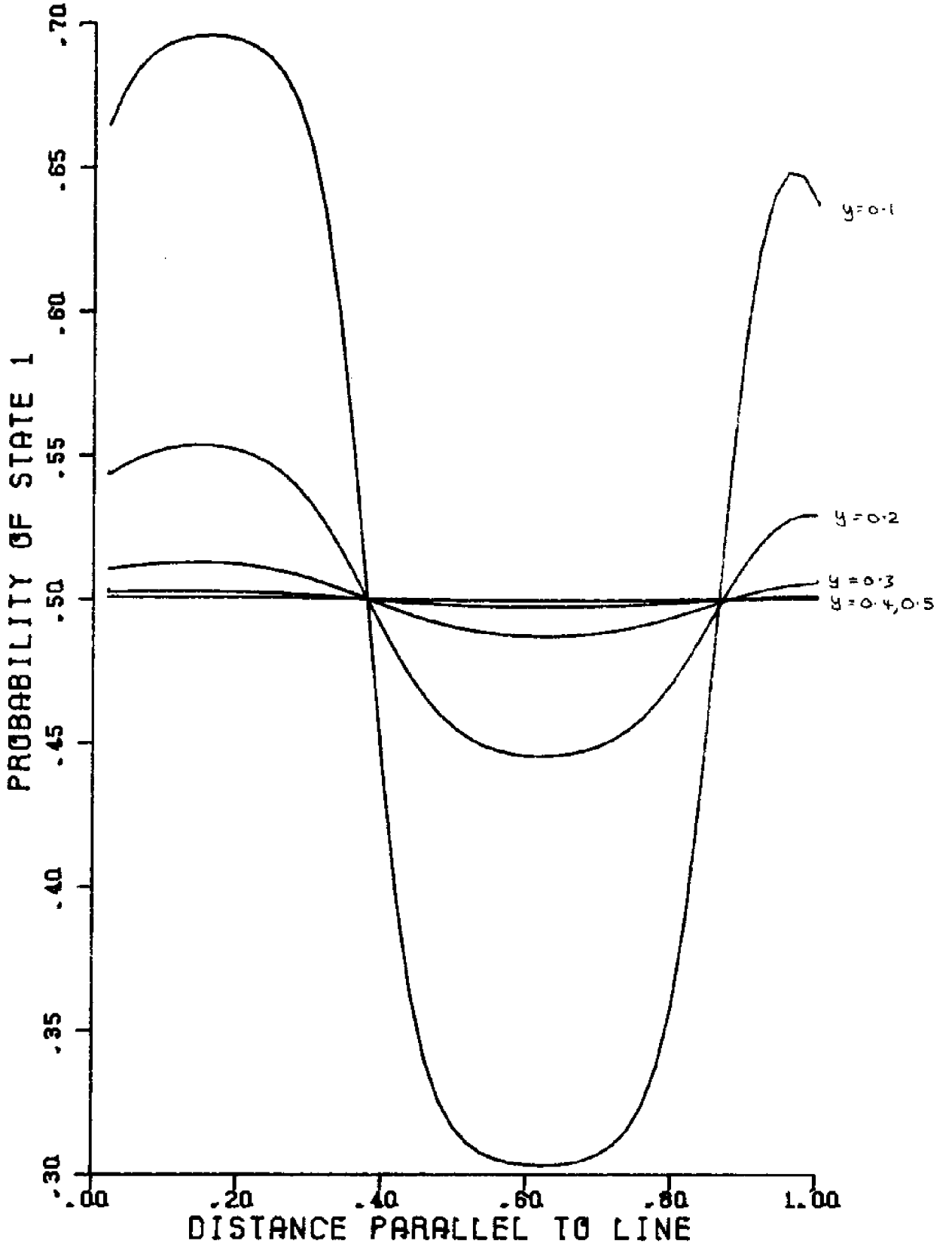

Figure 5.26 Probability variation from line 6-6, Map 1.

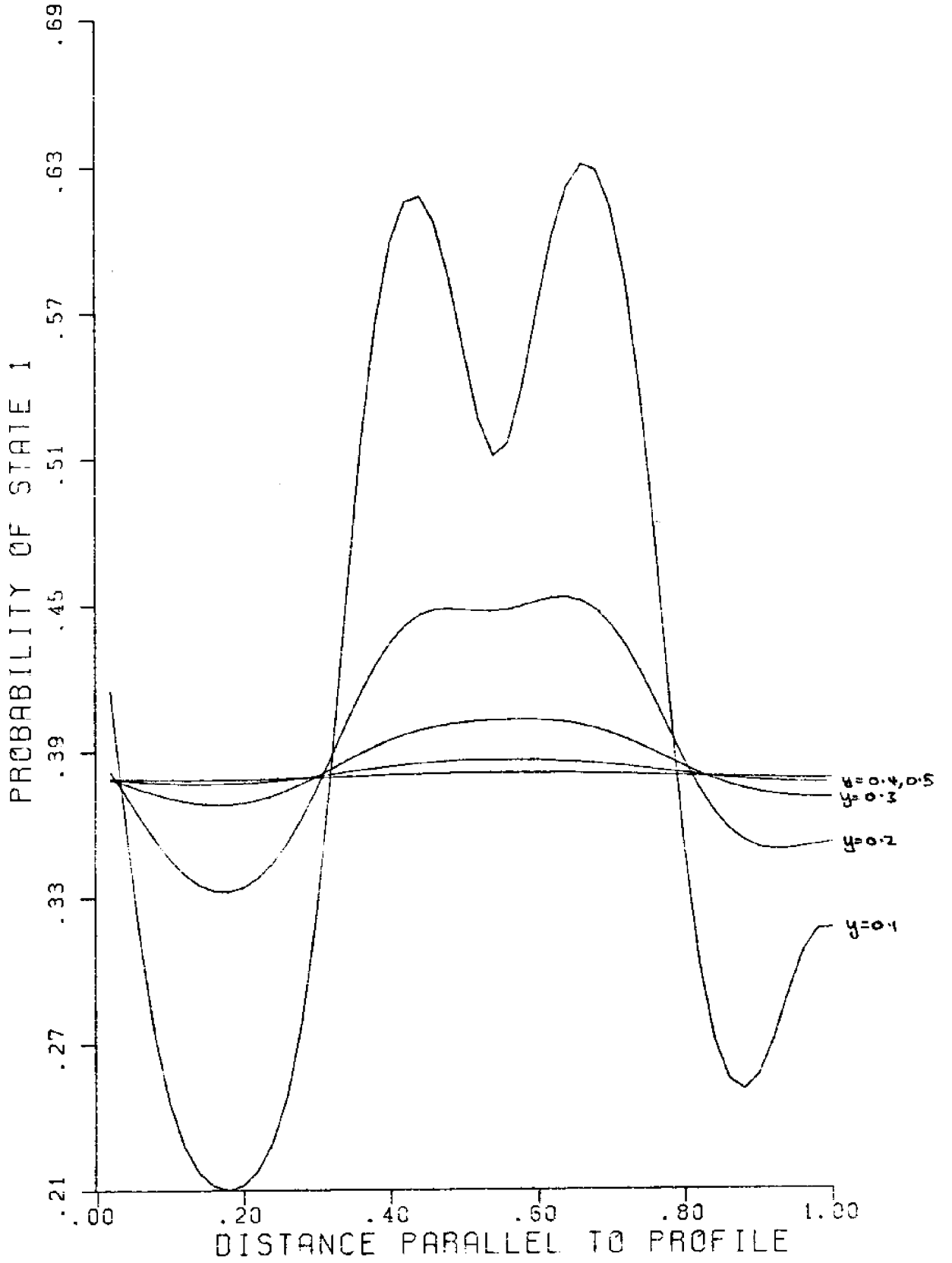

Figure 5.27 Probability variation from line OP, Map 4. δ=11.76.

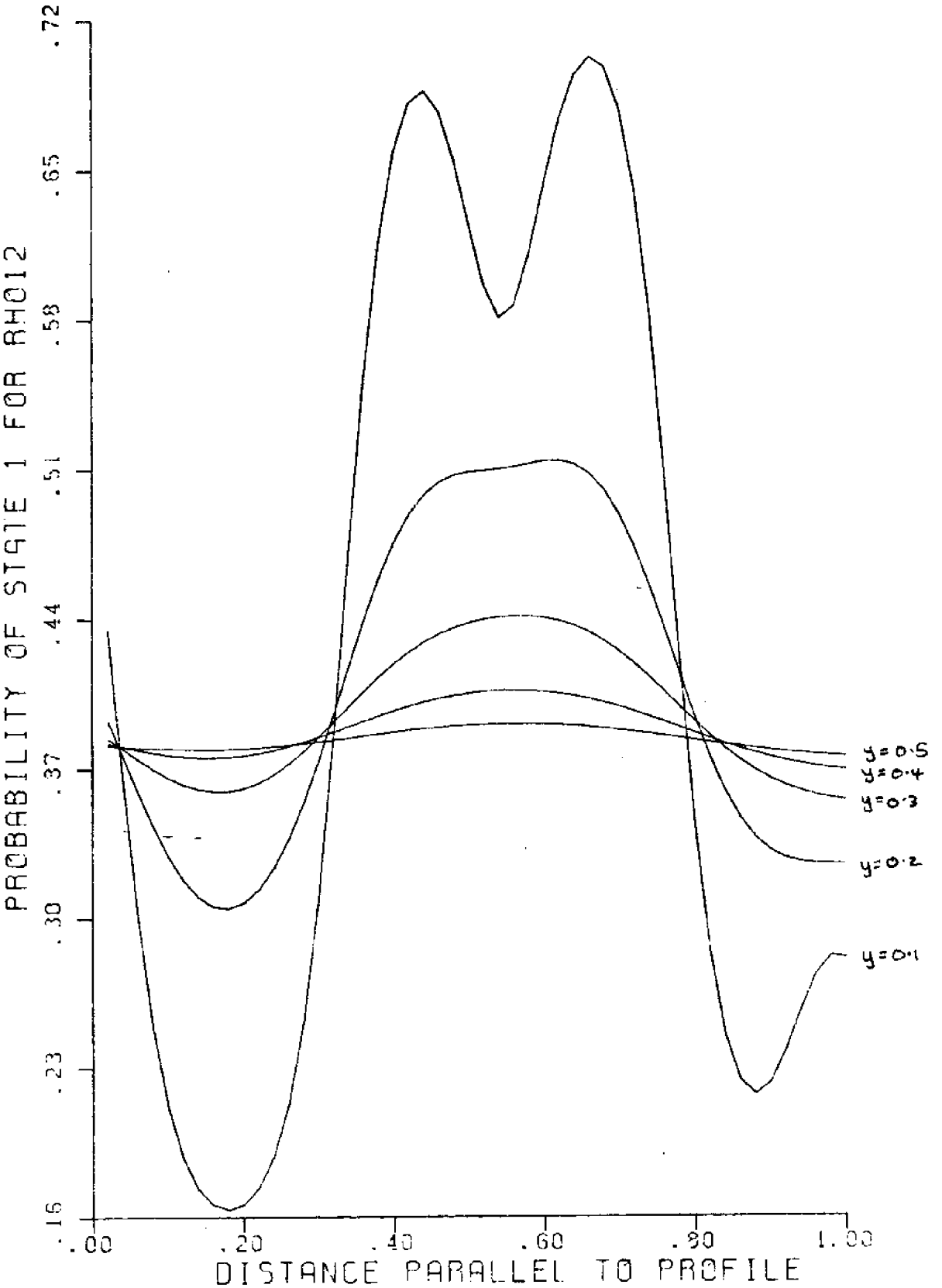

Figure 5.28 Probability variation from line OP, Map 4.
(σ=7.64, ϱ =12)

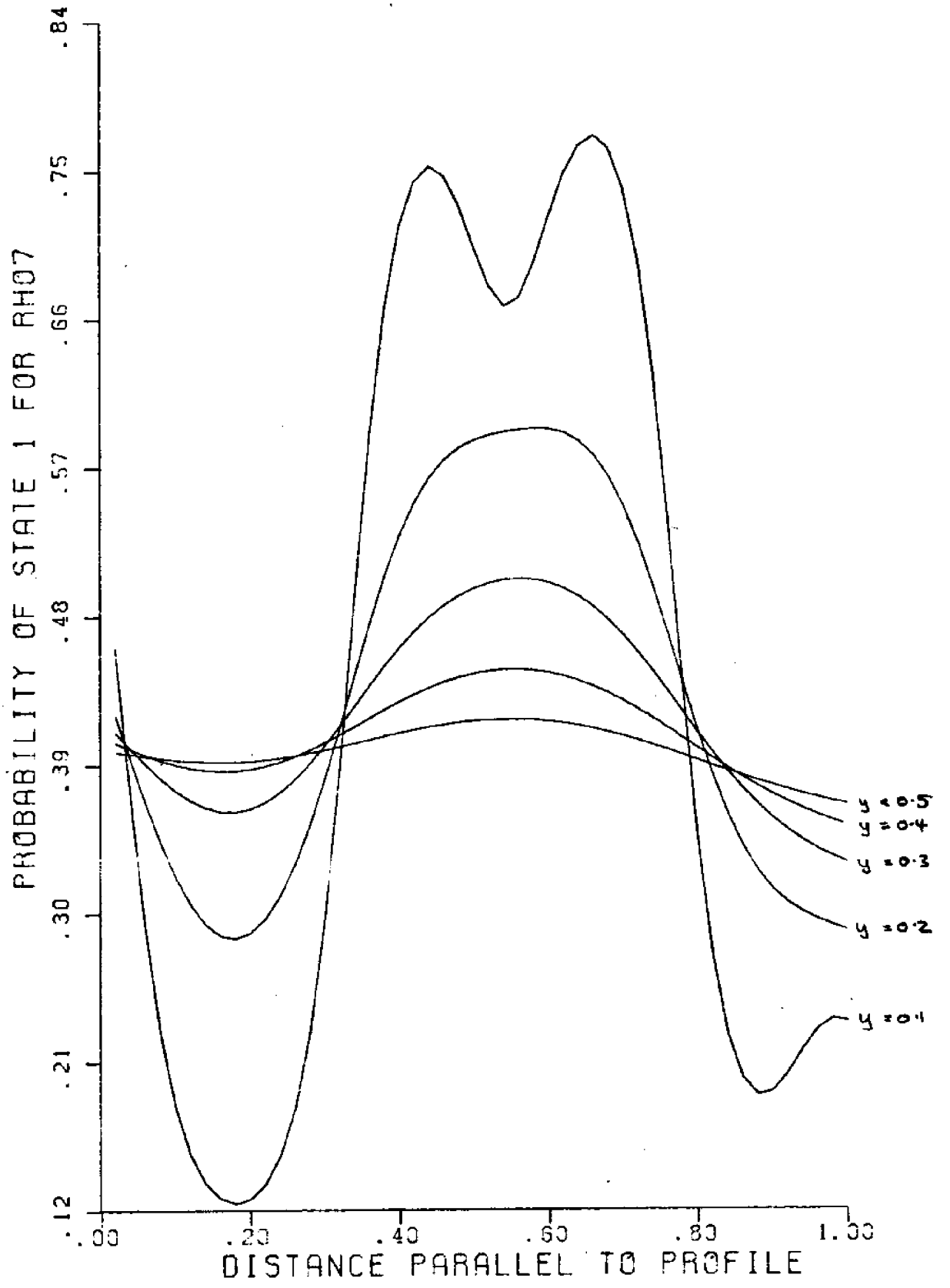

Figure 5.29 Probability variation from line OP, Map 4, (θ=4.46, ρ=7)

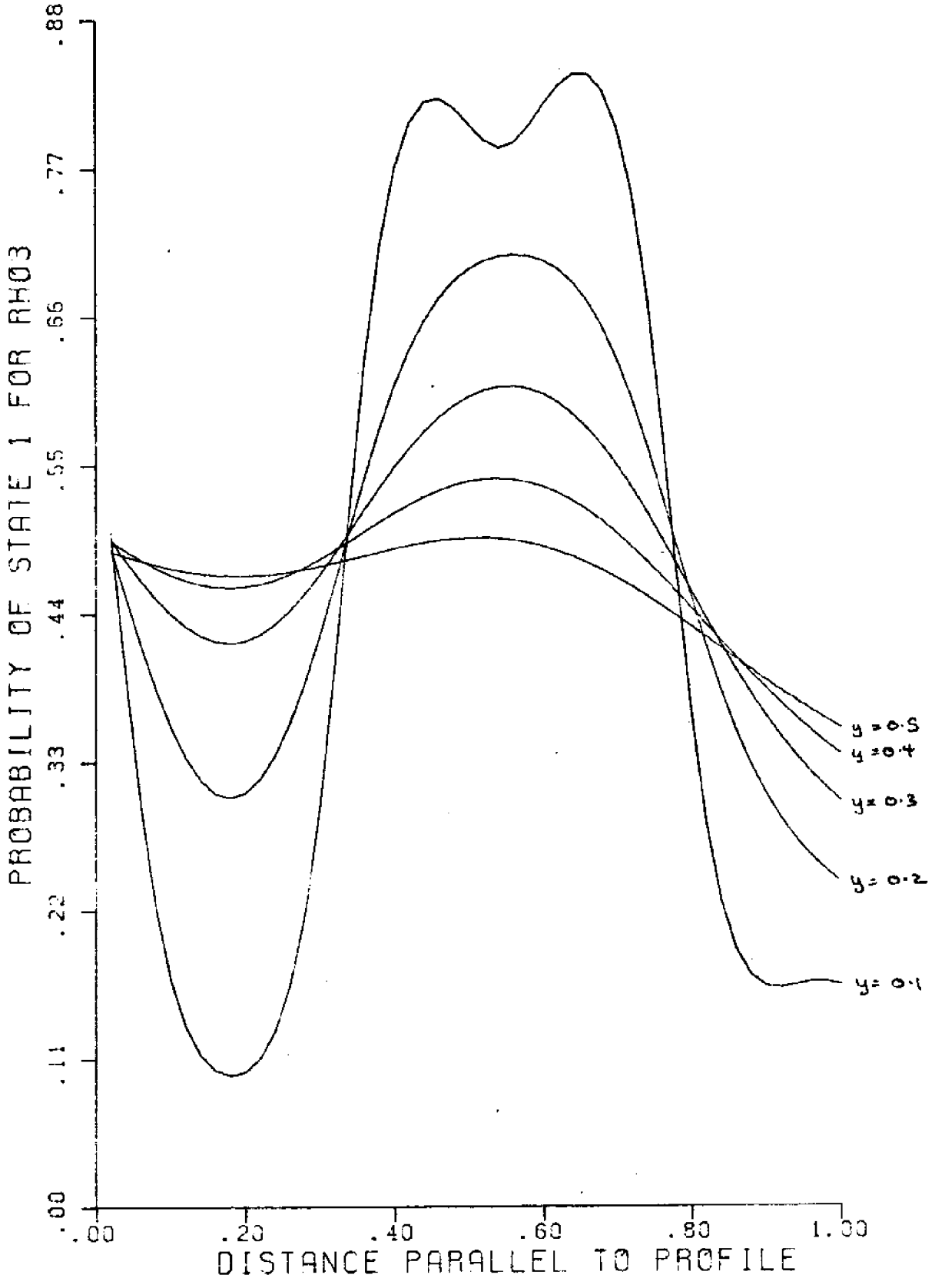

Figure 5.30 Probability variation from line OP, Map 4.
(γ =1.19, ρ =3)

A small value of the decay parameter would signify slow decay and the effect of line OP would extend over a greater distance (i.e. a larger r_c, the extrapolation distance). Figures 5.27 to 5.30 confirm this statement. The extrapolation distance for various decay parameter values are tabulated below:

γ	Range where Posterior Probability > 0.5
11.76	$0.1 < r_c < 0.2$
7.64	$0.2 < r_c < 0.25$
4.46	$0.25 < r_c < 0.3$
1.91	$0.4 < r_c < 0.5$

It is seen that the extrapolation distance generally increases with decreasing γ.

The true decay parameter for Map 4 is smaller than for Map 1 while the extrapolation distance is smaller in Map 4 than in Map 1. This seems to contradict the finding above that the smaller decay parameter should have the larger extrapolation distance. However, the prior probability (0.5) assumed in Map 1 is larger than for Map 4 (prior probability = 0.3788). It therefore appears that the choice of the prior probability has a significant influence on the extrapolation distance.

5.4.3 Checking the Applicability of the Model

The applicability of the model was checked by plotting the estimated probability of state 1 (horizontal axis) against

the actual frequency of state 1. Maps 1,2 and 3 and their corresponding decay parameters were used for this analysis. The method is described below.

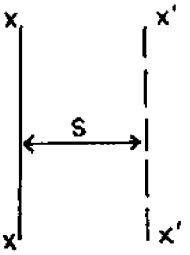

s = 1/33, 2/33, 3/33

In the figure above, line x-x is the reference line. The probability of state 1 is estimated at distance S from x-x (i.e. along x'-x') for every one of the 66 segments of x'-x' (line x'-x' was divided into 66 segments). The state of each of these segments is noted and is correlated with the estimated probability of state 1 on each segment. The estimated probabilities are then divided into ten equal ranges, i.e. 0.0-0.1, 0.1-0.2, ..., 0.9-1.0, and the frequency of actual occurrence of state 1 within each of these probability ranges is calculated. The calculated actual frequency of state 1 is then plotted against the mid-point of the probability range. The ideal plot is when the actual frequency of state 1 equals the estimated probability of state 1, and is indicated by a straight line through points (0,0) and (1,1) on the plot.

Figures 5.31 through 5.39 illustrate the results of this analysis. These figures show a good correlation between the experimental curve and the ideal curve, therefore indicating the general applicability of the model. In Figures 5.34 to 5.39, the dashed curve is the experimental curve obtained for

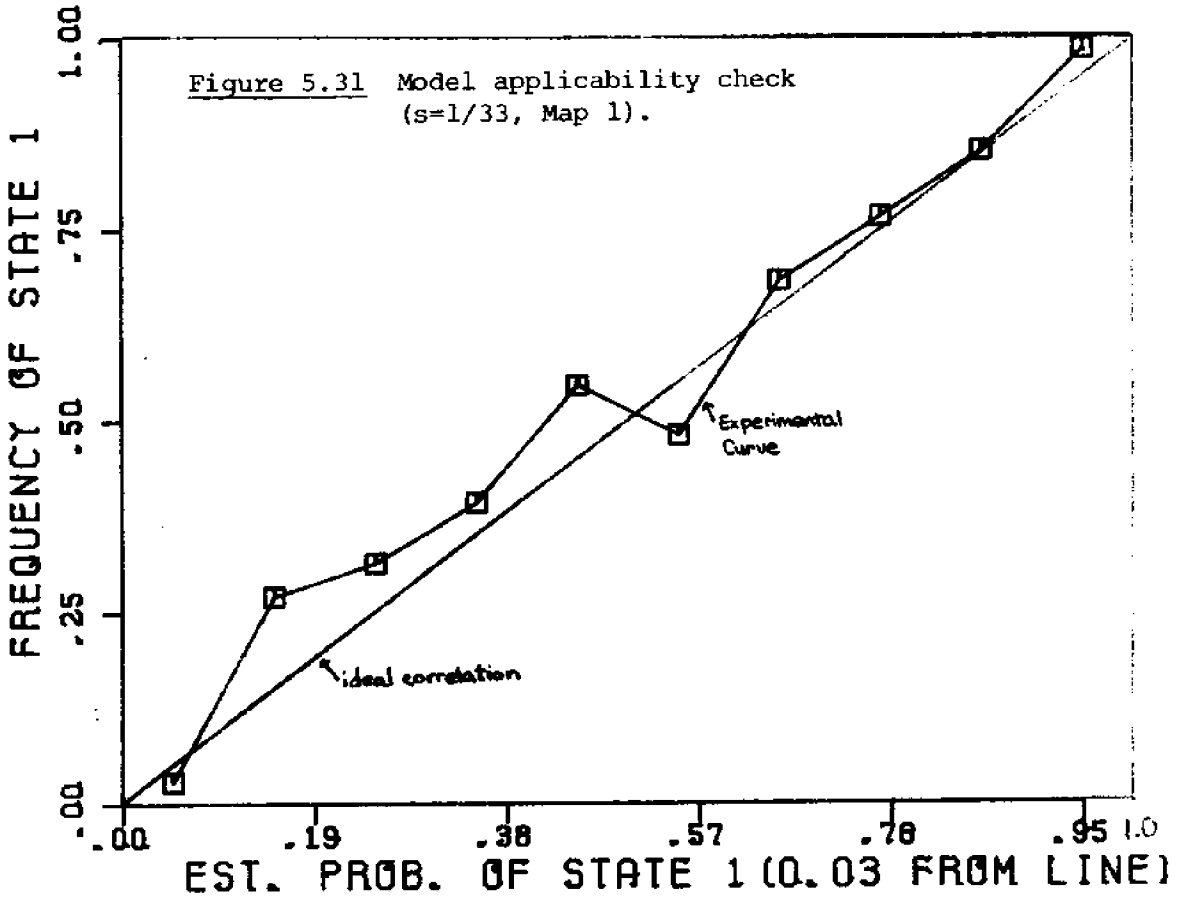

Figure 5.31 Model applicability check (s=1/33, Map 1).

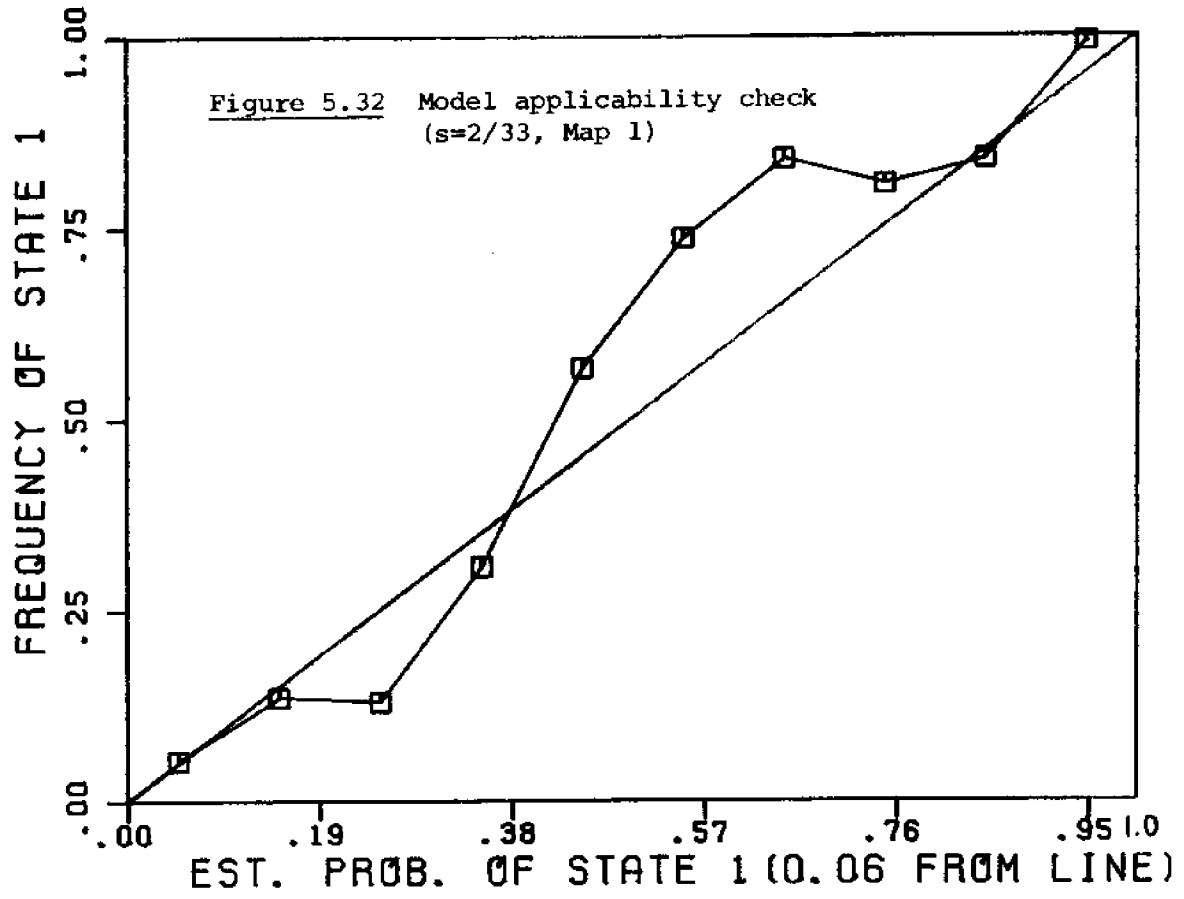

Figure 5.32 Model applicability check (s=2/33, Map 1)

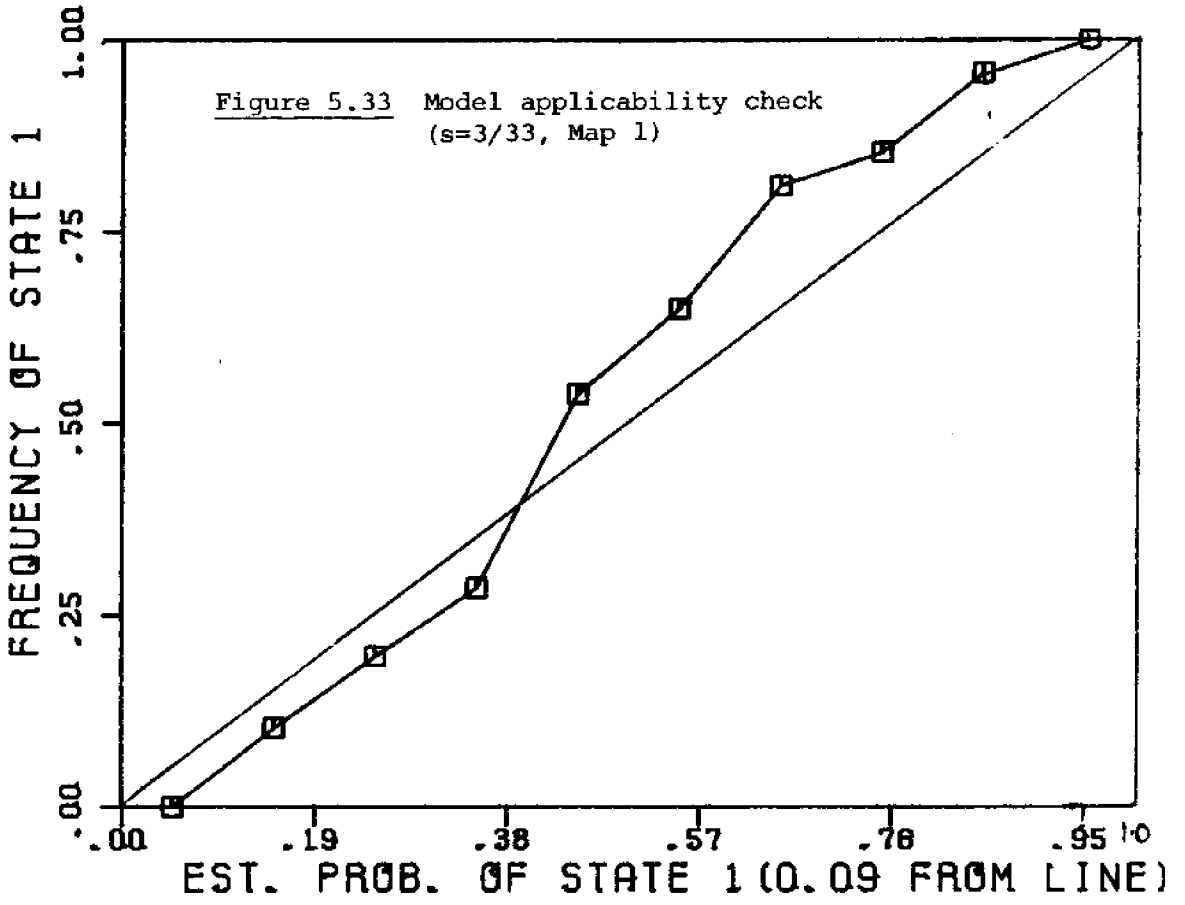

Figure 5.33 Model applicability check
(s=3/33, Map 1)

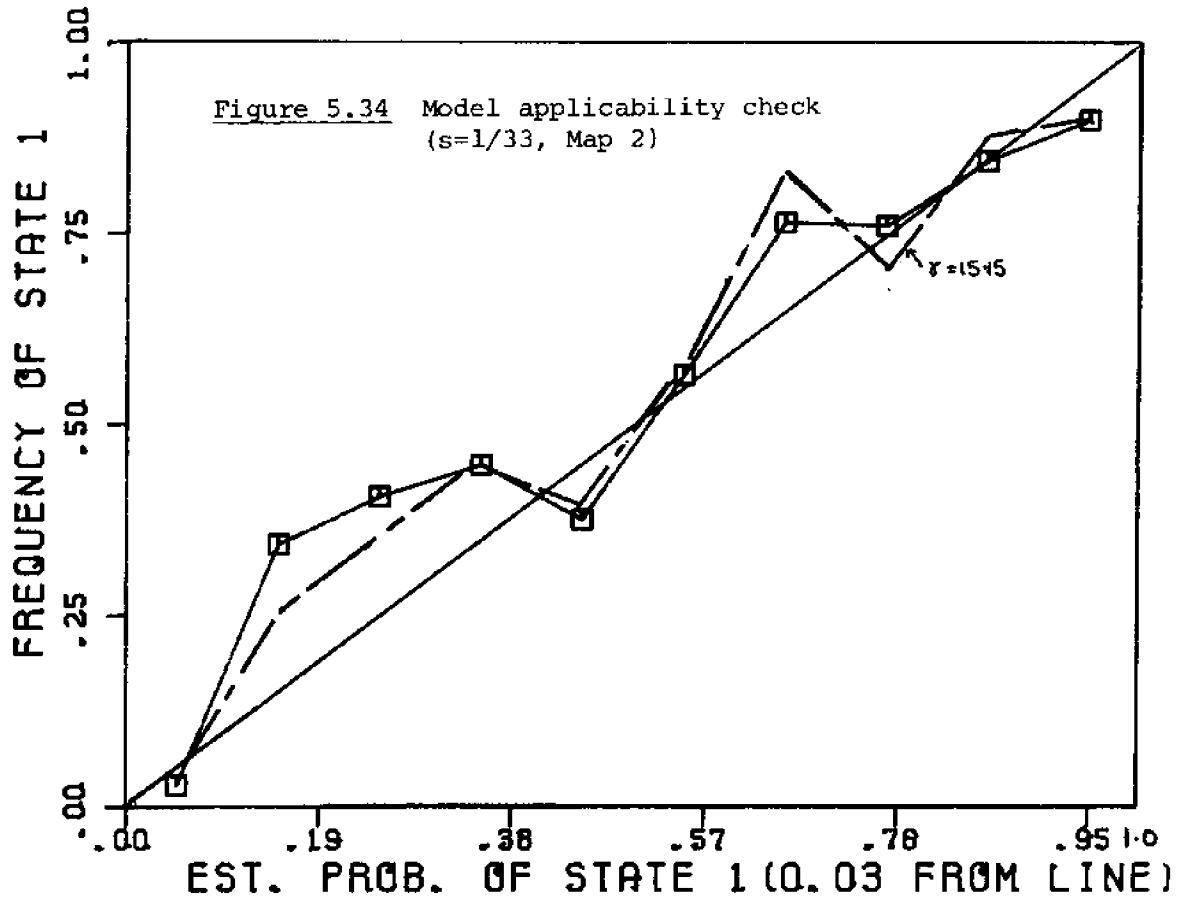

Figure 5.34 Model applicability check
(s=1/33, Map 2)

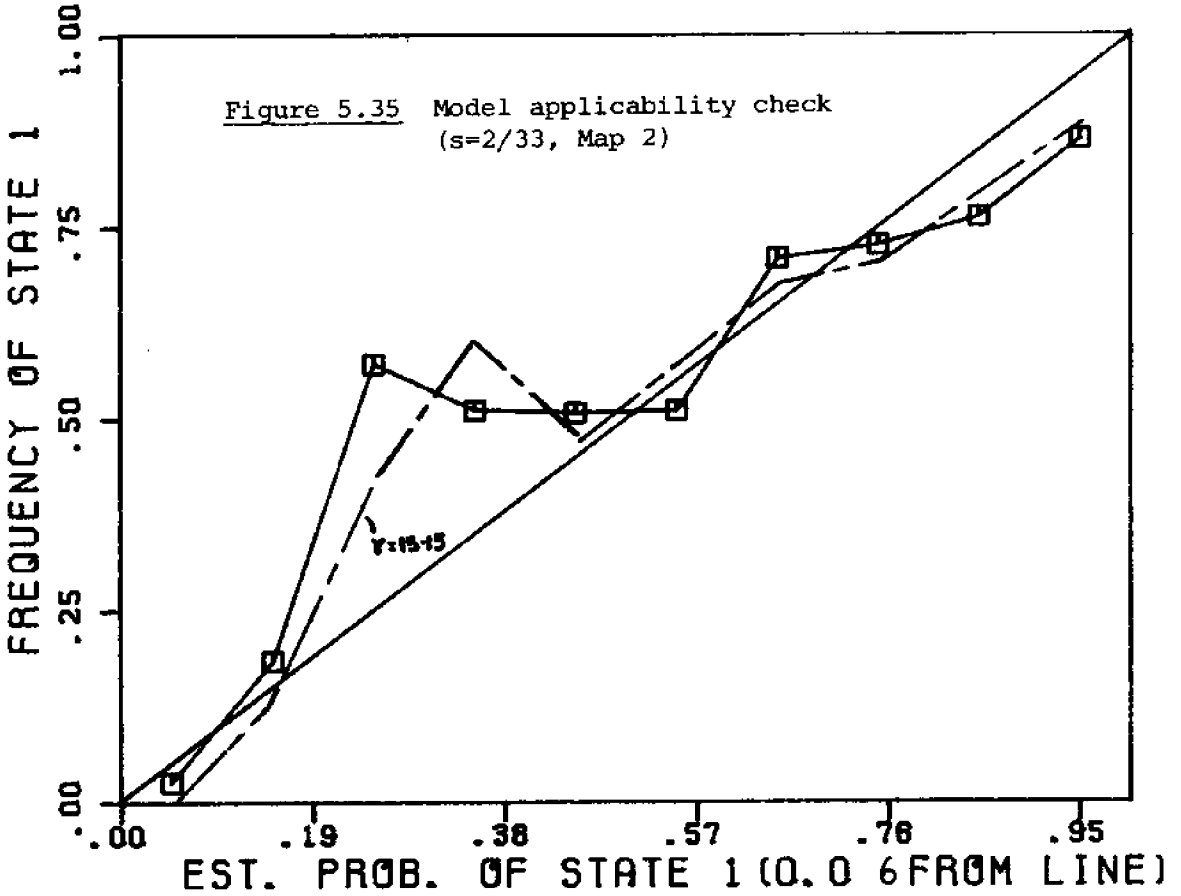

Figure 5.35 Model applicability check (s=2/33, Map 2)

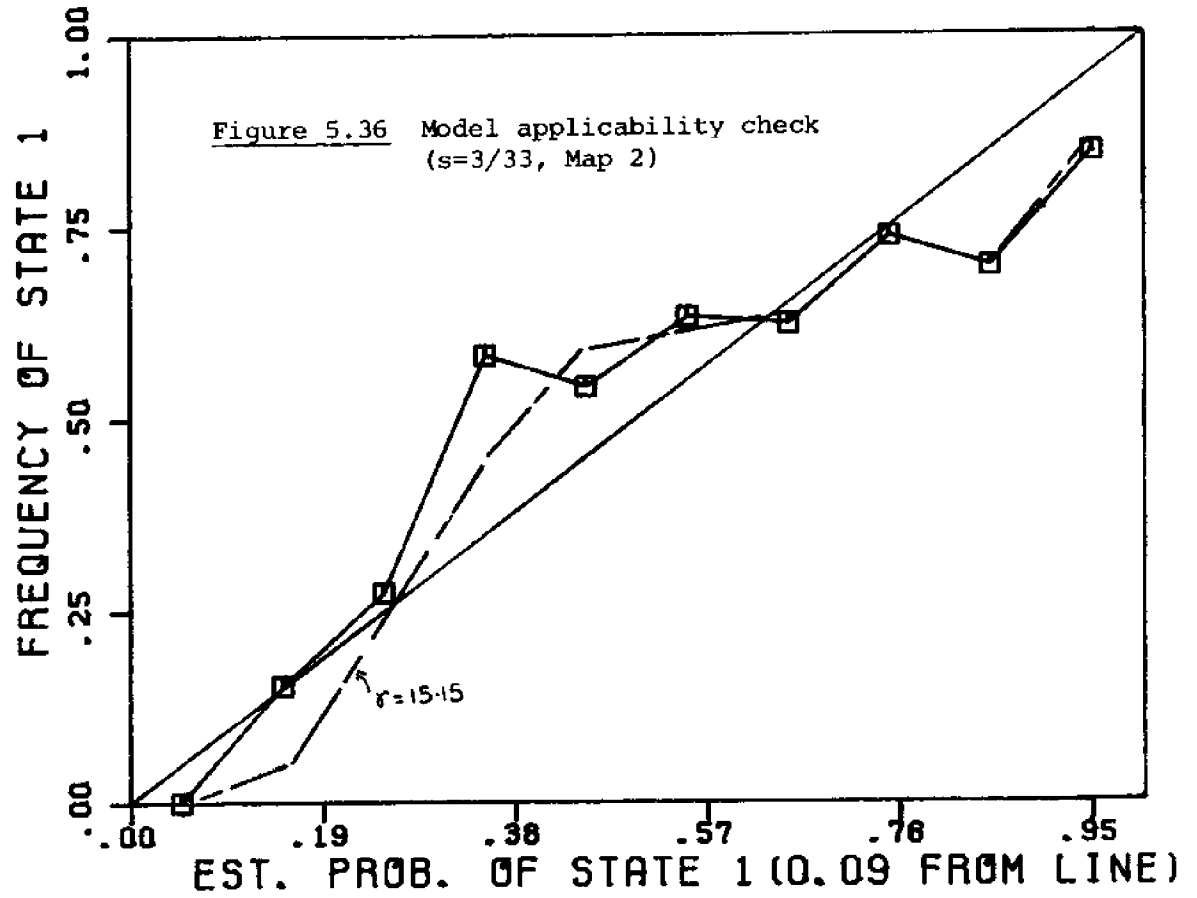

Figure 5.36 Model applicability check (s=3/33, Map 2)

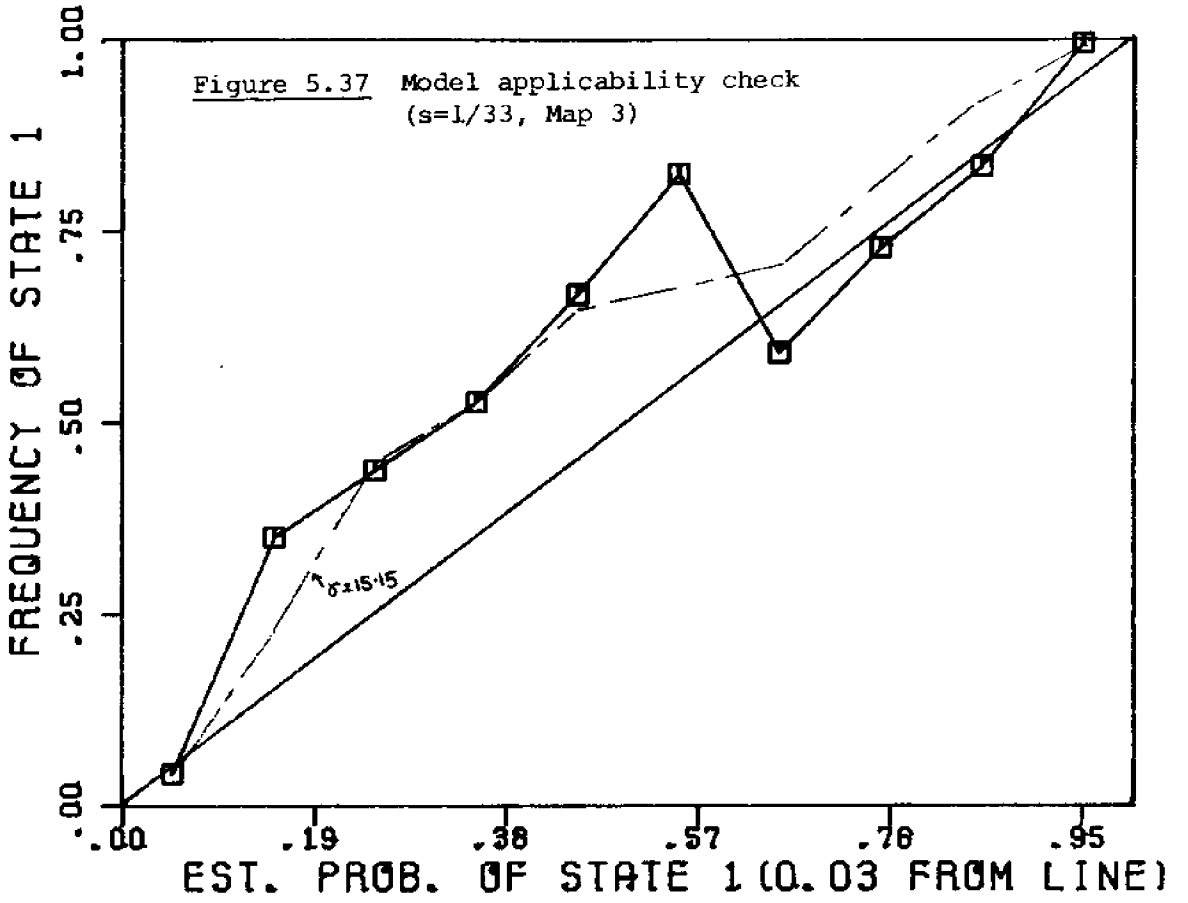

Figure 5.37 Model applicability check (s=1/33, Map 3)

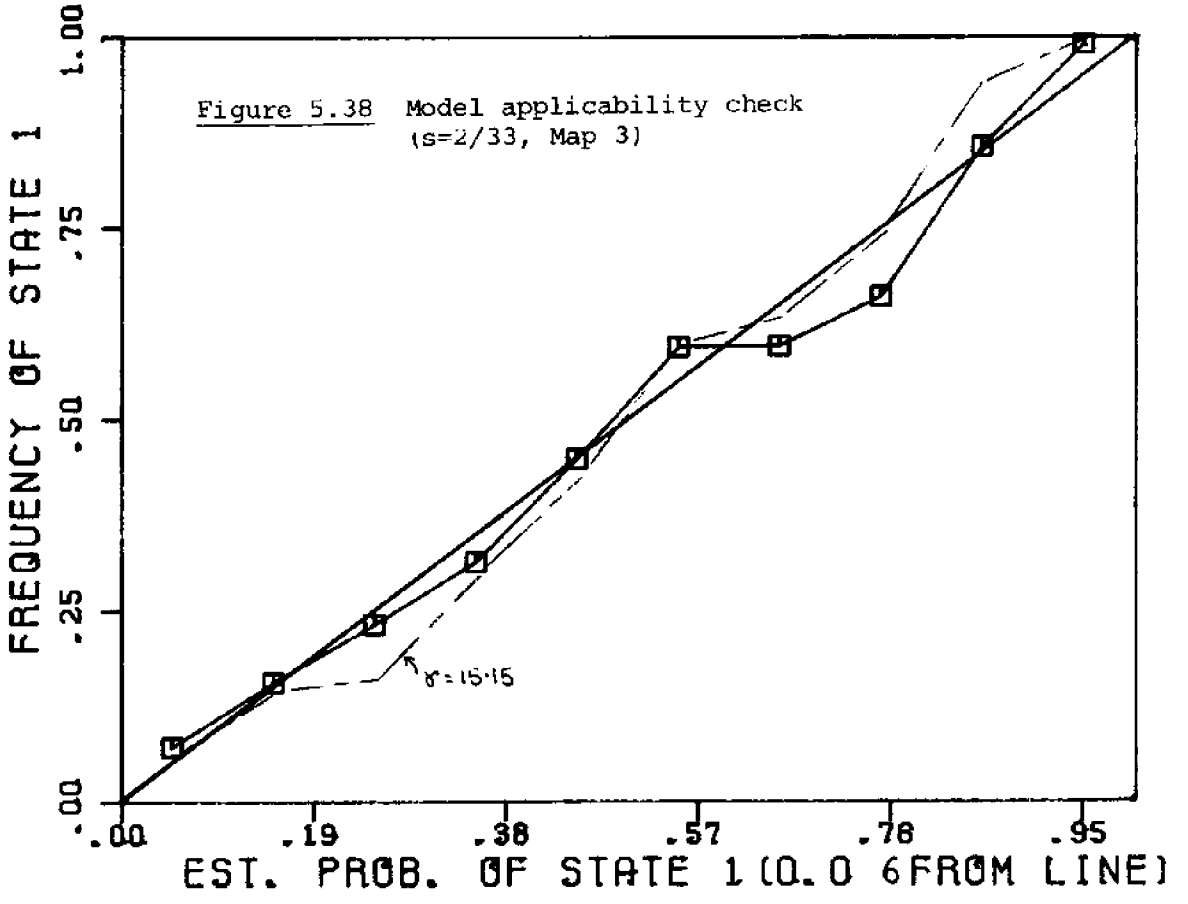

Figure 5.38 Model applicability check (s=2/33, Map 3)

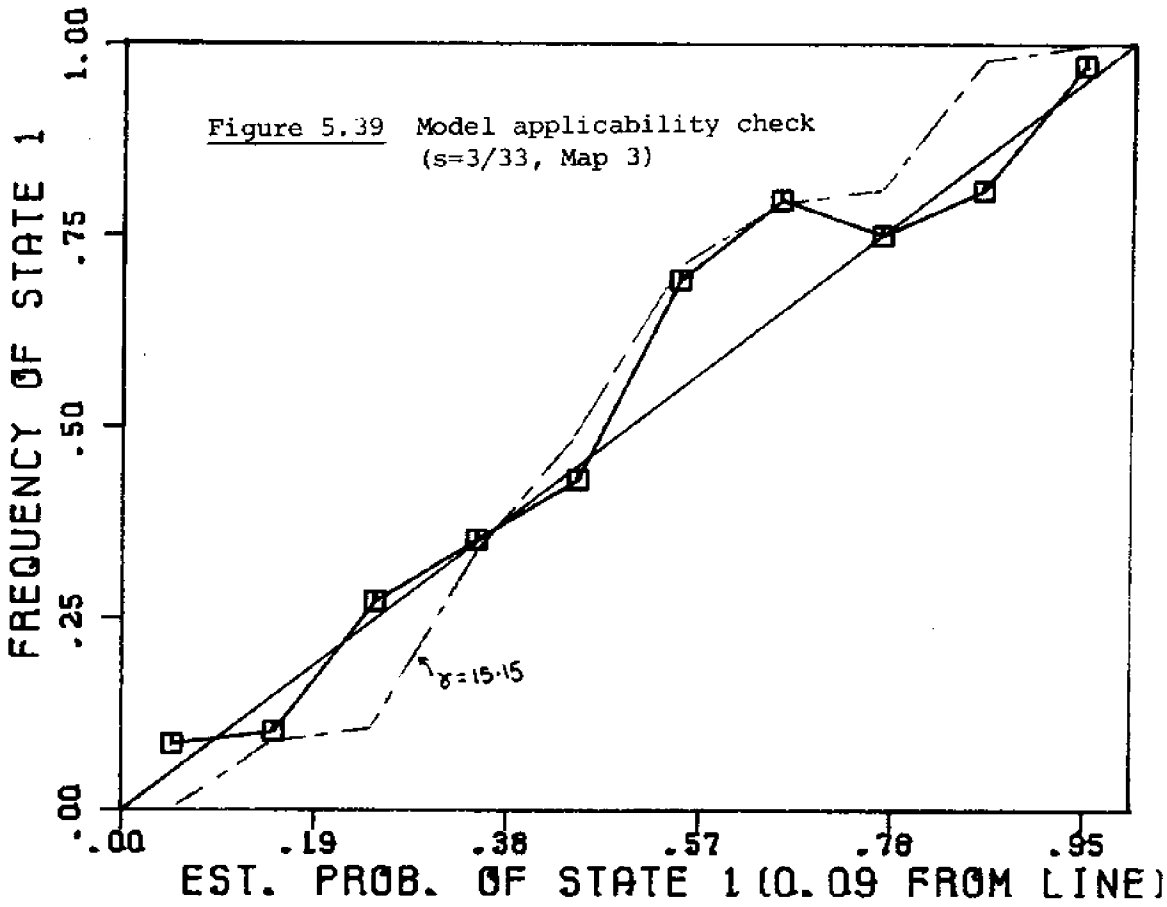

Figure 5.39 Model applicability check
(s=3/33, Map 3)

γ = 15.15 and the curve with the symbol ⊡ is the true experimental curve obtained with the true γ value (γ = 12.41 for Map 2, γ = 8.88 for Map 3). These figures show that the dashed curve correlates well with the ideal curve, therefore indicating that the model seems to apply even when the value of γ is changed from its actual value. The reason may be that the probabilities were estimated for small values of s(s = 1/33, 2/33, 3/33) such that the change in γ has little influence on the applicability of the model.

5.4.4 Probability Variation between Two Parallel Lines

The program to estimate the probability of the region between two known parallel lines is given in Appendix A2. This is a simple variation of the program in Appendix A1. Figures 5.40 to 5.44 illustrate the probability curves obtained along lines parallel to the profile lines. The pairs of lines used to obtain Figures 5.40 to 5.44 are from Map 1 (Fig. 5.6) and are respectively (0-0, 3-3), (1-1, 4-4), (2-2, 5-5), (3-3, 6-6) and (0-0, 6-6). Figures 5.40 to 5.43 show similar probability variation characteristics; large variations are observed near either of the pair of lines (i.e. at y = 0.05 and 0.45), while at the center (y = 0.25), the curve smooths out. The lines in Fig. 5.44 are spaced one unit apart. It is observed that at y = 0.5, the curve is a horizontal line at the prior probability value, indicating that the model is not able to estimate the state of the region

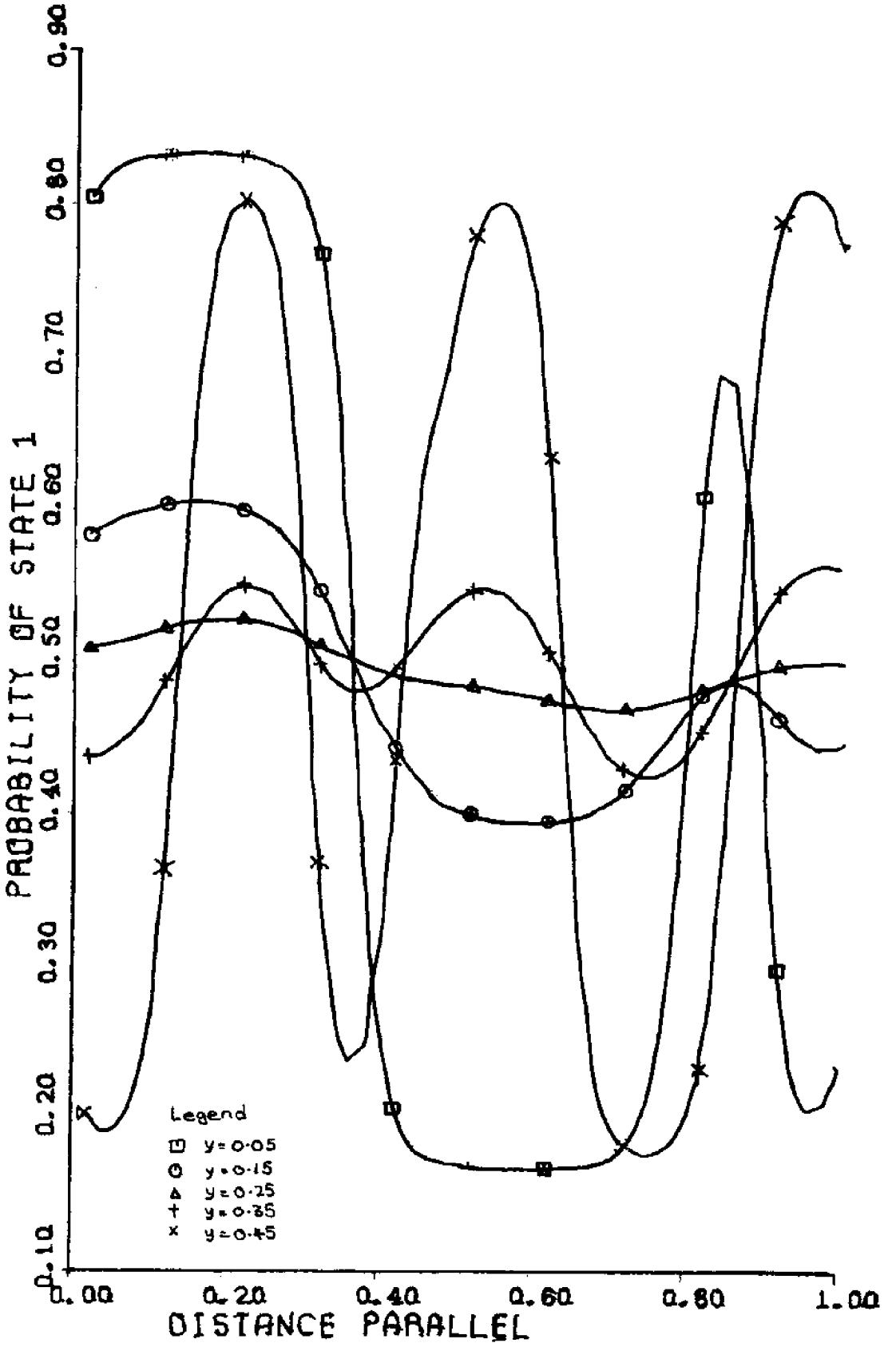

Figure 5.40 Probability variation between two parallel lines (Lines 0-0, 3-3)

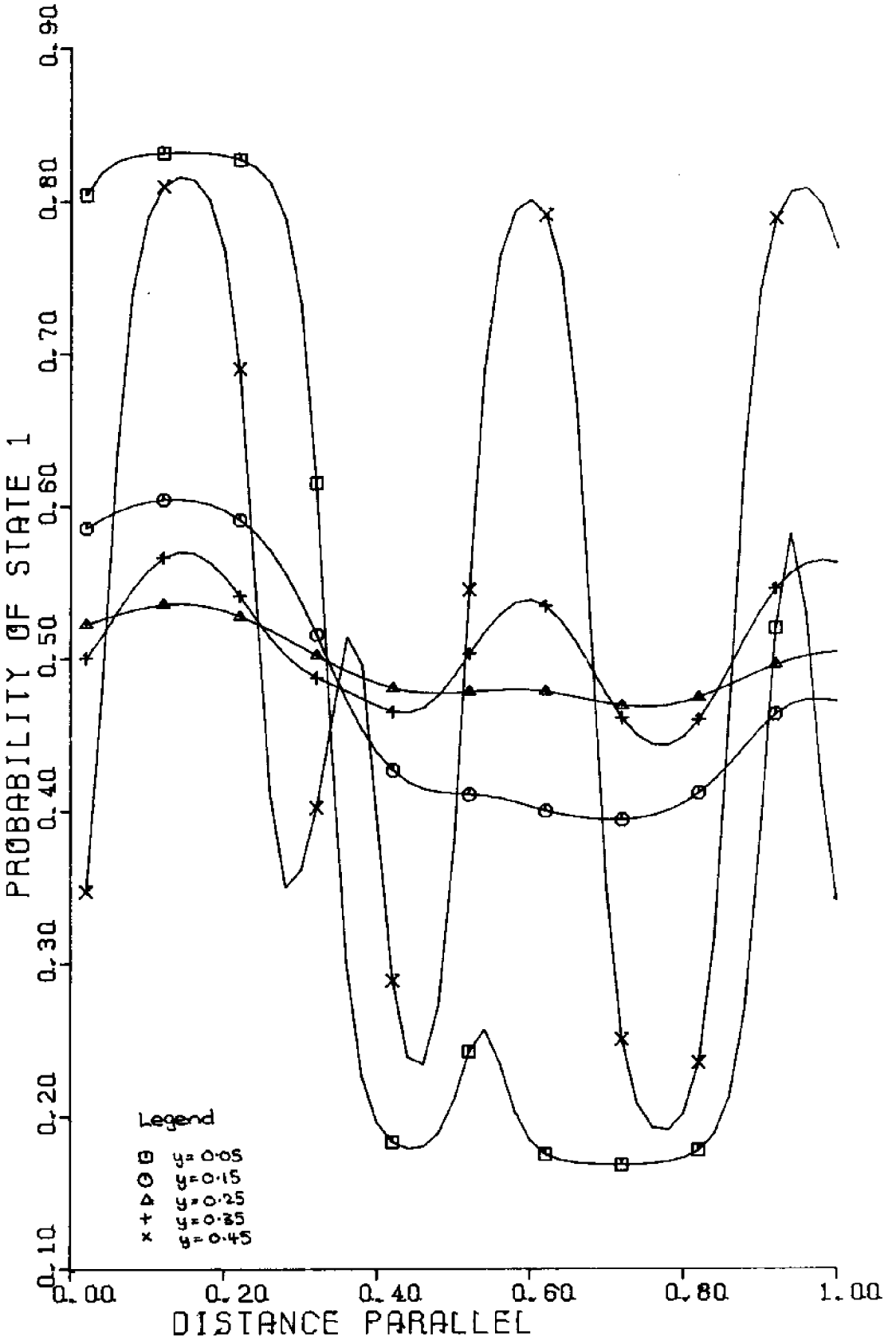

Figure 5.41 Probability variation between two parallel lines (lines 1-1, 4-4)

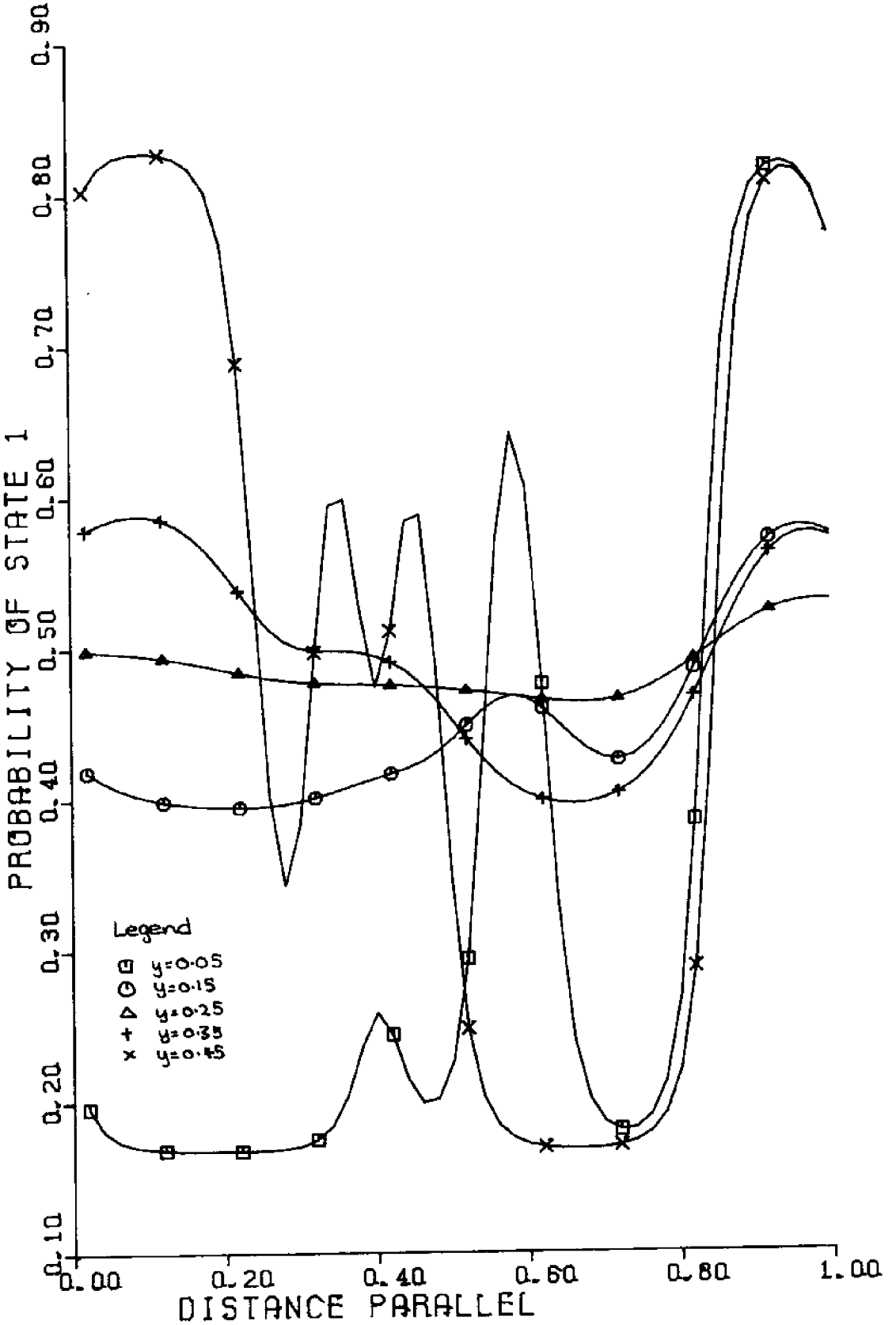

Figure 5.42 Probability variation between two parallel lines (lines 2-2, 5-5)

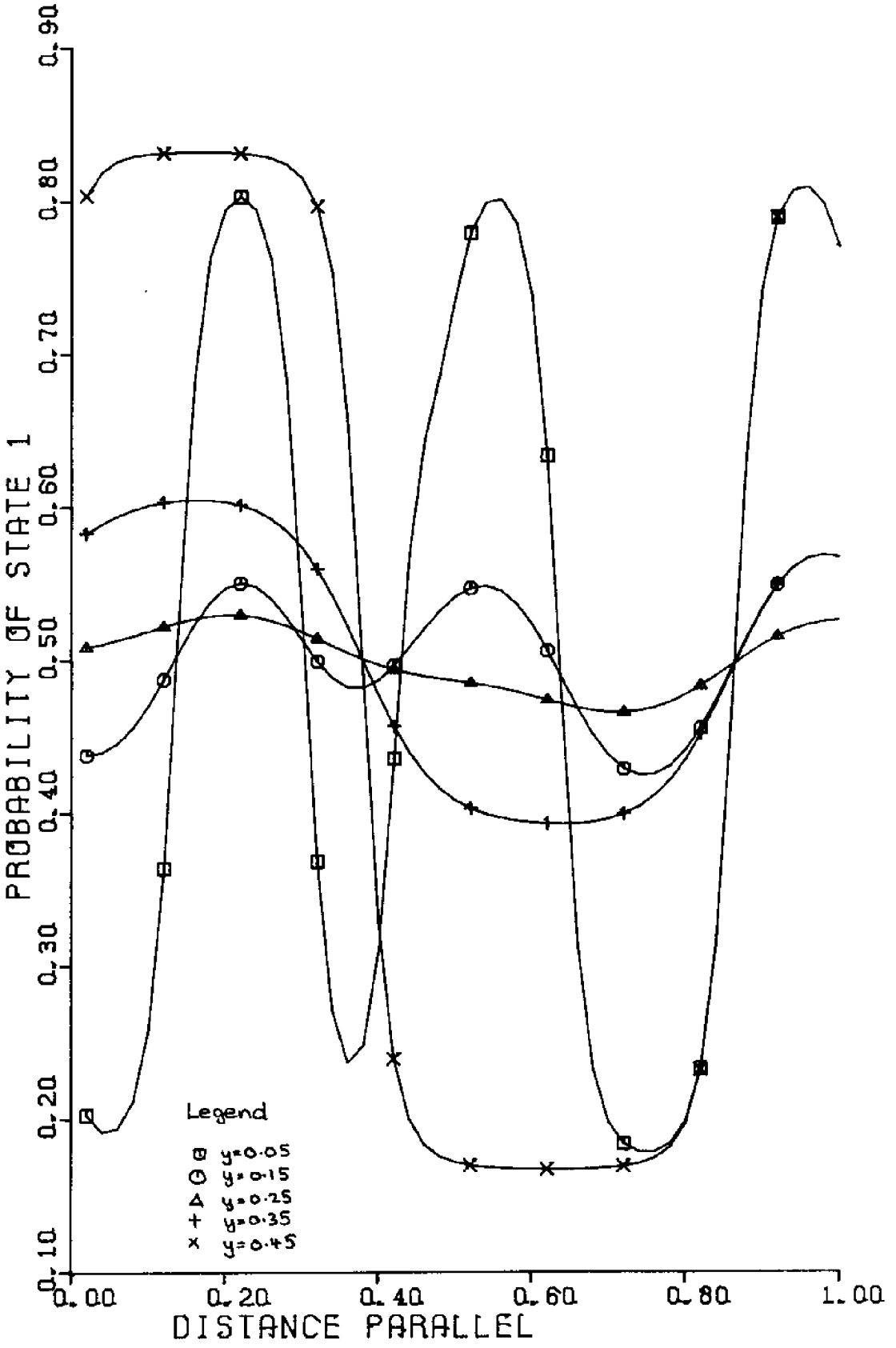

Figure 5.43 Probability variation between two parallel lines (lines 3-3, 6-6)

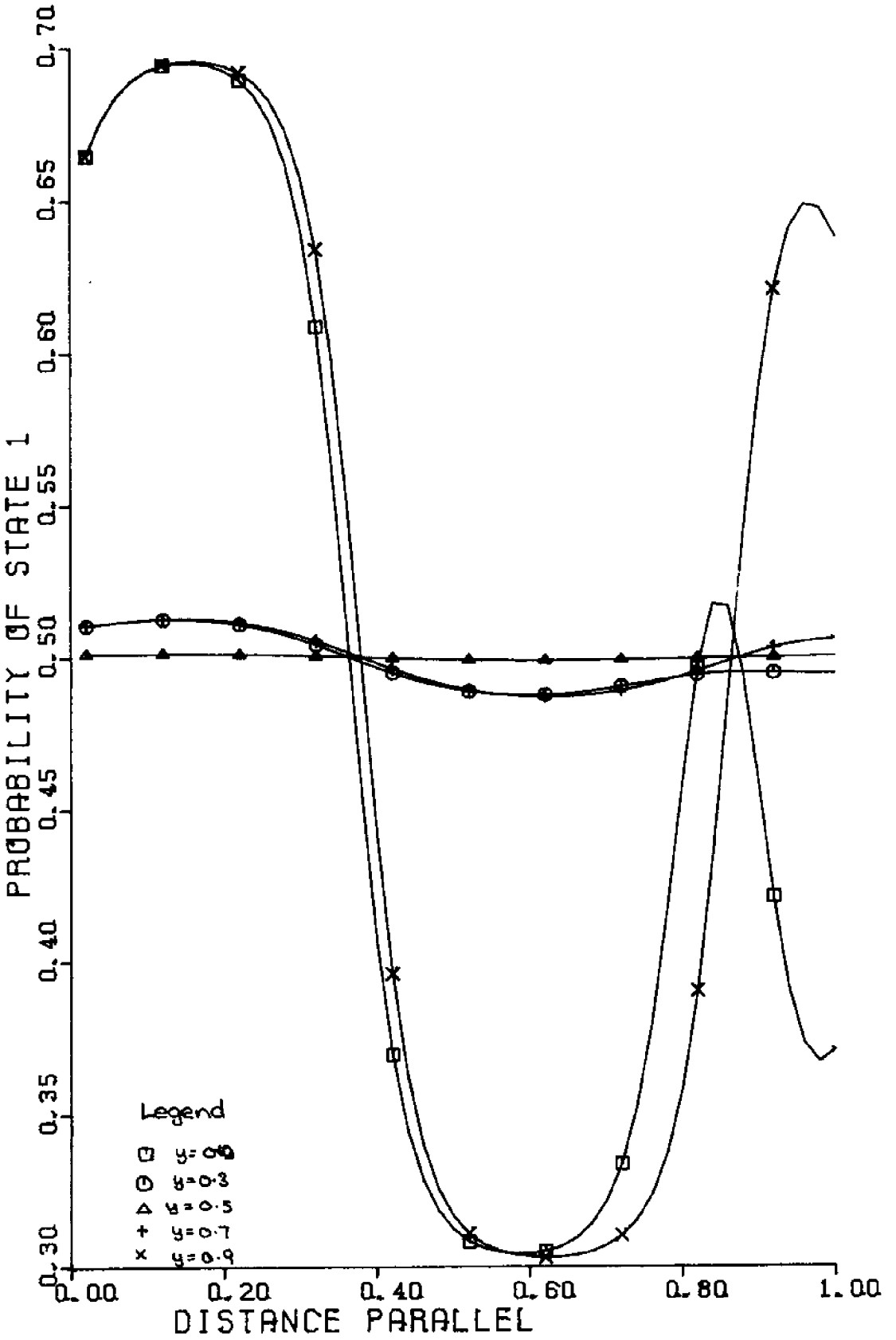

Figure 5.44 Probability variation between two parallel lines (lines 0-0,6-6)

between two lines if the region is 0.5 unit or greater from both the lines, and that at a distance close to one line, the other line has no influence on the predicted probabilities if the lines are spaced greater than or equal to 0.5 units apart. In all cases the line closest to the point of interest, will have the most influence on the predicted state of the point.

A comparison of Figures 5.40 to 5.44 with Figures 5.20 to 5.26 shows that at near distances to either one of the lines, the probability curve associated with single lines is similar to the curve associated with line pairs. This indicates that the model extrapolates well for single lines if the region to be extrapolated is close to the line, i.e. one need not have line pairs to achieve the same extrapolation advantage.

5.4.5 Maps

Figures 5.45 to 5.53 give the estimated maps for Map 1, Map 2 and Map 3, for three line-pair spacings (s = 1/3, 1/11, 1/6). These maps are obtained by estimating the posterior probability of 66 x 66 elements within the entire map and drawing the [1] where the posterior probability exceeds 0.5. The prior probability used in the model is obtained by calculating the spatial frequency of state 1 on each of the line-pairs, thus the 'prior' changes for every line-pair considered. This involves the assumption that the region

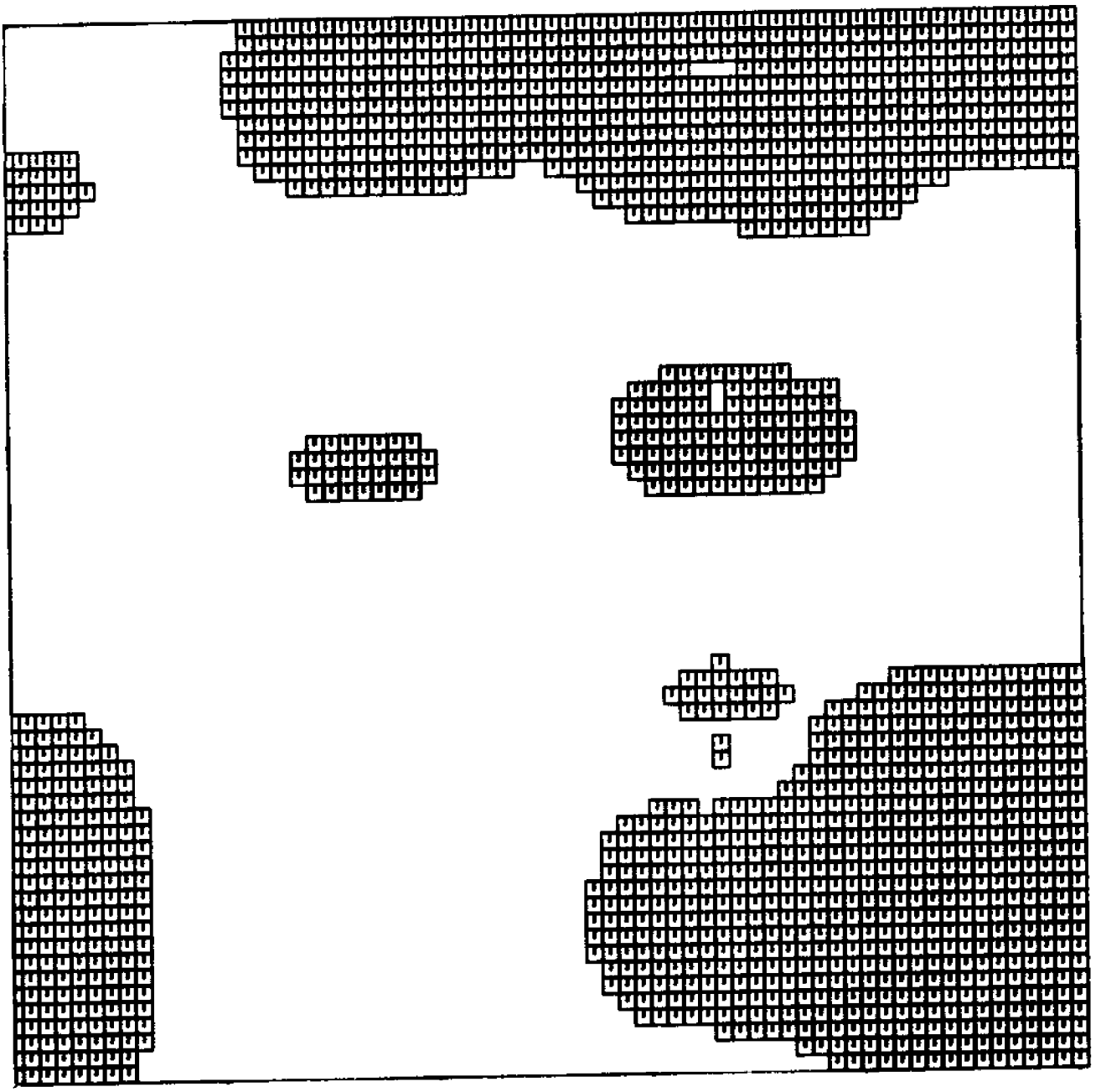

Figure 5.45 Estimated map for Map 1, s=1/3.

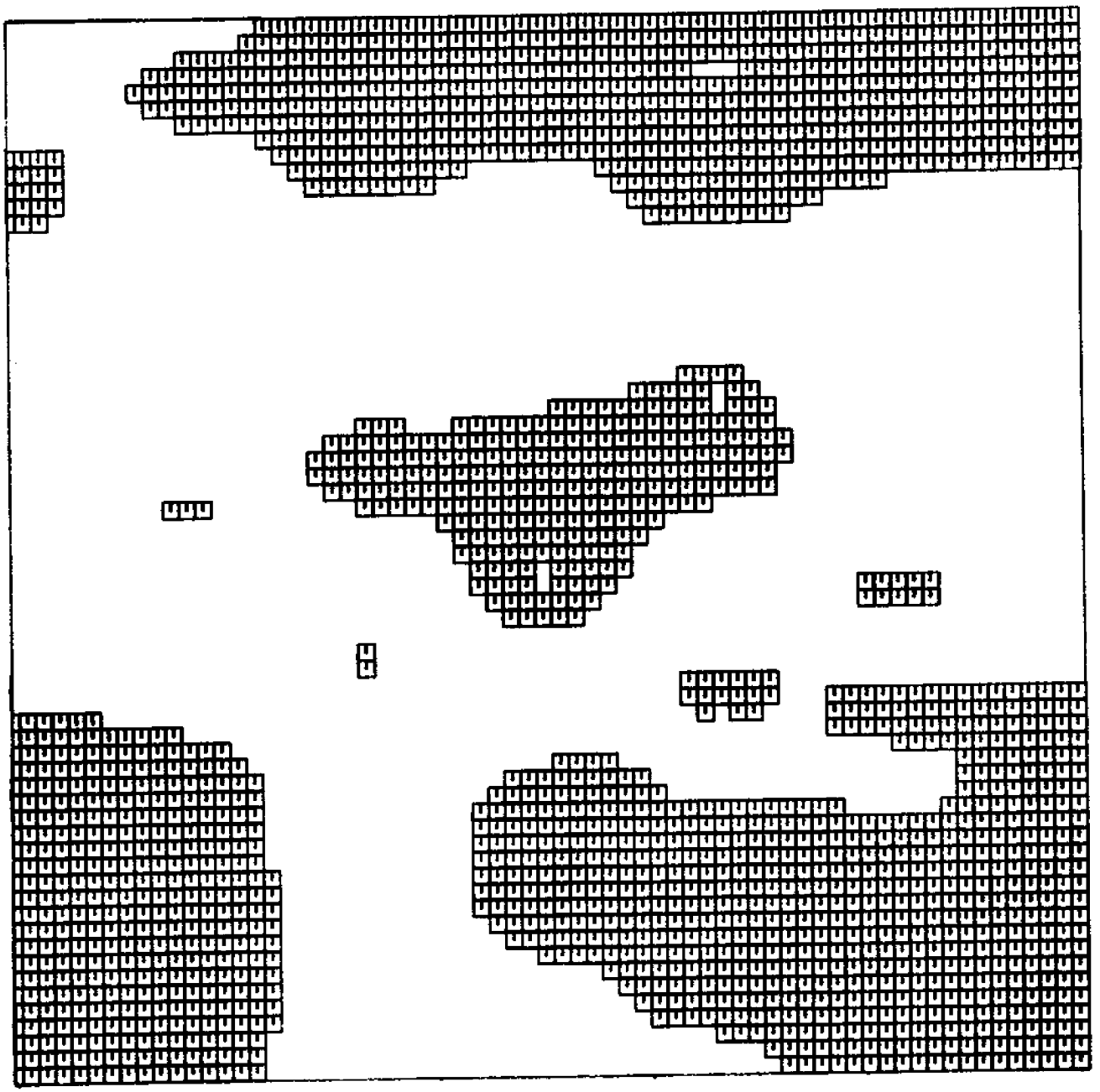

Figure 5.46 Estimated map for Map 1, s=1/6.

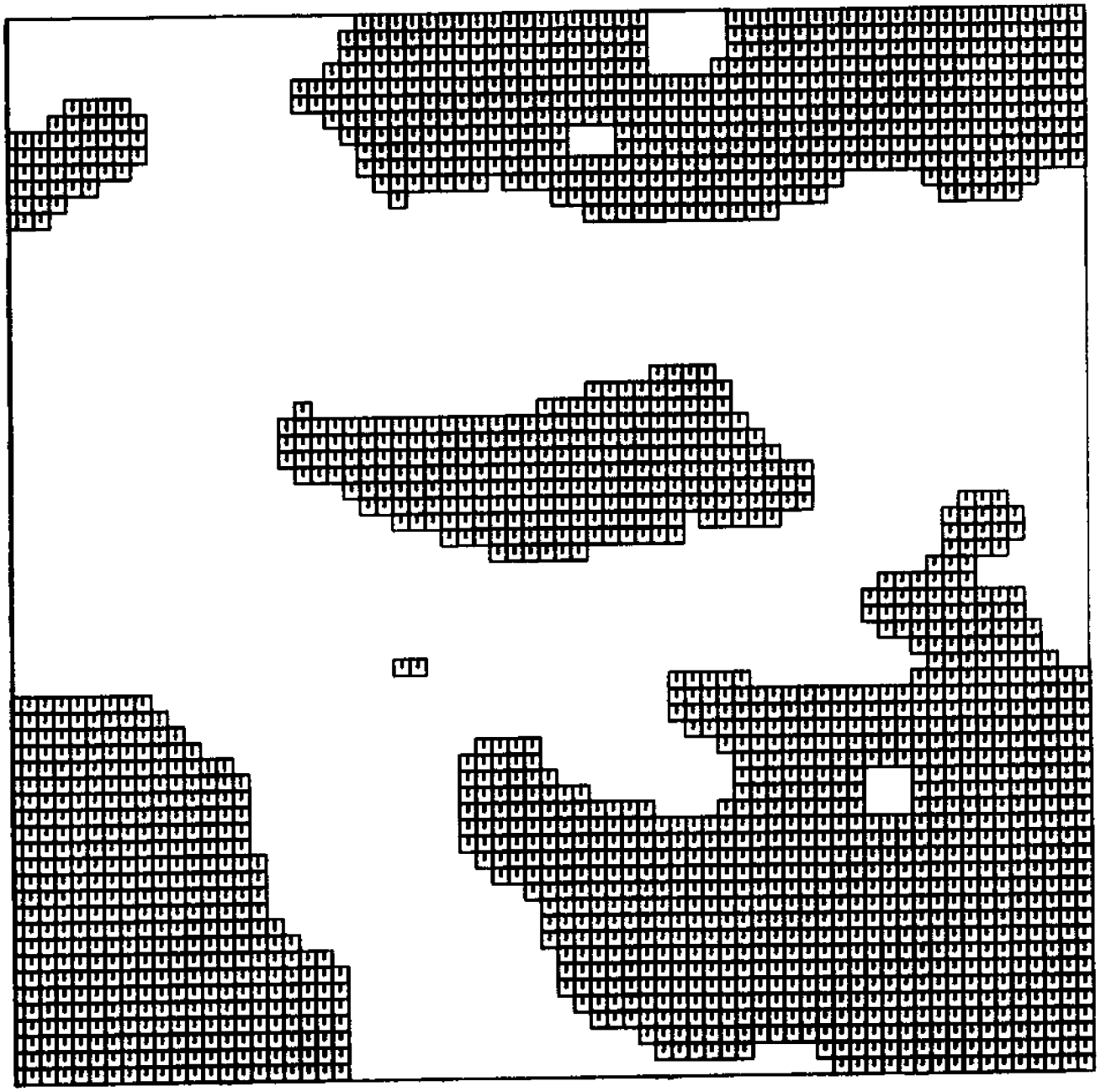

Figure 5.47 Estimated map for Map 1, s=1/11.

Figure 5.48 Estimated map for Map 2, s=1/3.

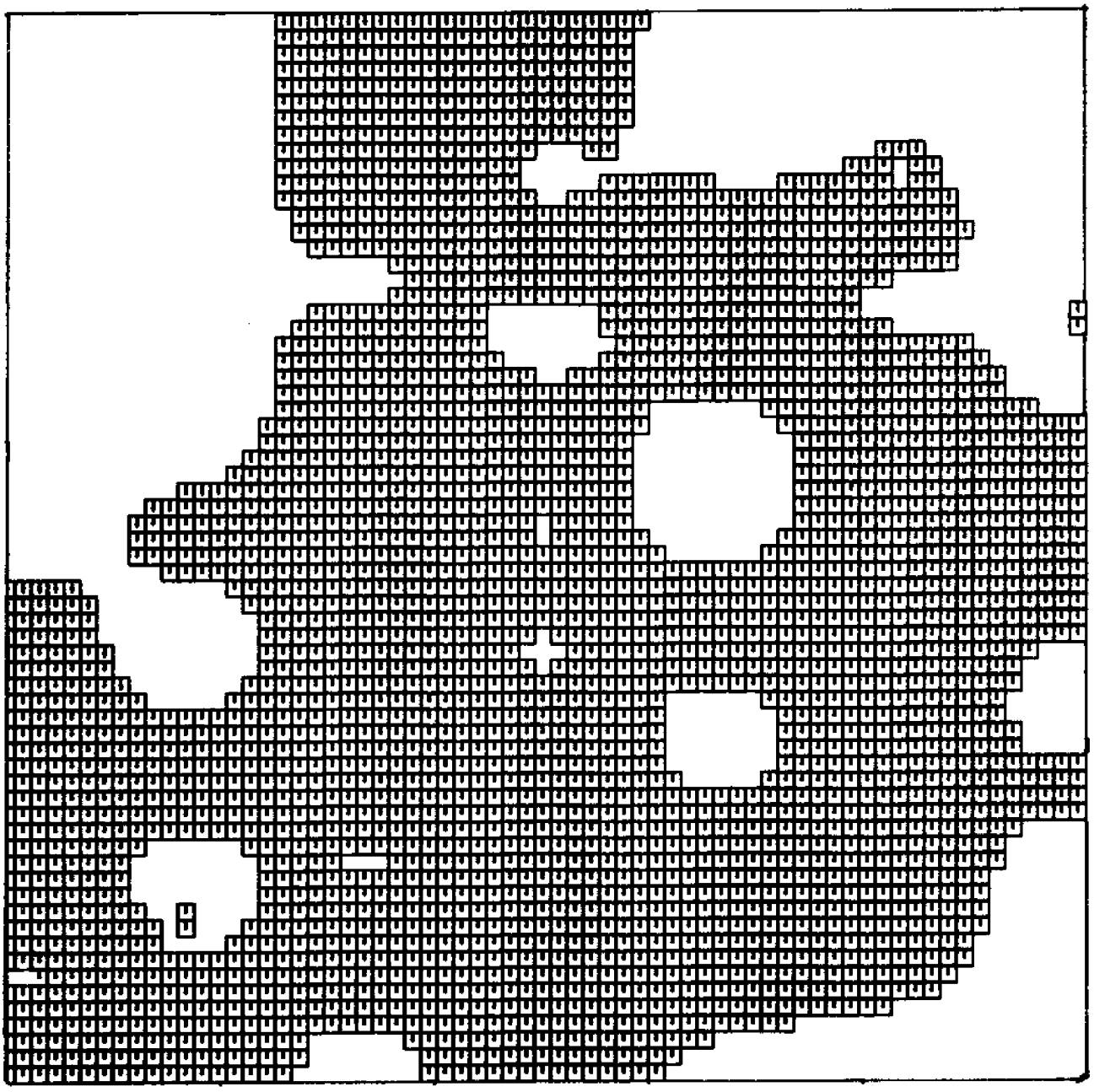

Figure 5.49 Estimated map for Map 2, s=1/6.

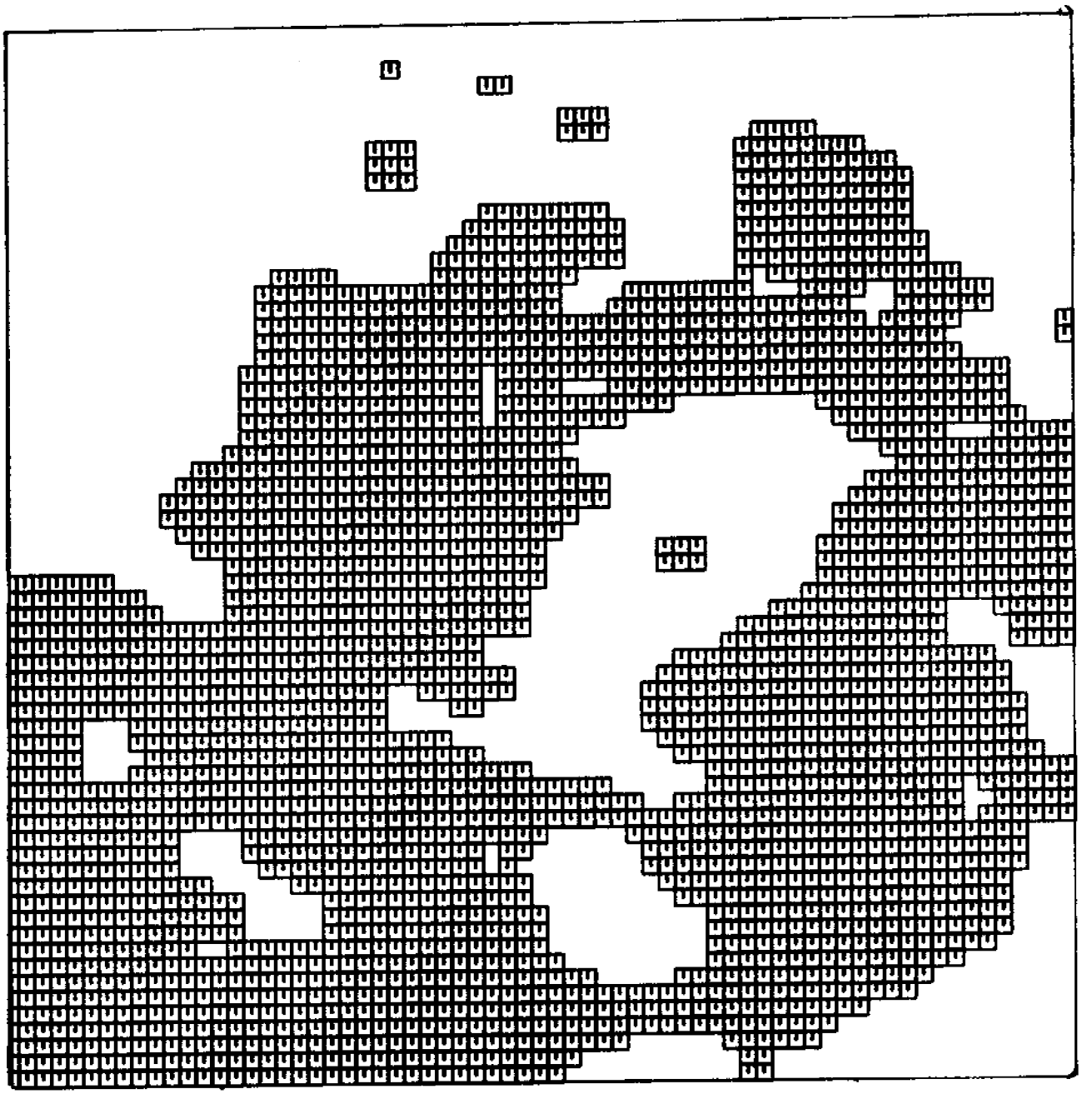

Figure 5.50 Estimated map for Map 2, s=1/11.

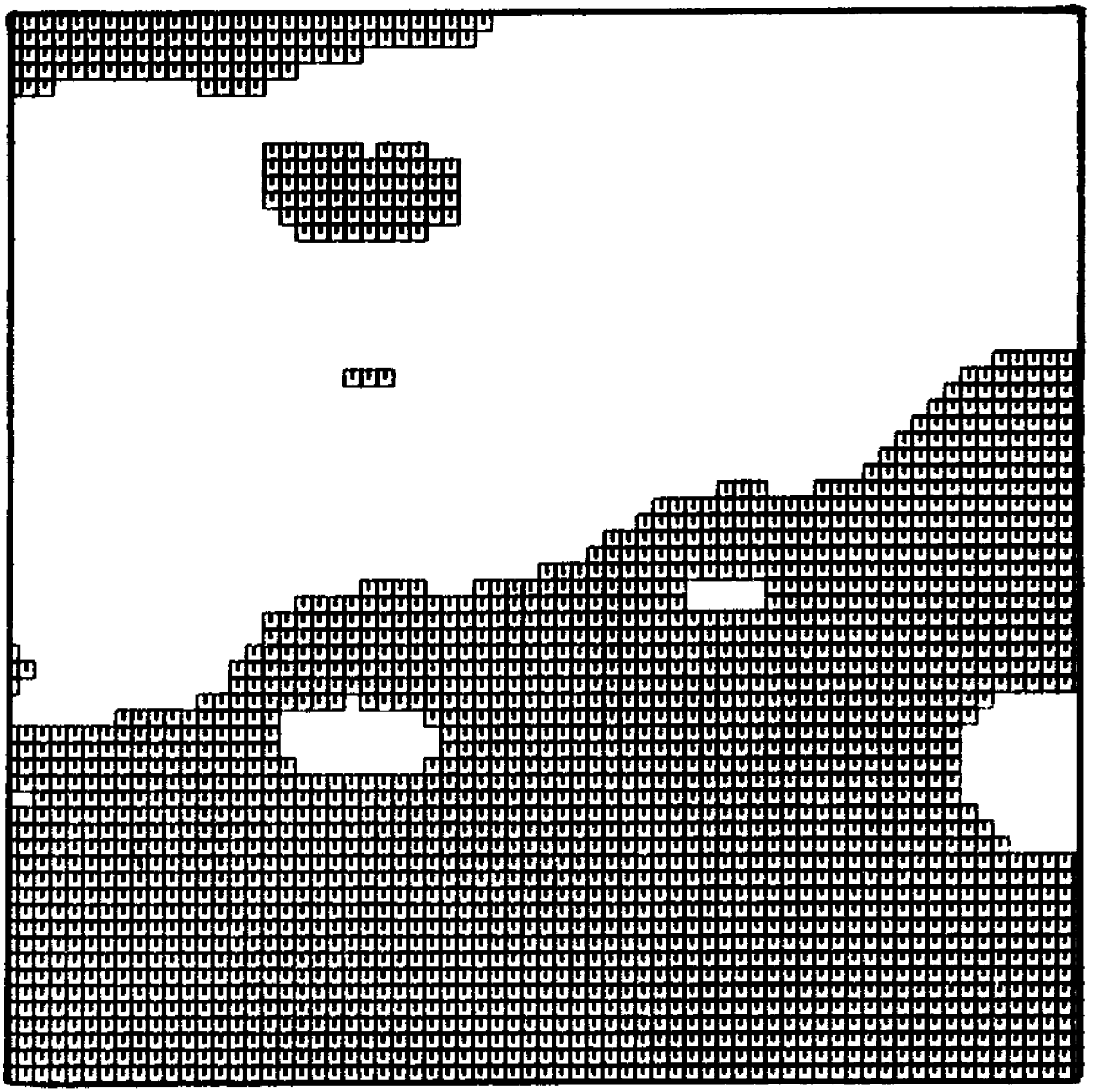

Figure 5.51 Estimated map for Map 3, s=1/3.

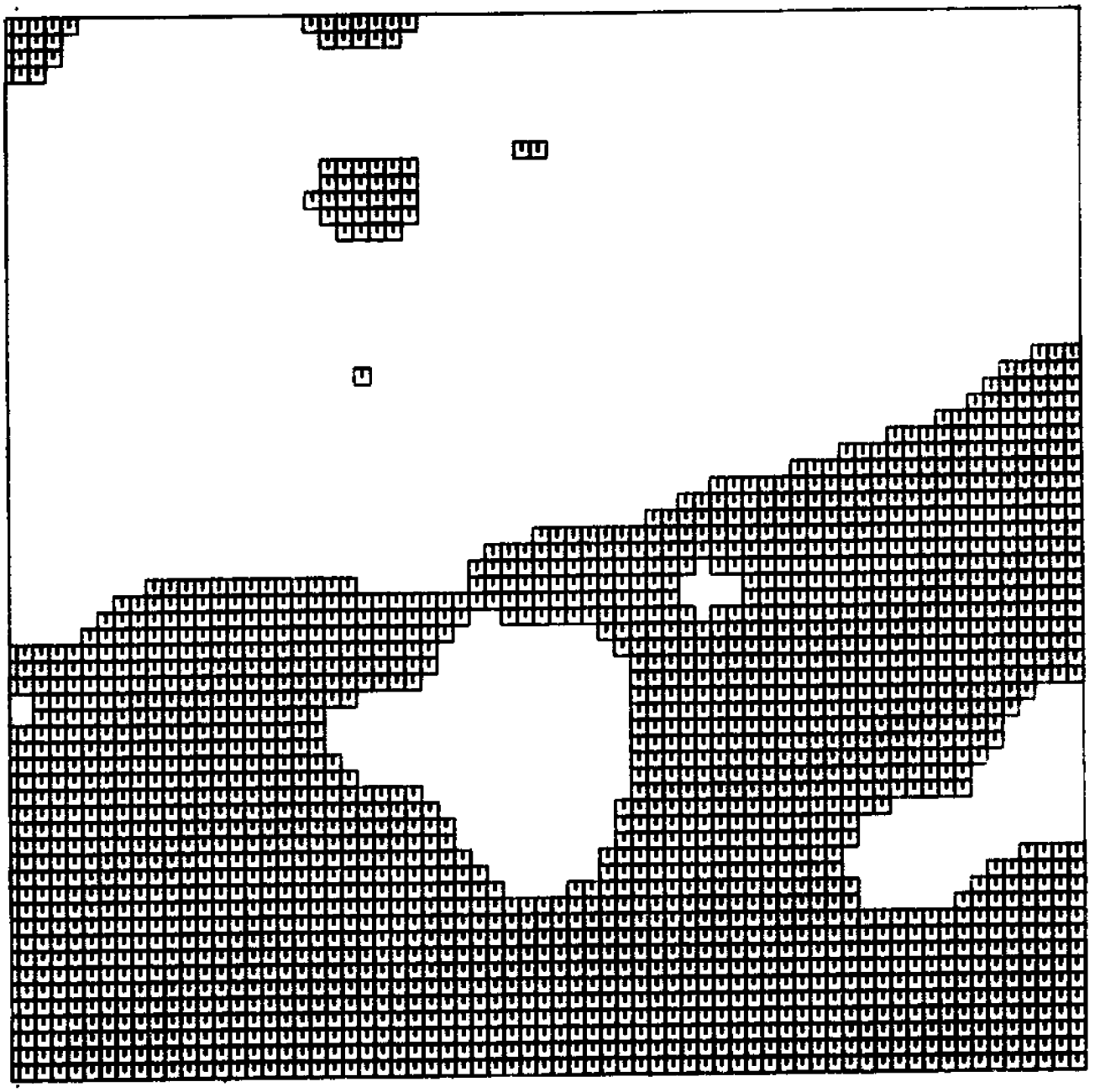

Figure 5.52 Estimated map for Map 3, s=1/6.

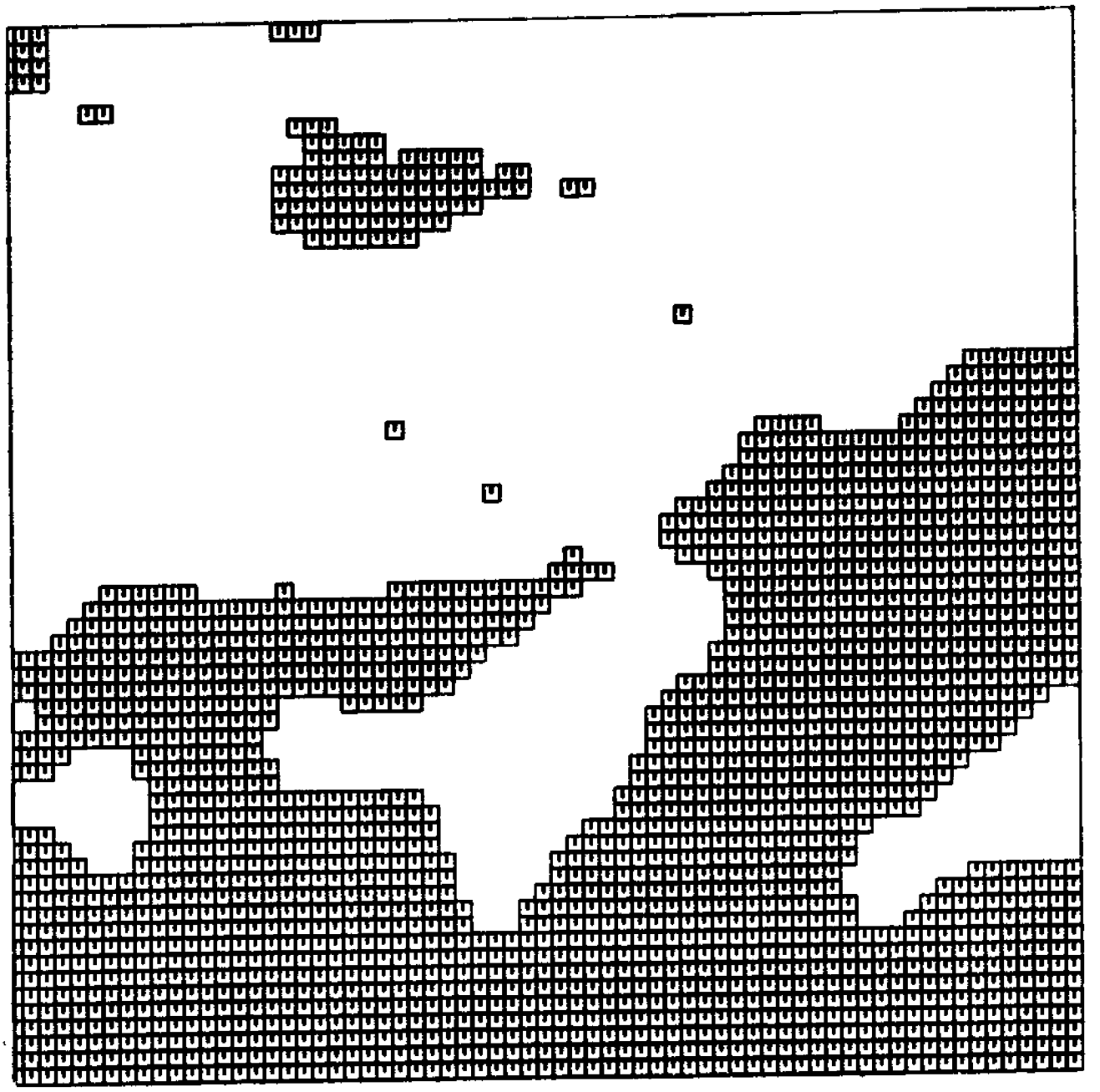

Figure 5.53 Estimated map for Map 3, s=1/11.

enclosed by each line-pair is an exclusive block (with the line-pair as the only known data) and is independent of neighboring blocks .

Comparison of Figures 5.45 to 5.53 with Nucci's estimated maps shows that this model gives better refinement to the maps and is more accurate (discussed with reference to misclassified area below). The model produces lower errors where small regions and uneven shapes are present.

Table 5.1 gives the predicted misclassification errors and actual misclassification errors for all the estimated maps. The predicted error is obtained by use of the following equation:

$$\text{Predicted Error} = \frac{1}{n} \sum_{1}^{n} (1-P_{max}) \qquad (5.38)$$

where $n = 66 \times 67 = 4422$

P_{max} = larger value of $[P_i, 1-P_i]$

The table indicates:

1. The smoother the symmetry and the larger the regions on the map, the smaller the actual error. Map 3 has the smoothest and largest bodies and therefore has the smallest predicted and actual errors. Map 2 has lots of small bodies and most asymmetric configurations, hence the largest actual and predicted errors.

Table 5.1

Tabulation of Predicted Error and Actual Misclassification Error for Figure 5.45 to 5.53

Map	Figure	S	Predicted Error %	Actual Error %
	5.45	1/3	13.2	9.5
1	5.46	1/6	8.5	6.3
	5.47	1/11	4.5	3.8
	5.48	1/3	13.7	18.7
2	5.49	1/6	9.6	13.6
	5.50	1/11	6.4	9.7
	5.51	1/3	10.2	8.6
3	5.52	1/6	5.2	5.5
	5.53	1/11	3.2	3.9

2. A smaller value of γ would be expected to yield smaller misclassification errors. Table 5.1 shows, however, that although Map 2 has a smaller γ value than Map 1, its misclassified area is actually larger. This is not sufficient to disqualify the value of small γ because the contradiction is probably due largely to Map 2 having a very irregular configuration and lots of small bodies.

3. The actual errors are generally small, most falling below 10%. The misclassification errors are mostly less than that obtained by using discrete sampling points (Section 5.2).

Figure 5.54 shows a plot of actual error vs. predicted error. The line Actual Error = Predicted Error forms a good regression line for the plotted points.

The Actual Error was plotted against log (spacing) in Figure 5.55. The figure shows that a linear relationship existed (for the limited data) between log spacing and actual error. The regression equations for the three lines are

$$\text{Map 1} \quad \text{Log}_e(S) = 0.23\ AE - 3.27 \tag{5.39}$$

$$\text{Map 2} \quad \text{Log}_e(S) = 0.15\ AE - 3.78 \tag{5.40}$$

$$\text{Map 3} \quad \text{Log}_e(S) = 0.29\ AE - 3.52 \tag{5.41}$$

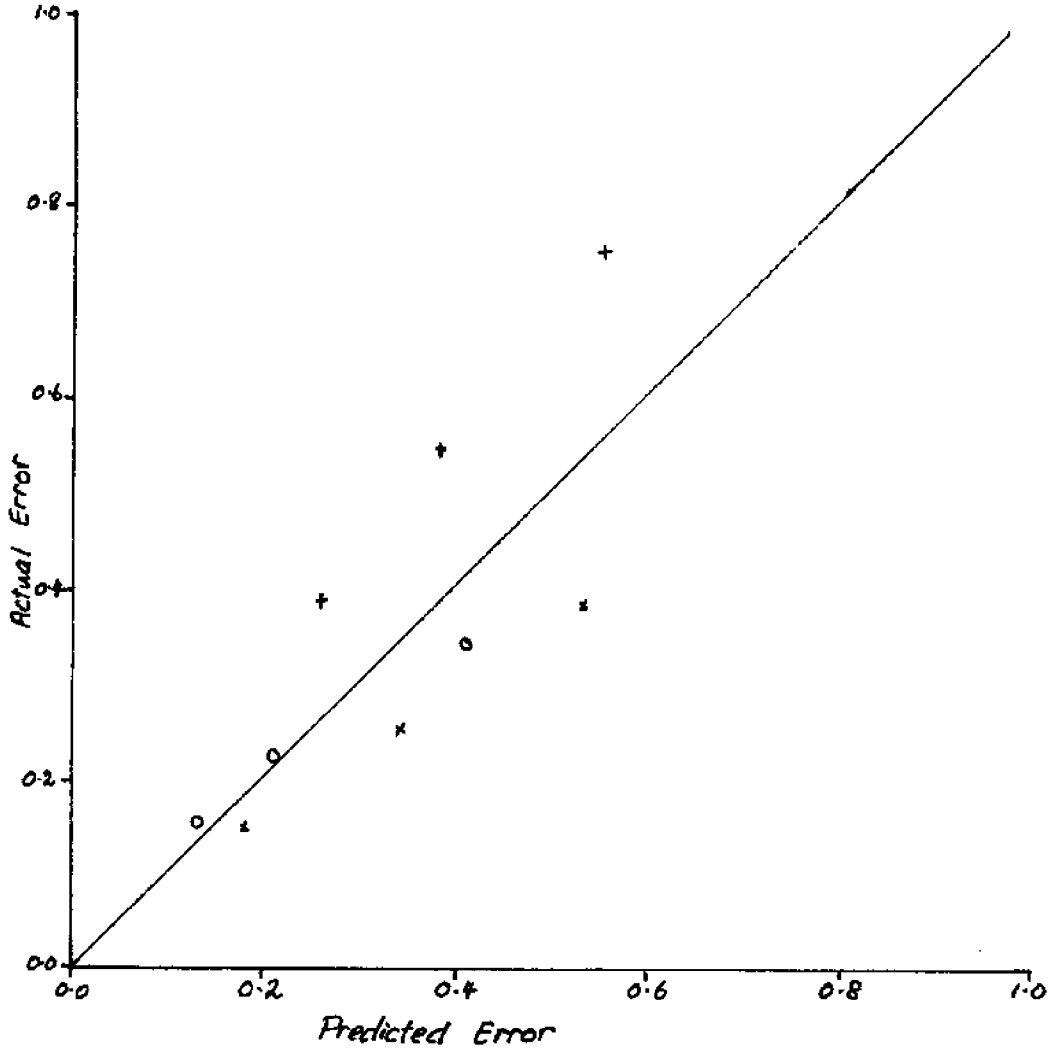

Figure 5.54 Plot of actual error vs. predicted error.

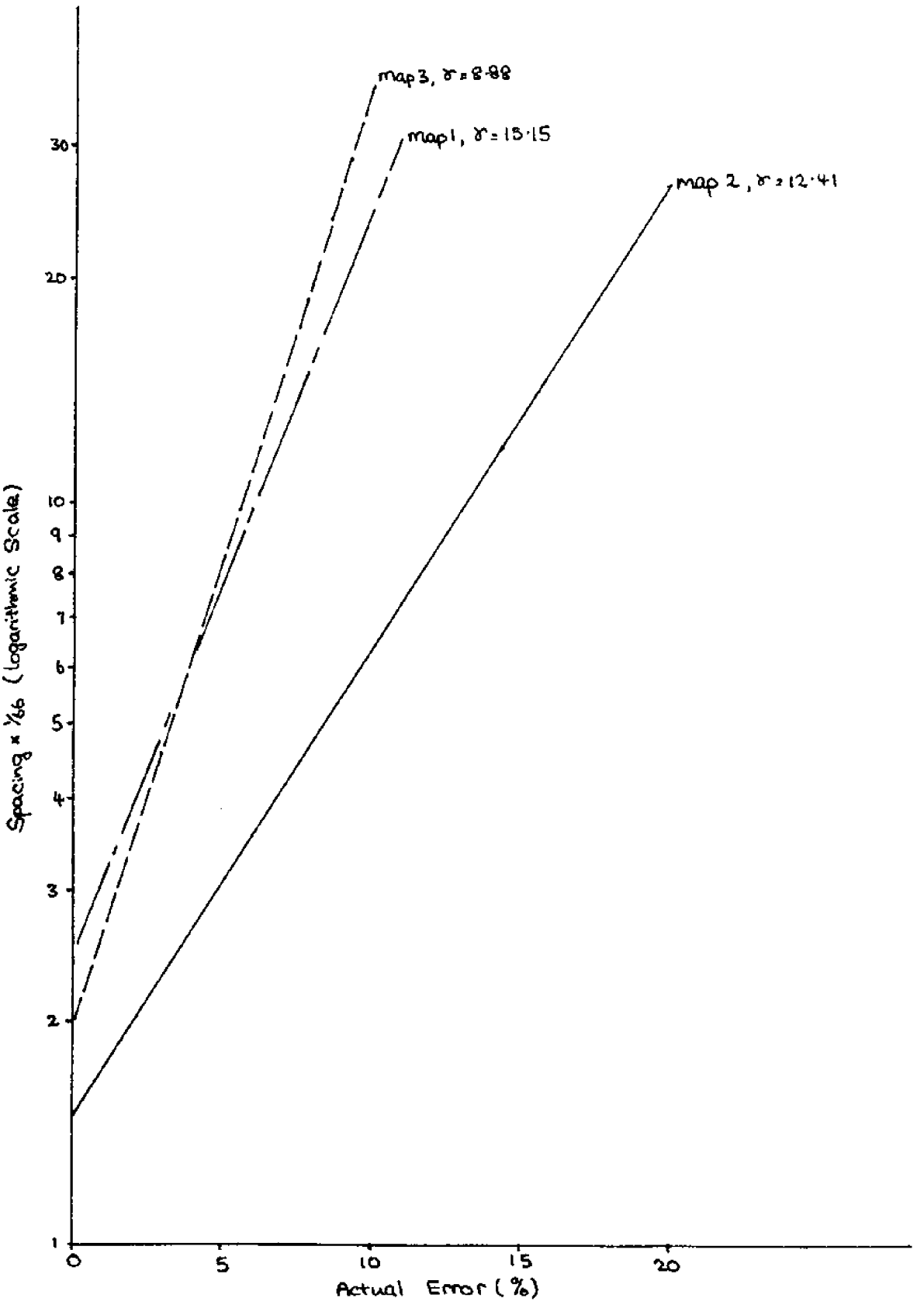

Figure 5.55 Plot of log (spacing) vs. actual error.

5.5 Conclusion

Acoustic profiling is the most frequently used method of obtaining information about the soil below the ocean bottom because it is the least expensive technique, can cover wide areas rapidly and is fairly reliable. To establish the states of the region between profile lines, the conventional method is by drilling boreholes. This operation is very expensive and covers only limited area. The computer program using the model allows the region to be mapped with reasonable accuracy (as was shown in Section 5.4), and the prospector can then choose, by looking at the estimated map, regions in which to drill boreholes or not to drill at all. The Government can also use the model to estimate the mineral potential of its offshore lands and to use this information to formulate development programs for its Outer Continental Shelf Lands. These arguments therefore establish the economic judgement that the model helps to achieve.

The model also helps to provide scientific judgement. When used to map over a very wide area, scientists can use the model to study the geological trend of the macro-region. These studies can be used to support or to refute their hypothesis of the geological form of the region.

6. A Policy Analysis of the OCS Leasing

6.1 Introduction

The OCS (Outer Continental Shelf) is defined as those portions of offshore lands beyond the three mile limit for the majority of coastal states. It is estimated that more than one third of the United States' oil resources available for the future will most likely be discovered in the OCS regions. This is important since U.S. dependence on foreign oil is so heavy that unreliable supply can create severe economic and social disruption in our society.

Exploration involves two major steps, geophysical surveys and exploratory drilling. In offshore land leasing, the Department of Interior's Bureau of Land Management specifies areas for intended lease based on both industry and government estimates of potential reserves and other factors. Then follows a period of accelerated collection and analysis of geophysical data from the specified region by both the United States Geological Survey and private companies to determine the best prospects for drilling and the amounts of reserves expected. Until the late 1970s, no exploratory drilling (which is the only means of determining the certain existence of oil deposits) was allowed. From the geophysical information, the value of each tract offered was estimated and opened to the highest bidder above this value.

Up 'til the end of the 1970s the 1953 OCS Lands Act provided wide authority to the Secretary of the Interior in regulating OCS development activities. During the 1970s however, the philosophy of this Act, which was based on the assumption that there would be few future OCS activities, became obsolete when faced with the burst of interest (caused by the Arab Oil embargo of 1973) in the OCS's oil resources. The Santa Barbara oil spill of 1969 caused widespread ecological damage to the Californian shores and the 1953 Act was not able to provide for precautionary and cleanup measures. State authorities were infuriated because they had no jurisdiction over and received no revenues from OCS exploitation off their shores. The Santa Barbara incident lit the fuse for intense lobbying by state authorities, environmentalists and certain interest groups to have Congress review the law. The issues that called for changes in the 1953 Act were the desire of state authorities to participate in the decision-making process in OCS development activities off their shores; the need to separate exploration from production and to try different leasing strategies so that maximum public return from OCS development could be obtained; the need to have precautionary and clean-up provisions in the Act in the event of side effects from OCS activities; and the general desire to update the Act.

The pressures for reform cumulated in the passing of the OCS Lands Act Amendments of 1978 and the signing into law by President Carter the same year. This chapter will examine the

leasing provisions of the OCSLAA, the strategies available to the Interior Secretary in formulating his OCS leasing policies and the evaluation of these stratigies.

6.2 The Outer Continental Shelf Act Amendments (1978); Provisions for Alternative Leasing Systems

The OCSLAA was signed into law on September 18, 1978, after nearly four years of arduous effort by Congress to amend and revitalize the OCSLA of 1953. Among the provisions of this amended Act are

- Section 201(a) defines lease as to not only lease for exploration, development and production, but also to allow a leasing system involving separate leases for exploration and then for subsequent development and production.
- Section 8(b)(4) specifies that any proposal to offer a lease just for exploration, or just for development and production or for exploration and partial development and production must be submitted to Congress which would have thirty days to review the proposal. Congress, by a joint resolution of disapproval, could then prohibit issuance of such a lease.
- Section 206 grants clear authority to the Interior Secretary to authorize any type of exploration before a lease sale, including private exploration, or public exploration, directly or by contract.

All the three sections of the OSCLAA (1978) described above are amendments to the OSCLA (1953). They represent a recognition by Congress that the traditional method of leasing OCS lands had been inadequate in achieving three basic objectives,

1. orderly and timely resource development
2. protection of the environment
3. receipt of a fair market value return for leased resources

The amendments and an examination of the legislative history of the OCSLAA (1978) indicate that Congress expects the Department of the Interior to look into new and efficient ways of managing OCS resources; to experiment with new systems of leasing OCS lands so that orderly and timely resources development can be achieved; and to study the feasibility of separating exploration from development so that more complete information of a lease potential can be obtained before bidding is opened for development of the lease area. With more complete information on the potential of lease areas, the value of the area can be more accurately assessed, thus assuming a fair market value return for the leased resource. State and local authorities whose jurisdiction are onshore of the lease prospects will be able to plan more adequately for environmental and social impacts of expected offshore oil development and production.

Prior to the Amendments, the amount of acreage (called a tract) that is leased out to individual bidders was fixed at 5760 acres. There is concern in Congress that this amount of acreage may lead

to inefficient exploration and development; and increased administrative burden to both the government and potential leasees. Section 205 of the Amendments eliminates the prior absolute limitation of 5760 acres and provides that a lease can cover any larger area that will make a reasonable economic production unit, thus allowing whole structures or geological traps to be leased.

6.3 Choices of Leasing Systems

This section examines the options available to the Secretary of the Interior in formulating OCS leasing policies. The options will be examined as a general choice model and will be divided into three scales, namely macro, intermediate and micro. The macro-option looks at the oil supply situation as a whole, the intermediate option examines the choices for leasing policies on OCS lands and the micro-option looks at the methods in which leasing systems can be used in an optimum manner. The last two options (i.e. intermediate and micro) consider three basic questions.

1. Will the policies help achieve an orderly and timely resource development of the OCS?
2. Is the public receiving an adequate return for the potential resources being leased to the oil firms?

3. Are there safeguards to ensure that the expected boom in offshore petroleum operations does not cause environmental damage or have any adverse impacts on adjacent coastal regions and communities?

Subsection 6.3.1 considers the macro-option, subsection 6.3.2 the intermediate-option and subsection 6.3.3 the micro-option.

6.3.1 Macro-option

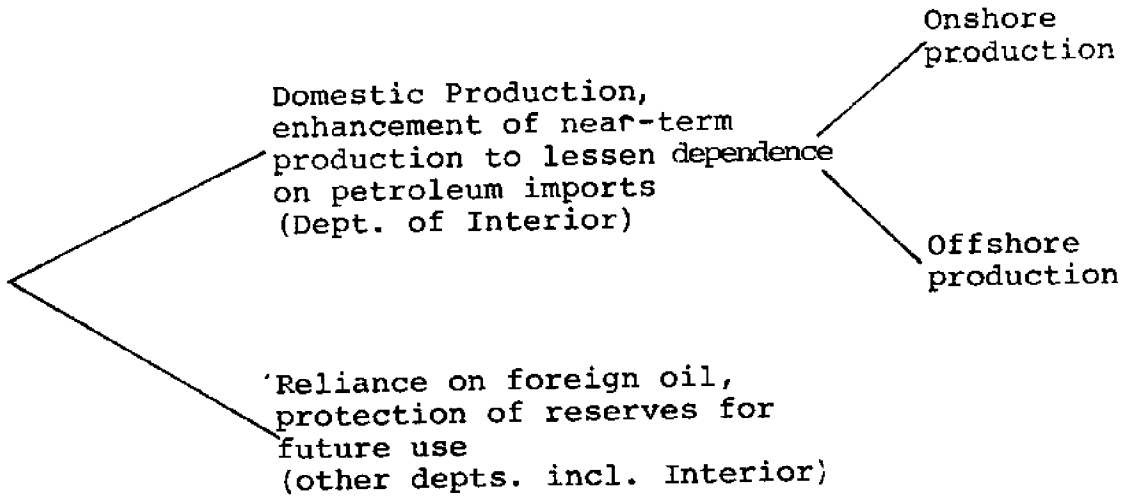

Figure 6.1: Macro-option policy choice

Figure 6.1 illustrates a policy issue usually confronted by the President of the United States, and several departments in addition to Interior (for example, Commerce and State). The reliance on foreign oil option allows domestic reserves to be protected for future use. This option is, however, not socially desirable because it places the country in a national security risk should the oil supply be cut off suddenly; it

creates an unfavorable international balance of payments to the United States; and it destroys incentive to search for an alternative source of energy (example fusion energy and solor energy) because if an alternative source of energy is discovered, then the value of the domestic reserves will be reduced and the initial decision to rely on foreign oil will be a bad decision. The second option, enhanced domestic production, will not create the three problems just mentioned.

The Domestic production is categorized into two divisions, i.e. onshore production and offshore production. Onshore oil resources of the United States have been well documented, and it is expected that no more large oil fields, that will have a significant effect at satisfying domestic demand, will be discovered. Large oil fields are expected to be discovered only on offshore lands and various estimates have indicated that more than half of the United States' existing oil resources exist offshore on the continental shelf. However offshore production presents a risky issue to the Interior Department. The particular characteristics of offshore production that create high potential risks are listed below.

1. Unlike onshore production, side effects (such as spills and blow-outs) from offshore production are carried by the waves to the coastal regions and can cause widespread damage to the coastal ecology. Rough sea conditions often make the control and monitoring of these accidents more difficult

than at onshore fields when spills and blowouts are localized and can be closely monitored and controlled.

2. Because of the difficult operating conditions, high design uncertainties in ground and wave conditions, and high cost of construction, offshore development often incurs much higher cost than onshore development.

The central issue in offshore development is therefore the availability of sufficient geological information of offshore lease areas such that the surrounding uncertainties of offshore development can be reduced. Subsection 6.3.2 shall consider various policy options for leasing offshore lands, with the view that the best option should provide the most amount of useful geological information prior to leasing for development and production.

6.3.2 Intermediate-option

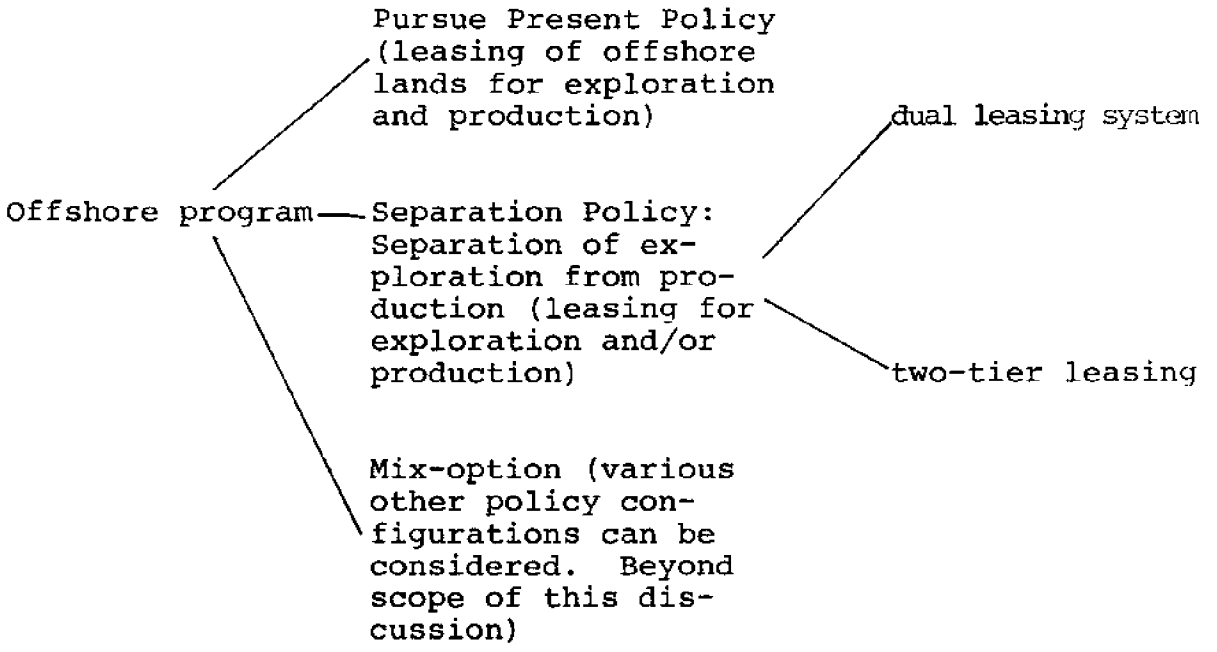

Figure 6.2: Leasing Policy for offshore lands

Figure 6.2 indicates two leasing policy options that the Secretary can pursue in an offshore exploitation program, i.e. the present policy or the separation policy. He can adopt a mixture of both options but this mix-option will not be discussed here since an understanding of either of the two earlier options will determine the attributes of the mix-option.

By present policy, is meant the cash bonus system which dominates past and current leasing policies. In this system, the Secretary offers tracts for lease sale. The minimum values of these tracts are determined by limited geophysical surveys undertaken by the United States Geological Survey. No

exploratory drilling is allowed. Hence the real values of the tracts are indeterminate. Industry bids on the leases and the successful bidders pay a cash bonus of about 17% on the minimum values of the tracts to the United States Treasury. A single bid covers both exploration and production on the tract.

Data are therefore inadequate under the present policy to determine if geological characteristics necessary for petroleum accumulation exist in the OCS frontier areas. Although geophysical data and extrapolation of geological trends can identify potentially attractive geological structures, the geological characteristics and specific potential for oil and gas are unknown until boreholes have been sunk. Since exploratory drilling is not done until after leasing, policy makers must rely on geological inference and speculation as to whether petroleum actually exists. Actual information on shelf resources would generally require a major drilling effort but would better identify areas favorable for oil and gas accumulation before leasing. Drilling stratigraphic holes in the vicinity of known structures would improve the geological information on potential petroleum accumulation. For the separation policy option, it is assumed that the exploration phase includes stratigraphic drilling as well as geophysical exploration.

In the separation policy, exploration on the tract is leased out separately from production. The effect of this is that exploration results can be made non-proprietary (not so in the present policy) and accessible to the public. There will also be a time lag between the end of the exploration lease to the start of the development lease, thus allowing oil companies, Interior officials,and state and local government authorities to study the data and arrive at a fair estimate of the value of the lease area and to prepare for the onshore impacts of offshore development.

Two systems of separation are available. These are the dual leasing system where lease for exploration would not include any right to subsequently develop and produce the resources discovered, and the two-tier leasing system where the lease awarded for exploration will include a right to subsequent development and production of the resources on a portion of the lease area.

In dual leasing system, the government offers, by means of competitive bidding, exploration leases to private firms who would manage and conduct exploratory drilling. The government can also do the exploration itself and lease out the tracts for subsequent development and production. Bid factors for the exploration leases can be the percentage of costs to be assumed by the bidder, the percentage of revenues to be received by the bidder (revenues on the sale of the lease areas for development), or a combination of both. The

benefit of this system is that it introduces a way to acquire exploratory data for planning purposes, environmental decisions, and coastal state review, without an extensive government managed exploratory drilling program and therefore at lower cost to the government; it provides a more rational basis for development leasing since the information collected allows prospects to be properly evaluated and fair value obtained; and it encourages greater competition for development and production of leases because smaller firms who might not otherwise bid because of the high information cost, will now know more about the prospects before bidding for development and production.

In the two-tier system, the exploration lease is also awarded on the basis of competitive bids. This system is presently used in Australia and in Canada where the exploratory permit awarded grants the holder the right to comprehensive exploration within the permit area. The permit holder can, after the exploration phase, select a portion of the permit area to which he is entitled to obtain a lease or license for development and production. The remainder of the lease area is leased by the government to the rest of the industry for development and production. The two-tier system has most of the benefits of the dual leasing system. Bidding factors are similar to that for the dual-leasing system, except in here an additional bid factor can be the fraction of the leased

area that the successful bidder for the exploration phase will be allowed to develop.

Both systems discussed above allow for the separation of exploration from production. The two-tier system has the particular advantages that it has been tested in countries similar in society structure, political system and offshore environment to the United States, and it affords incentive to the operator of the exploration phase to do a thorough job by rewarding him with the right to develop a portion of the lease area. The dual leasing system is advantageous in that it allows independent companies, interested only in offshore exploration and not in the development and production of offshore areas, to join oil companies in exploration lease bidding, thus creating a bigger pool of bidders and therefore probably resulting in a higher bid on the exploration lease; and the operator of the exploration phase will be non-biased towards the outcome of this phase since automatic right to the development and production of the lease area is not granted,and therefore will do an impartial and perhaps better job.

The two-tier system is faulted in some ways. The operators of the exploration phase often choose the best areas for development, leaving less valuable areas to the government. If a rich oil field is found, the operator makes a tremendous profit if he has obtained the right to the development phase at a price that reflects the unknown potential of the area which

is often much lower then the value of the area when the presence of substantial oil is confirmed. Of course, the converse is true and the operator may lose heavily if the area turns out to be barren. This characteristic of the two-tier system can be rectified by setting the price of the right to later development of a portion of the lease area to a value equal to the value of the portion of area after the exploration phase (computed from the value/unit area of the remaining area, obtained from the successful bidder) minus the total cost of the exploration phase plus the cost of exploring the portion of the operator's development area . I suggest that both systems should be tried in future leasing policies and the success of each system evaluated.

It is believed that the separation policy will provide a better estimate of the resource potential of an offshore lease area, since all exploratory results will be made public and stratigraphic drilling is allowed. This better estimate will ensure a fairer market value on the lease when the area is opened for bids. A fair market value however may not indicate better returns to the public from OCS development. A review of the leasing record from 1970 to 1975 (when the present policy was the only policy) shows that the oil industry had consistently been overoptimistic and a greater than fair value has usually been obtained. It is feared that with the separation policy, and a better knowledge of the value of the lease areas, the return to the public may drop since the

winning bid will probably be closer to the true value. It is not certain that given the tight money situation and better geophysical exploration techniques in the 1980s oil companies will still overbid on the lease areas, if the present policy is used. They may underbid since competition is reduced by the depressed economic situation. Hence the separation system is probably still the better policy.

6.3.3 Micro-option

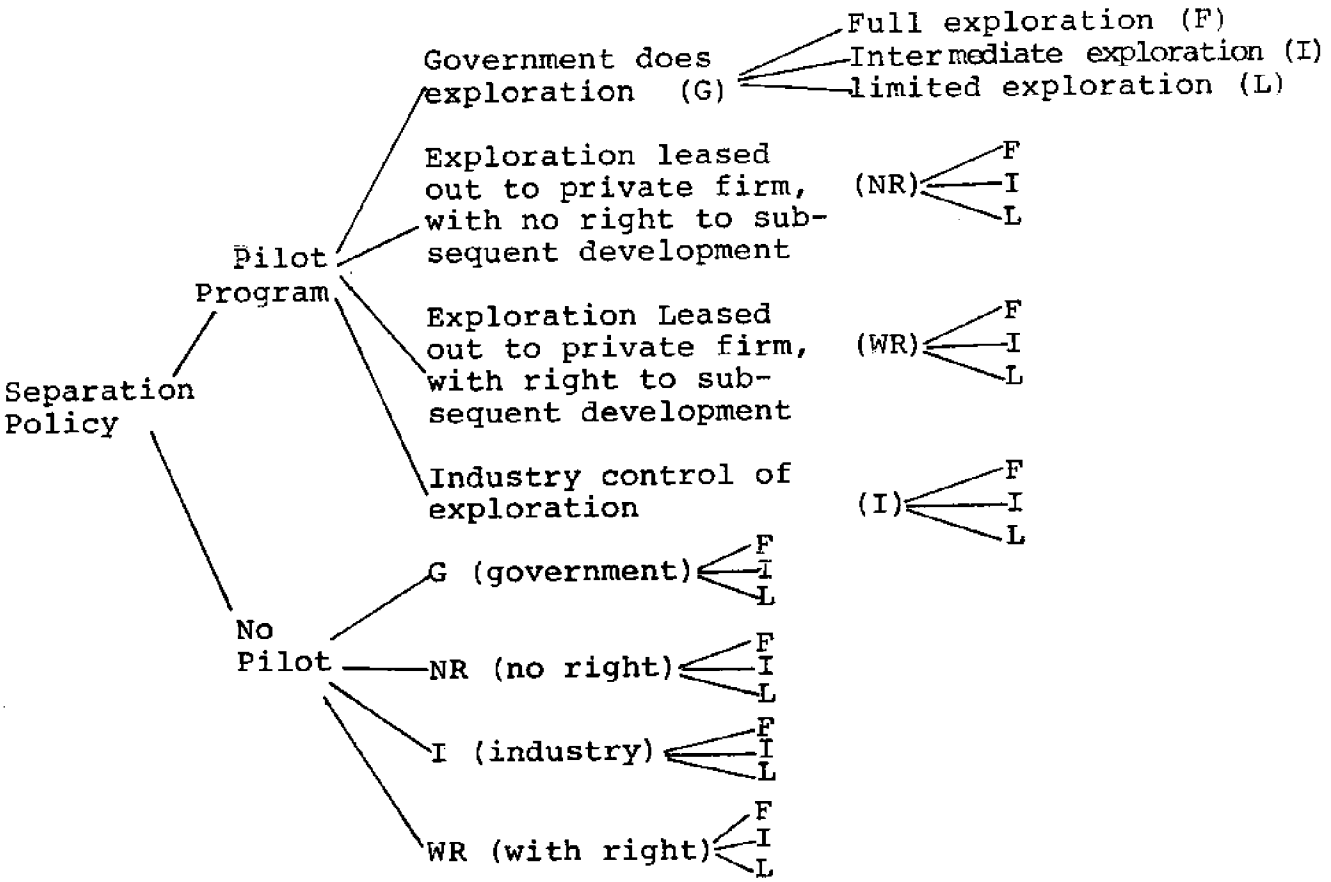

Figure 6.3: Methods of Separation

Figure 6.3 indicates by means of a probability tree, how the Interior Secretary can formulate his separation policy. First, the decision is reached as to whether a pilot program which commits certain areas to the separation system; or a no-pilot program which commits the entire industry to the separation system, should be used. The no-pilot option will enable rapid transition into the separation system but carries the danger that if the untested separation system did not work, then the entire offshore oil industry might be in a jam, creating possible loss of revenues amounting to billions of dollars. The pilot option is a cautious policy option, and allows Interior to test the success of its separation program against the cash-bonus system under the same socio-economic environment and is probably the better option since the stakes are so high and the economic environment depressed.

The next step considers how the exploration work is to be allocated. Four options can be distinguished.

1. exploration done by the government, with government personnel and facilities (G-option).
2. exploration done by a private firm with the contract terminating at the end of the exploration phase, i.e the firm has no automatic right to subsequently develop part or whole of the exploration lease area.
3. exploration done by a private firm, with subsequent right to develop a portion of the exploration lease area.

4. exploration done and financed by industrial groups with government approval.

In the G-option the Department of Interior will take over the task of exploratory drilling on its own initiative. (Drilling is specifically considered here because it is the only method that can determine with certainty the existence of oil. The other part of the exploration phase, geophysical exploration, is not at issue here since it has always been done by the government or by the oil industry and is a much less expensive operation than exploratory drilling.) The oil industry has been very wary of a government takeover of the exploration phase. They warn that this could lead to the creation of a federal agency to produce and own the undersea oil and gas because they cannot conceive that the feds will turn it over to the industry once they have found oil. They used this argument in the 1977 Congressional hearings on the bills proposing OCSLA (1953) amendments, as the principal reason why the bills should be defeated. However there is nothing in the then pending bills or in the OSCLAA (1978) that would enable the government to undertake full-scale production activities of any sort. The argument is therefore unfounded. Another argument is that with government takeover of exploration, the oil industry's experienced exploratory arm would wither away; and exploration research would be stifled, with the loss of technological advances critical to locating

increasingly harder-to-find offshore oil and gas deposits. This argument is not entirely true. In order to maintain the level of exploration activities, the government will require a large amount of expert personnel who will be drawn from the 'withered' exploratory arm of the oil industry and exploration research can still be supported by the government. There are certain disadvantages associated with government control of exploration. Firms that deal principally with offshore exploration will find themselves having to close down since there is no more work from the government or from the oil industry. It may also cost more for government to do the exploration than for the industry since a start-up time is needed to recruit and train personnel and to procure equipment. Government resources in terms of personnel and equipment are much smaller than the whole industry's, and therefore government exploration may take longer and cover smaller areas. The delay in exploration will result in delays in production and the basic aim of the 1978 Amendments to achieve orderly and timely development of the OCS's oil resources will not be achieved. A final argument is that although the Secretary has wide discretion in designing exploration policies, legislative intent throughout the legislative history of the Amendments has been that private firms, not the government should carry out the exploration operations. A complete government takeover of exploration may run into legal difficulties in the courts.

The next option (NR-option) is that the government should lease out the exploration phase to private firms, with no automatic right to subsequently develop a part of the leased area. This option has none of the disadvantages associated with the previous option. Since the government can lease out the exploration phase to firms specialized in offshore exploration, the data gathering can be achieved more rapidly and more efficiently. Data could be released early to the public to ease information disadvantages in smaller oil companies and encourage participation by them in the bidding for the development and production lease. This option can also encourage the growth of small specialized private firms that deal with leasing government exploration functions.

Both the above two options are identified with the dual leasing system. The next two options I will discuss can be identified with the two-tier leasing system.

In the WR-option, the exploration phase is leased out to private firms, with the automatic right to subsequently develop a portion of the lease area. This option has most of the benefits associated with the NR-option but it also inherits the drawbacks associated with the two-tier leasing system,i.e difficulty in assuring a fair return to the public and unethical practice on the part of the industry-partner.

The final option, industry takeover of exploration, can be achieved through unitization agreements. Unitization agreements are voluntary agreements by the various oil companies

interested in exploiting a particular OCS region, to form a group that will be approved by the Secretary, and will have the responsibility of performing the exploratory work on behalf of all its members. The operator with a major interest in the unitized area is the unit operator or unit manager and acts on behalf of all the other operators. For this principle to be effective, entire structures will have to be leased for the exploration phase. All tracts identified to a given structure will also be combined into and considered as a single lease unit for development purposes. In the development phase, unit operation encompassing an entire structure is contented to be most efficient and will enable the greatest volume of petroleum from any reservoir to be recovered. There is a new dimension in this option in that unitization in the development phase is included. It may seem that the advantages associated with the separation of exploration from development (example equal public access to exploration data) will be foregone. This is not so since we are dealing here with a single unit and therefore there is no incentive for anyone to keep exploration information proprietary hence information can still be accessible to the general public.

Despite its benefits, unitized agreements have some major problems, three of which are itemized below:

1. Choice of an appropriate sharing formula.
2. Selection of a unit operator and the determination of a drilling plan.

3. The risk that unitization may become a lease-holding device because as long as a unit plan is in force, some drilling or production anywhere on the acreage included in the unit will maintain the lease on all lands in the unit.

The difficulties with trying to solve these three problems diminishes the attractiveness of the unitized agreement.

I suggest that the NR-option and WR-option be used as possible policy options in deciding on a leasing strategy. The G-option is discouraged because of its inefficient nature and potential legal problems. The I-option is attractive and rather innovative but difficulties in agreeing on an appropriate sharing formula and on the selection of the unit operator and the problem of assuring a fair market return on the leased resources (since no bidding occurs when the agreement is made), discourages the practice of this option.

The final step deals with the question of no matter who does the exploration, should the full, intermediate or limited exploration programs be performed? A limited exploration program takes 4 to 6 years and should be concentrated on the major prospects in an OCS region. Cost of this program ranged from $0.6 billion to $1.6 billion in 1975. The intermediate program lasts 8 years and cost ranged from $1.3 billion to $2.4 billion (in 1975). It is an extension of the limited program. The full program can last much longer and cost much more than the intermediate program, depending on how much

information is required, and is not recommended since the outcome of the program is not worth the cost to public funds. It is recommended that the limited program be chosen since the economics of offshore production lie in the discovery of major traps (not in minor traps which are abundant onshore). Futhermore, if the bidding process for the development phase turns out to be a failure (because of industry perception of poor potential of the explored regions), then a smaller loss of public funds will be the result.

Appendix A1: Fortran IV Program for estimating the posterior probability of State 1 away from a known line.

```
      DIMENSION M(70),R(70),T(70),X(66)
      REAL LLIKE1, LLIKEO
C
C INITIALISE VALUES : RHO = CORRELATION COEFFICIENT, 2S = SPACING
C BETWEEN PARALLEL LINES, TL = TOTAL LENGTH OF EACH LINE,
C P = INITIAL PROBABILITY OF STATE 1 .
C
      S = 1.0/6.0
      TL = 1.0
      P = 0.5
      PI = 3.14159
      GAMA = 15.15
      RHO = PI * GAMA/2.
      Q = 1.00000 - P
C
C START WITH AN INITIAL VALUE OF Y, AND LOOP WITH A CONSTANT
C INCREMENT. WRITE HEADING.
C FIRST READ IN THE STATES OF THE 66 SEGMENTS.
C
      READ(5,400) (M(I), I=1,66)
C
C START LOOP FOR X
C
      DO 70  K=1,66
      X(K) = FLOAT(K)*TL/66.
C
C INITIALISE LIKELIHOOD FNS : LIKE1 FOR STATE 1, AND LIKEO FOR STATE O
C
      LLIKE1 = 0.0
      LLIKEO = 0.0
C
C CALCULATE DISTANCES R OF EXTERIOR PT. U TO LINE AT EACH OF 66 SEGMENTS
C
      DO 10  I = 1,66
      T(I) = FLOAT(2*I-1)*TL/66.
      R(I) = SQRT((X(K) - T(I)/2.)**2 + S**2)
 10   CONTINUE
C
C THEN START CALCULATING THE LIKELIHOOD FNS, KNOWING THE STATES AT
C THE VARIOUS SEGMENTS.
C
      A4 = EXP(-RHO*2.*T(1)/PI)
      C = P + Q*A4
      DO 55 I = 2,66
C
C FIRST CALCULATE ALL THE PARAMETERS.
C
      A2 = EXP(-RHO*2.*R(I-1)/PI)
      A1 = (R(I-1) + R(I) + T(1))/PI
      A3 = EXP(-RHO*2.*R(I)/PI)
      A = P*P + (1.-3.*P+2.*P*P)*EXP(-RHO*A1) + (P-P*P)*(A2+A3+A4)
      B = P + Q*A3
      D = P + Q*A2
      E = Q*Q + (1.-3.*Q+2.*Q*Q)*EXP(-RHO*A1) + (Q-Q*Q)*(A2+A3+A4)
      F = Q + P*A3
```

```
C
C THEN DIFFERENTIATE BETWEEN THE STATES OF NEIGHBOURING SEGMENTS.
C WHEN BOTH M(I-1) AND M(I) ARE OF STATES O :
C
      IF(M(I-1).NE.1 .AND. M(I).NE.1) GO TO 20
C
C WHEN M(I-1) IS STATE 1 AND M(I) STATE O :
C
      IF(M(I-1).EQ.1 .AND. M(I).NE.1) GO TO 30
C
C WHEN M(I-1) IS STATE O AND M(I) STATE 1 :
C
      IF(M(I-1).NE.1 .AND. M(I).EQ.1) GO TO 40
C
C CALCULATE FN. P(M(I-1)/M(I),U=1) = FY1 AND FN. P(M(I-1)/M(I),U=O)
C = FYO WHERE U IS THE EXTERIOR PT. (X,Y). THIS CASE IS FOR M(I-1)
C , M(I)=1 AND U=O,1.
C
      FY1 = A/B
      FYO = (C - A)/(1. - B)
      GO TO 50
C
C DITTO.....M(I-1) = O, M(I) = O
C
  20  FY1 = 1. - (D - A)/(1. - B)
      FYO = E/F
      GO TO 50
C
C DITTO.....M(I-1) = 1, M(I) = O
C
 30   FY1 = (D - A)/(1. - B)
      FYO = 1. - E/F
      GO TO 50
C
C DITTO.....M(I-1) = O, M(I) =1
C
 40   FY1 = 1. - A/B
      FYO = 1. - (C - A)/(1. - B)
C
C NOW CALCULATE LIKELIHOOD FNS. FOR U=1, I.E. LIKE1 AND FOR U=O, LIKEO
C
 50   LLIKE1 = LLIKE1 + ALOG(FY1)
      LLIKEO = LLIKEO + ALOG(FYO)
 55   CONTINUE
C
C CALCULATE THE VALUE OF P(M(66)/U). FOR U=1 M(66)=1 FN.=F11,
C U=O M(66)=1 FN.=F1O, U=O M(66)=O FN.=FOO, U=1 M(66)=O FN.=FO1
C
      IF(M(66).NE.1) GO TO 60
      F11 = B
      F1O = P*(1. - A3)
C
C CALCULATE LIKELIHOOD FN. FOR M(66) = 1
C
      LLIKE1 = LLIKE1 + ALOG(F11)
```

```
      LLIKE0 = LLIKE0 + ALOG(F10)
      GO TO 65
C
C CALCULATE LIKELIHOOD FN. FOR M(66) = 0
C
 60   F01 = Q*(1. - A3)
      F00 = F
      LLIKE1 = LLIKE1 + ALOG(F01)
      LLIKE0 = LLIKE0 + ALOG(F00)
C
C NOW CALCULATE VALUE OF P(X) = PL(X/U=1) + QL(X/U=0). CALL THI
C CALCULATE THE POSTERIOR PROBABILITY OF STATE 1, CALL IT POST1.
C
 65   APOST1 = ALOG(Q) + LLIKE0 - ALOG(P) -LLIKE1
      POST1 = 1/(EXP(APOST1) + 1.)
      POST0 = 1. - POST1
      WRITE(6,300) X(K), S, POST1, POST0
 70   CONTINUE
 100  FORMAT('1','THE Y-COEFFICIENT IS  ',F6.4)
 200  FORMAT('0',1X,'XCOEFF.',15X,'YCOEFF.',15X,'PROB.1',16X,'PROB.0')
 300  FORMAT('0',2X,F6.4,14X,F6.4,14X,F6.5,14X,F6.5)
 500  FORMAT(4F10.5)
 400  FORMAT (2(22I3/), 22I3)
      STOP
      END
```

Appendix A2: Fortran IV program for estimating the posterior probability of State 1 between two known lines.

```
      DIMENSION M(66),R(66),T(66),X(100),M1(66),MO(66)
      REAL LLI1, LLIO
C
C ****************************************************************
C
      READ(5,400)(MO(I),I=1,66)
      READ(15,400)(M1(I),I=1,66)
      KCO=0
      KC1=0
      MCO=0
      MC1=0
      DO 2 I=1,66
      IF(MO(I).EQ.1)KC1=KC1+1
      IF(MO(I).EQ.0)KCO=KCO+1
      IF(M1(I).EQ.1)MC1=MC1+1
      IF(M1(I).EQ.0)MCO=MCO+1
 2    CONTINUE
      P=FLOAT(MC1+KC1)/FLOAT(MC1+MCO+KC1+KCO)
      GAMA = 8.88
      S = 1.0/33.0
      TL = 1.0
      Q=1.00000-P
      PI=3.14159
      RHO = PI * GAMA/2.
      DO 4 I=1,66
      T(I)=FLOAT(2*I-1)*TL/66.
 4    CONTINUE
      A4=EXP(-RHO*2.*T(1)/PI)
      C=P+Q*A4
C
C ****************************************************************
C
      DO 70  K=1,66
      X(K) = FLOAT(K)*TL/66.
C
C ****************************************************
C
      N=0
 5    N=N+1
      IF(N.EQ.1) GO TO 7
      DO 6 I=1,66
      M(I)=M1(I)
 6    CONTINUE
      GO TO 9
 7    DO 8 I=1,66
      M(I)=MO(I)
 8    CONTINUE
C
C ****************************************************
C
 9    LLI1 = 0.0
      LLIO = 0.0
C
C
C
```

```
      DO 10  I = 1,66
      R(I) = SQRT((X(K) - T(I)/2.)**2 + S**2)
 10   CONTINUE
C
C
C
      DO 55 I = 2,66
      A2 = EXP(-RHO*2.*R(I-1)/PI)
      A1 = (R(I-1) + R(I) + T(1))/PI
      A3 = EXP(-RHO*2.*R(I)/PI)
      A = P*P + (1.-3.*P+2.*P*P)*EXP(-RHO*A1) + (P-P*P)*(A2+A3+A4)
      B = P + Q*A3
      D = P + Q*A2
      E = Q*Q + (1.-3.*Q+2.*Q*Q)*EXP(-RHO*A1) + (Q-Q*Q)*(A2+A3+A4)
      F = Q + P*A3
C
      IF(M(I-1).NE.1 .AND. M(I).NE.1) GO TO 20
C
      IF(M(I-1).EQ.1 .AND. M(I).NE.1) GO TO 30
C
      IF(M(I-1).NE.1 .AND. M(I).EQ.1) GO TO 40
C
      FY1 = A/B
      FYO = (C - A)/(1. - B)
      GO TO 50
C
 20   FY1 = 1. - (D - A)/(1. - B)
      FYO = E/F
      GO TO 50
C
 30   FY1 = (D - A)/(1. - B)
      FYO = 1. - E/F
      GO TO 50
C
 40   FY1 = 1. - A/B
      FYO = 1. - (C - A)/(1. - B)
C
 50   LLI1 = LLI1 + ALOG(FY1)
      LLIO = LLIO + ALOG(FYO)
 55   CONTINUE
C
C ********************************************************
C
      IF(M(66).NE.1) GO TO 60
      F11 = B
      F10 = P*(1. - A3)
C
C
      LLI1 = LLI1 + ALOG(F11)
      LLIO = LLIO + ALOG(F10)
      GO TO 65
C
C
 60   FO1 = Q*(1. - A3)
      FOO = F
```

```
      LLI1 = LLI1 + ALOG(FO1)
      LLIO = LLIO + ALOG(FOO)
C
 65   IF(N.EQ.2)GO TO 67
C
      ALI1=LLI1
      ALIO=LLIO
      GO TO 5
C
C ***************************************************************
C
 67   LLI1=LLI1 + ALI1
      LLIO=LLIO + ALIO
      APOST1 = ALOG(O) + LLIO - ALOG(P) -LLI1
      POST1 = 1/(EXP(APOST1) + 1.)
      POSTO = 1. - POST1
      WRITE(6,600)POST1
 70   CONTINUE
C
C ***********************************************************
C
 200  FORMAT('O',2X,'XCOEFF',14X,'YCOEFF',14X,'PROB.1',14X,'PROB.O')
 300  FORMAT('O',2X,F6.4,14X,F6.4,14X,F6.5,14X,F6.5)
 400  FORMAT (2(22I3/), 22I3)
 500  FORMAT(4F10.5)
 600  FORMAT(40X,F10.8)
      STOP
      END
```

Appendix B: Table of probability of State 1 for various values of x and y, Map 4, line OP.

XCOEFF	YCOEFF	PROB.1
0.1000	0.1000	.24634
0.2000	0.1000	.21203
0.3000	0.1000	.32490
0.4000	0.1000	.59868
0.5000	0.1000	.55433
0.6000	0.1000	.57168
0.7000	0.1000	.61290
0.8000	0.1000	.34887
0.9000	0.1000	.25693
1.0000	0.1000	.31688
0.1000	0.2000	.34612
0.2000	0.2000	.33403
0.3000	0.2000	.37455
0.4000	0.2000	.43462
0.5000	0.2000	.44797
0.6000	0.2000	.45117
0.7000	0.2000	.44150
0.8000	0.2000	.38502
0.9000	0.2000	.35016
1.0000	0.2000	.35197
0.1000	0.3000	.37086
0.2000	0.3000	.36887
0.3000	0.3000	.37970
0.4000	0.3000	.39458
0.5000	0.3000	.40174
0.6000	0.3000	.40265
0.7000	0.3000	.39696
0.8000	0.3000	.38324
0.9000	0.3000	.37254
1.0000	0.3000	.37014
0.1000	0.4000	.37696
0.2000	0.4000	.37680
0.3000	0.4000	.37963
0.4000	0.4000	.38350
0.5000	0.4000	.38590
0.6000	0.4000	.38619
0.7000	0.4000	.38427
0.8000	0.4000	.38064
0.9000	0.4000	.37753
1.0000	0.4000	.37632
0.1000	0.5000	.37841
0.2000	0.5000	.37846
0.3000	0.5000	.37920
0.4000	0.5000	.38024
0.5000	0.5000	.38094
0.6000	0.5000	.38102
0.7000	0.5000	.38046
0.8000	0.5000	.37947
0.9000	0.5000	.37857
1.0000	0.5000	.37812

0.1000	0.6000	.37872
0.2000	0.6000	.37877
0.3000	0.6000	.37895
0.4000	0.6000	.37923
0.5000	0.6000	.37943
0.6000	0.6000	.37946
0.7000	0.6000	.37930
0.8000	0.6000	.37903
0.9000	0.6000	.37876
1.0000	0.6000	.37861
0.1000	0.7000	.37878
0.2000	0.7000	.37880
0.3000	0.7000	.37887
0.4000	0.7000	.37893
0.5000	0.7000	.37897
0.6000	0.7000	.37898
0.7000	0.7000	.37895
0.8000	0.7000	.37889
0.9000	0.7000	.37879
1.0000	0.7000	.37874
0.1000	0.8000	.37879
0.2000	0.8000	.37880
0.3000	0.8000	.37881
0.4000	0.8000	.37884
0.5000	0.8000	.37887
0.6000	0.8000	.37885
0.7000	0.8000	.37883
0.8000	0.8000	.37880
0.9000	0.8000	.37879
1.0000	0.8000	.37879
0.1000	0.9000	.37879
0.2000	0.9000	.37879
0.3000	0.9000	.37880
0.4000	0.9000	.37881
0.5000	0.9000	.37881
0.6000	0.9000	.37881
0.7000	0.9000	.37881
0.8000	0.9000	.37880
0.9000	0.9000	.37880
1.0000	0.9000	.37879
0.1000	1.0000	.37879
0.2000	1.0000	.37879
0.3000	1.0000	.37879
0.4000	1.0000	.37879
0.5000	1.0000	.37879
0.6000	1.0000	.37880
0.7000	1.0000	.37880
0.8000	1.0000	.37879
0.9000	1.0000	.37879
1.0000	1.0000	.37879

BIBLIOGRAPHY

Addy, S.K., Behrens, E.W. and Haines, R.R. (1979): 'Correlation of Some Lithologic and Physical Characteristics of Sediments with High Frequency Sub-bottom Reflection Types', Offshore Technology Conference paper No. 3569, 1979.

Akal, T. (1972): 'The Relationship between the Physical Properties of Underwater Sediments that affect Bottom Reflection', Marine Geology 13, 251-266.

Baecher, G.B. (1972): 'Site Exploration, A Probabilistic Approach', Ph.D. Thesis, Massachusetts Institute of Technology.

Bell, D.L. and Porter, W.J. (1974): 'Remote Classification Potential of Reflected Acoustic Signals', Physics of Sound in Marine Sediments, ed. Hampton, L.D., New York, Plenum Press, 1974, pp. 319-336.

Benjamin, J.R. and Cornell, C.A. (1970): Probability, Statistics and Decision for Civil Engineers, McGraw Hill Book Company, New York.

Breslau, L.R. (1965): 'Classification of Sea-Floor Sediments with a Ship-borne Acoustical System', Petroleum and the Sea, Proceedings of International Congress, Monte Carlo, Volume 2, Sec. 1, No. 132, Paris, La Revue Petroliere.

Buchan, S., Dewes, F.C.D., McCann, D.M. and Taylor Smith, D. (1967): 'Measurements of the Acoustic and Geotechnical Properties of Marine Sediment Cores', Marine Geotechnique, ed. Richards, A.F., University of Illinois Press.

Claerbout, J. (1976): Fundamentals of Geophysical Data Processing, McGraw Hill, New York (1976).

Clay, C.S. and Rona, P.A. (1965): 'Studies of Seismic Reflections from thin Layers on the Ocean Bottom in the Western North Atlantic', Journal of Geophysical Research, Vol. 70, No. 4, Feb. 15, 1965, pp. 855-869.

Danbom, S.H. (1976): 'Sediment Classification by Seismic Reflectivity - Oceans '76', Proceedings of MTS-IEEE Annual Meeting, 1976, pp. 16D-1-16D-6.

Dix, C.H. (1955): 'Seismic Velocities from Surface Measurements', Geophysics 20, 68-86.

Dobrin, M.B. (1976): Introduction to Geophysical Prospecting, McGraw-Hill, New York.

Faas, R.W. (1969): 'Analysis of the Relationship between Acoustic Reflectivity and Sediment Porosity', Geophysics, Vol. 34, No. 4, Aug. 1969, pp. 549-553.

Fountain, J.D. (1979): 'Foundation Information from Exploration Seismic Data', Offshore Technology Conference paper No. 3663, 1979.

Griffith, D.J. and King, R.F. (1965): Applied Geophysics for Engineers and Geologists, Pergamon Press, New York.

Hamilton, E.L. (1970): 'Sound Velocity and Related Properties of Marine Sediments', Journal of Geophysical Research, Vol. 75, No. 23, 1970.

Hamilton, E.L. (1971a): 'Elastic Properties of Marine Sediments', Journal of Geophysical Research, Vol. 76, No. 2 (1971).

Hamilton, E.L. (1971b): 'Prediction of In-Situ Acoustics and Elastic Properties of Marine Sediments', Geophysics, Vol. 36, No. 2 (1971).

Hamilton, E.L. (1974): 'Prediction of Deep-Sea Sediment Properties', Deep Sea Sediments, ed. A.L. Inderbitzen, Plenum Press, 1974, New York.

Hamilton, E.L. (1976a): 'Sound Attenuation as a Function of Depth in the Sea Floor', J. Acoustical Soc. Am., Vol. 59, No. 3, 1976.

Hamilton, E.L. (1976b): 'Shear-wave Velocity versus Depth in Marine Sediments: A Review', Geophysics, Vol. 41, No. 5, 1976.

Hampton, L.D. (1967): 'Acoustical Properties of Sediments', Acoustical Society of America Journal, Vol. 42, No. 4, 1967.

Hampton, L.D., editor (1974): Physics of Sound in Marine Sediments, Plenum Press, New York, 1974.

Horn, D.R., Horn, B.M. and Delach, M.N. (1968): 'Correlation between Acoustic and Other Physical Properties of Deep Sea Cores', J. Geophy. Res. 73, 1939-57.

Hubral, P. (1978): 'On Getting Reflection Coefficients from Waves', Geophysical Prospecting 26, 627-630.

Kalter, R.J., Tyner, W.E. and Hughes, D.W. (1975): Alternative Energy Leasing Strategies and Schedules for the Outer Continental Shelf, Department of Agricultural Economics, 1975, Cornell University.

Kesmarky, I. (1977): 'Estimation of Reflector Parameters by the Virtual Image Technique', Geophysical Prospecting 25, 621-635.

Larner, K. Hale, D., and Misener, S. (1979): 'Desired Seismic Characteristics of an Air Gun Source', Offshore Technology Conference paper No. 3617, 1979.

Lee, H. and Malloy, R.J. (1977): Acoustic Retrieval of Seafloor Geotechnics

Levin, F.K. (1971): 'Apparent Velocity from Dipping Interface Reflections', Geophysics 36, 510-516.

Mahmood, A. and Hough, J.C. (1978): 'Sea-bottom Soil Properties and Acoustics', Offshore Technology Conference paper No. 3208 (1978).

Matheron, G. (1971): The Theory of Regionalized Variables and its Applications, Les Cahiers du Centre de Morphologie Mathematique de Fontainebleau, Vol. 5.

Mayne, W.H. and Palmer, H.D. (1967): 'Offshore Seismic Reflection Surveys', Civil Engineering in the Oceans, Proceedings of ASCE Conference, San Francisco, California, September 6-8, 1967, New York, ASCE 1968, pp. 789-806.

Mayne, W.H. (1969): 'Physical Properties of Marine Sediments and Relation to Seismic Velocities', Geophysics, Vol. 34, No. 4, Aug. 1969, pp. 529-545.

Nafe, J.E. and Drake, C.L. (1957): 'Variation with Depth in Shallow and Deep Water Marine Sediments of Porosity, Density and the Velocities of Compressional and Shear Waves', Geophysics 22, 523-552.

Nooteboom, J.J. (1978): 'Signature and Amplitude of Linear Air Gun Arrays', Geophysical Prospecting 26, 194-201.

Nucci, L.R. (1979): "An Analysis of the Rate of Error in Two Color Maps', SM Thesis, Mass. Inst. of Technology.

Paynton, C.E. (1977): Seismic Stratigraphy - Applications to Hydrocarbon Exploration, editor, American Association of Petroleum Geologists.

Nucci, L.R. (1979): 'An Analysis of the Rate of Error in Two Color Maps', SM Thesis, Mass. Inst. of Technology.

Payton, C.E. (1977): Seismic Stratigraphy - Applications to Hydrocarbon Exploration, Editor, American Association of Petroleum Geologists.

Porter, W.J. and Bell, D.L. (1975): 'Development of Quantitative Remote Acoustic Indices for Locating and Mapping of Sea Floor Spoil Deposits', Offshore Technology Conference paper No. 2288, 1975.

Ramsayer, G.R. (1979): 'Seismic Stratigraphy, A Fundamental Exploration Tool', Offshore Technology Conference paper No. 3568, 1979.

Reed, D.H. and Hardison, J.E. (1977): 'New Marine Seismic Source of the Gas Exploder Type', Offshore Technology Conference paper No. 2781.

Roksandic, M.M. (1978): 'Seismic Facies Analysis Concepts', Geophysical Prospecting 26, 383-398.

Self, G.W. and Mahmood, A. (1978): 'Assessment of Relative Slope Stability of Kodiak Shelf, Alaska', Marine Geotechnology, Vol. 2, 1978.

Stone, D.G. (1979): 'Using Seismic Data to Extrapolate Well Logs', Offshore Technology Conference paper No. 3658, 1979.

Switzer, P. (1967): 'Reconstruction Patterns from Sample Data', Annals of Mathematical Statistics, Vol. 3.

Switzer, P. (1971): 'Mapping a Geographically Correlated Environment', Statistical Ecology.

Switzer, P. (1973): 'Estimation of the Accuracy of Qualitative Maps', Display and Analysis of Spatial Data, J.C. Davis and M.J. McCullagh, eds., Wiley.

Tufekcic, D. (1978): 'A Prediction of Sedimentary Environment from Marine Seismic Data', Geophysical Prospecting 26, 329-336.

United States Comptroller General, Report to the Congress: Outer Continental Shelf Oil and Gas Development - Improvements needed in determining Where to Lease and at What Dollar value. Wasington: Government Printing Office, 1975.

United States Congress, House Select Committee on the Outer Continental Shelf; Offshore Oil and Gas: The Five-Year Leasing Program and Implementation of the Outer Continental Shelf Lands Act Amendments of 1978, Washington: Government Printing Office, 1980.

United States Congress, Office of Technology Assessment (1975); An Analysis of the Feasibility of Separating Exploration from Production of Oil and Gas on the Outer Continental Shelf. Washington: Government Printing Office, 1975.

United States Congress, Senate Subcommittee on Energy Resources and Materials Production, of the Senate Committee on Energy and Natural Resources; OCS Oil and Gas Leasing Program Hearings (96th. Congress, 2nd Session), Washington: Government Printing Office, 1980.

Veneziano, D. (1980): 'Probabilistic Model of Joints in Rock', Unpublished M.I.T. Report, Massachusetts Institute of Technology.

Wilson, W.D. (1960): J. Acoust. Soc. Am., 23: 1357.

Ziolkowski, A. and Lerwill, W.E, (1979): 'A Simple Approach to High Resolution Seismic Profiling for Coal, Geophysical Prospecting 27, 360-393.